A genome-wide arrayed CRISPR screen identifies PLSCR1 as an intrinsic barrier to SARS-CoV-2 entry that recent virus variants have evolved to resist

Authors

Jérémie Le Pen[1,*], Gabrielle Paniccia[1,*], Volker Kinast[2,3,#], Marcela Moncada-Velez[4,#], Alison W. Ashbrook[1,#], Michael Bauer[1,#], H.-Heinrich Hoffmann[1,#], Ana Pinharanda[5,#], Inna Ricardo-Lax[1,#], Ansgar F. Stenzel[1,6,#], Edwin A. Rosado-Olivieri[7,8,#], Kenneth H. Dinnon III[1], William C. Doyle[1,9], Catherine A. Freije[1], Seon-Hui Hong[1], Danyel Lee[4,10,11], Tyler Lewy[1], Joseph M. Luna[1,12], Avery Peace[1], Carltin Schmidt[4,13], William M. Schneider[1], Roni Winkler[1], Elaine Z. Yip[1], Chloe Larson[14], Timothy McGinn[14], Miriam-Rose Menezes[14], Lavoisier Ramos-Espiritu[14], Priyam Banerjee[15], John T. Poirier[16], Francisco J. Sànchez-Rivera[17,18], Aurélie Cobat[4,10,11], Qian Zhang[4,10,11], Jean-Laurent Casanova[4,10,11,19,20], Thomas S. Carroll[21], J. Fraser Glickman[14], Eleftherios Michailidis[1,22,§], Brandon Razooky[1,23,§], Margaret R. MacDonald[1,§], Charles M. Rice[1,§]

[*] Contributed equally to this work

[#] Contributed equally to this work

[§] Contributed equally to this work

Correspondence: Jérémie Le Pen: jlepen@rockefeller.edu; Charles M. Rice: ricec@rockefeller.edu

Affiliations:

1. Laboratory of Virology and Infectious Disease, The Rockefeller University, New York, NY, USA.

2. Department of Medical Microbiology and Virology, Carl von Ossietzky University Oldenburg, Oldenburg, Germany.

3. Department for Molecular and Medical Virology, Faculty of Medicine, Ruhr University Bochum, Bochum, Germany.

4. St Giles Laboratory of Human Genetics of Infectious Diseases, Rockefeller Branch, The Rockefeller University, New York, NY, USA.

5. Department of Biological Sciences, Columbia University, New York, NY 10027, USA.

6. Present address: Department of Infectious Diseases, Molecular Virology, Heidelberg University, Heidelberg, Germany.

7. Laboratory of Synthetic Embryology, The Rockefeller University, New York, NY, USA.

8. Present address: Department of Molecular Pathobiology, New York University.

9. Present address: Laboratory of Host-Pathogen Biology, The Rockefeller University, New York, NY, USA.

10. Laboratory of Human Genetics of Infectious Diseases, Necker Branch, INSERM U1163, Paris, France, EU.

11. Paris City University, Imagine Institute, Paris, France, EU.

12. Present address: Department of Biochemistry and Center for RNA Science and Therapeutics, Case Western Reserve University, Cleveland, OH, USA.

13. Present address: Medical Faculty, Heinrich Heine University Dusseldorf, Germany.

14. Fisher Drug Discovery Resource Center, The Rockefeller University, New York, NY, USA.

15. Bio-Imaging Resource Center, The Rockefeller University, New York, NY, USA.

16. Laura and Isaac Perlmutter Cancer Center, New York University Grossman School of Medicine, NYU Langone Health, New York, NY.

17. Department of Biology, Massachusetts Institute of Technology, Cambridge, 02142, Massachusetts, USA.

18. David H. Koch Institute for Integrative Cancer Research, Massachusetts Institute of Technology, Cambridge, 02142, Massachusetts, USA.

19. Department of Pediatrics, Necker Hospital for Sick Children, Paris, France, EU.

20. Howard Hughes Medical Institute, New York, NY, USA.

21. Bioinformatics Resource Center, The Rockefeller University, New York, NY, USA.

22. Present address: Laboratory of Biochemical Pharmacology, Department of Pediatrics, Emory University School of Medicine, Atlanta, GA, USA.

23. Present address: National Resilience, Inc., La Jolla, CA, USA.

Abstract

Interferons (IFNs) play a crucial role in the regulation and evolution of host-virus interactions. Here, we conducted a genome-wide arrayed CRISPR knockout screen in the presence and absence of IFN to identify human genes that influence SARS-CoV-2 infection. We then performed an integrated analysis of genes interacting with SARS-CoV-2, drawing from a selection of 67 large-scale studies, including our own. We identified 28 genes of high relevance in both human genetic studies of COVID-19 patients and functional genetic screens in cell culture, with many related to the IFN pathway. Among these was the IFN-stimulated gene *PLSCR1*. PLSCR1 did not require IFN induction to restrict SARS-CoV-2 and did not contribute to IFN signaling. Instead, PLSCR1 specifically restricted spike-mediated SARS-CoV-2 entry. The PLSCR1-mediated restriction was alleviated by TMPRSS2 over-expression, suggesting that PLSCR1 primarily restricts the endocytic entry route. In addition, recent SARS-CoV-2 variants have adapted to circumvent the PLSCR1 barrier via currently undetermined mechanisms. Finally, we investigate the functional effects of PLSCR1 variants present in humans and discuss an association between PLSCR1 and severe COVID-19 reported recently.

Introduction

Viruses maintain a complex relationship with their host cells, co-opting host factors for their replication while being targeted by cellular defense mechanisms. Such cellular defenses include the interferon (IFN) pathway, where the infected cell senses foreign molecules and secretes IFN to trigger an antiviral state in neighboring cells [1].

Approximately 1-5% of critical COVID-19 patients have mutations that compromise the production of or response to type I IFNs, while an additional 15% possess autoantibodies that neutralize type I IFNs [2-8]. This highlights the essential role of type I IFN in the defense against the SARS-CoV-2 virus that caused the COVID-19 pandemic [9, 10]. Consequently, investigating IFN-stimulated genes (ISGs) is crucial to our understanding of the remarkable antiviral systems that evolved in nature and could enhance our preparedness for future pandemics.

Several recent studies have identified ISGs restricting SARS-CoV-2. Most of these studies involved gain-of-function genetic screens, over-expressing individual ISGs. The factors bone

85 marrow stromal cell antigen 2 (BST2), cholesterol 25-hydroxylase (CH25H), lymphocyte antigen 6
86 family member E (LY6E), 2'-5'-oligoadenylate synthetase 1 (OAS1), and receptor transporter
87 protein 4 (RTP4) were notably identified as SARS-CoV-2 antivirals in these studies [10-15]. One
88 advantage of the gain-of-function approach is that it circumvents potential genetic redundancies
89 between ISGs [16, 17]. However, this approach is biased towards ISGs that act autonomously
90 when over-expressed and does not mimic the cellular context of the IFN response, where
91 hundreds of genes and gene products are differentially regulated to establish an antiviral state.
92 To counter this limitation, two recent publications examined the effects of ISG loss of function in
93 IFN-treated cells. They conducted pooled CRISPR knockout (KO) screens in cells pre-treated with
94 IFN before SARS-CoV-2 infection [18, 19]. By sorting for cells with high SARS-CoV-2 viral load, they
95 identified SARS-CoV-2 restriction factors such as death domain associated protein (DAXX).

96 Here, we conducted a human whole-genome arrayed CRISPR KO screen to identify genes
97 that influence SARS-CoV-2 infection in cells with or without pretreatment with a low dose of IFN.
98 The arrayed approach, though logistically challenging, has advantages over the pooled format in
99 capturing both proviral and antiviral genes, genes affecting virus egress, and those coding for
100 secreted products that exert their impact on neighboring cells. It reliably captures genotype-
101 phenotype correlations while also unveiling the effects of single gene perturbation on cell growth
102 and death [20]. Additionally, the shorter culture time and lack of competition among cells with
103 different gene KO in the arrayed screen allow the inclusion of genes that would be depleted and
104 deemed essential in a pooled format [21]. The arrayed format thus enables the identification of
105 crucial cellular functions that may be co-opted by the virus or are vital for the cell's defense
106 against infection.

107 We then compiled a comprehensive list of genes interacting with SARS-CoV-2,
108 incorporating findings from our own screen as well as existing literature. This meta-analysis
109 revealed several host genes of interest, both previously described and novel. Notably, the ISG
110 product phospholipid scramblase 1 (PLSCR1) emerged as a prominent antiviral factor. PLSCR1 is
111 involved in several biological processes [22], including regulating the movement of phospholipids
112 between the two leaflets of a cell membrane (lipid scrambling) [23] and IFN signaling in the
113 context of virus infection [24].

114 Follow-up experiments revealed that PLSCR1 is a cell intrinsic factor that restricts spike-
115 mediated SARS-CoV-2 entry, independently of the IFN pathway, via currently undetermined
116 mechanisms. Our genetic screen data and meta-analysis provide a valuable resource to broaden
117 our understanding of coronavirus infection and innate immunity. Furthermore, we extend the
118 recent characterization of PLSCR1 as an antiviral against SARS-CoV-2 impacting COVID-19
119 outcomes (**Supp Fig. 1**)[19, 25, 26].

120 Results

121 A genome-wide arrayed CRISPR KO screen identifies known and novel factors
122 influencing SARS-CoV-2 infection.

123 While the liver is not the primary target organ of SARS-CoV-2 infection, human
124 hepatocellular carcinoma Huh-7.5 cells naturally express SARS-CoV-2 dependency factors,
125 including the receptor angiotensin converting enzyme 2 (ACE2), and proved unexpectedly useful
126 in SARS-CoV-2 research [19, 27-34]. Huh-7.5 cells are defective in virus sensing and do not
127 commonly produce IFN during infection [35]. We confirmed that Huh-7.5 cells do not induce ISG
128 expression during SARS-CoV-2 infection (**Fig 1A, Supp Tables 2 and 3**). This is likely due to a defect
129 upstream of IFN production, as these cells did induce ISG expression when treated with
130 recombinant IFN (**Fig 1B, Supp Tables 4 and 5**). Thus, Huh-7.5 cells are a convenient model for
131 studying controlled IFN responses during viral infection. Furthermore, IFN treatment restricted
132 SARS-CoV-2 (**Fig 1C**), indicating that some ISGs are effective in limiting SARS-CoV-2 infection in
133 Huh-7.5 cells. This allows us to study the functional landscape of SARS-CoV-2 restriction,
134 examining both intrinsic factors and those induced in response to IFN signaling. Similar to A549-
135 ACE2 cells [11, 36], Huh-7.5 cells do not express transmembrane serine protease 2 (TMPRSS2)
136 (**Supp Fig 1B**). As a result, SARS-CoV-2 entry is restricted to the endocytic route [37, 38].
137 Using these cells, we conducted a whole-genome arrayed CRISPR KO screen designed to
138 identify both SARS-CoV-2 proviral and antiviral genes, whose KO reduces or enhances SARS-CoV-
139 2 infection, respectively. In particular, we aimed to identify factors involved in the IFN response,
140 from IFN sensing to ISG induction, including effector ISGs that directly influence the virus life
141 cycle. With this arrayed approach performed in 384-well plates, the cells in each well received a

142 pool of four gRNAs targeting a single host gene. Each well was then either treated with 1 pM IFN-
143 α2a or left untreated before being infected with SARS-CoV-2, followed by SARS-CoV-2
144 nucleoprotein (N) immunofluorescence staining and high content microscopy (**Fig 1D**). This low
145 dose of IFN was chosen to mimic a cellular environment where IFN triggers an antiviral state
146 before infection. We anticipated that a saturating amount of IFN would lead to high ISG
147 transcription and functional redundancy between effectors, biasing hits towards factors in IFN
148 signaling. In contrast, a low dose of IFN, around the IC50, might enable identification of the
149 specific roles of individual effector ISGs.

150 We conducted the functional assays four days after KO to allow sufficient time for full
151 protein depletion, considering both cell division and protein half-life (**Supp Fig 2E**).

152 We included control gRNAs with known proviral and antiviral effects in our screening
153 plates. As expected, the SARS-CoV-2 receptor angiotensin-converting enzyme 2 (ACE2) [9]
154 behaved as a proviral gene with and without IFN pretreatment. The interferon-alpha/beta
155 receptor alpha chain 1 (IFNAR1) [39-41] was essential for the IFN-mediated restriction of SARS-
156 CoV-2. The ISG15 ubiquitin-like modifier (ISG15) has been previously described as a negative
157 regulator of the IFN response. ISG15 stabilizes ubiquitin-specific peptidase 18 (USP18) [42-44],
158 which in turn binds to the interferon-alpha/beta receptor alpha chain 2 (IFNAR2) and blocks signal
159 transduction [45, 46]. Accordingly, ISG15 was proviral in IFN-treated cells (**Fig 1E**).

160 Of the 16,790 screened genes, we selected 16,178 genes where KO did not lead to changes
161 in cellular fitness, as assessed by nuclei count (-2 ≤ z-score ≤ 2) (**Supp Fig 2B**). Of these, we
162 selected 12,119 genes expressed in three cell lines relevant for SARS-CoV-2 research (A549, Calu-
163 3, Huh-7.5 cells) and human lung cells, the primary target cell type *in vivo*, for downstream
164 analysis [47-49](Supp Table 6). We then binned the genes into two groups for data visualization,
165 depending on whether they were induced by IFN-α2a treatment in Huh-7.5 cells as determined
166 by mRNA-seq (log 2 FC ≥ 2 and padj ≤ 0.05) (**Supp Fig 2C, Supp Tables 7-9**).

167 We classified 448 genes with a SARS-CoV-2 infection z-score ≥ 2 as antiviral hits and 507
168 genes with a SARS-CoV-2 infection z-score ≤ -2 as proviral hits (**Supp Table 9**).

169 Our screen found known and previously unidentified host factors influencing SARS-CoV-2
170 infection (**Fig 1F**). As expected, positive regulators of IFN signaling, such as IFNAR1,2 [39-41],

171 interferon regulatory factor 9 (IRF9) [50, 51], Janus kinase 1 (JAK1) [52], and signal transducer and
172 activator of transcription 2 (STAT2) [53, 54] were antiviral only in IFN pretreated cells. Known
173 negative regulators of IFN signaling, such as ISG15 [42-44], suppressor of cytokine signaling 1
174 (SOCS1) [55], and USP18 [45, 46] were proviral only in IFN pretreated cells.

175 The receptor ACE2 was required for infection [9]. In our mRNA-seq analysis, IFN treatment
176 was found to significantly upregulate ACE2 mRNA levels (**Supp Fig. 2C**). Prior studies indicate that
177 IFN induces transcription of a truncated ACE2 isoform, rather than the full-length receptor for
178 SARS-CoV-2 [56, 57]. The lysosomal cysteine protease cathepsin L (CTSL), required for SARS-CoV-
179 2 spike protein activation during endocytosis [58-60], was also a proviral hit in our screens (**Fig**
180 **1F**).

181 The screen data likely contains false negatives. For example, STAT1 and tyrosine kinase 2
182 (TYK2) [61, 62] did not influence infection alongside other positive regulators of IFN signaling,
183 which we attribute to the fact that some gRNAs in the library may have not efficiently directed
184 Cas9 to cut at their respective target gene loci.

185 Collectively, the identification of known proviral and antiviral factors confirms the validity
186 of our screening method.

187 We performed a Gene Set Enrichment Analysis (GSEA) to identify cellular pathways
188 exhibiting proviral or antiviral properties in our screen. The full GSEA results, including the genes
189 driving each pathway enrichment (so-called *leading edge*), can be found in **Supp Table 10**. Some
190 top pathways ranked by adjusted p-value are summarized in **Supp Fig 2D**. Notably pathways
191 associated with RNA pol II transcription and mRNA maturation, as well as pathways related to
192 cellular respiration, exhibited antiviral activity independent of IFN (**Fig 2**). Surprisingly, RNA pol III
193 transcription, in part driven by the genes RNA polymerase III subunit A (*POLR3A*) and RNA
194 polymerase III subunit B (*POLR3B*), were critical to the antiviral response mediated by IFN.
195 Conversely, factors involved in translation, such as eukaryotic translation initiation factor 3
196 subunits F and G (EIF3G and EIF3F), likely co-opted for producing viral proteins, were identified
197 as proviral. Similarly, factors regulating cholesterol homeostasis, likely crucial for SARS-CoV-2
198 entry [14, 63], were also identified as proviral. For instance, the gene sterol regulatory element
199 binding transcription factor 2 (*SREBF2*) was one of the top proviral genes (**Fig 2**).

200 Our arrayed CRISPR KO screen results constitute a valuable resource for research on
201 coronavirus infection specifically, as well as on innate immunity in general. These can be used to
202 help characterize human genes influencing SARS-CoV-2 infection and the IFN response.
203

204 The ISG PLSCR1 is associated with COVID-19 outcomes and exhibits antiviral effects 205 in functional SARS-CoV-2 genetic screens

206 To provide a thorough perspective on human genes that impact SARS-CoV-2 infection and
207 to place our arrayed CRISPR KO screen results within the context of existing research, we have
208 compiled a table that includes findings from a selection of 67 large-scale 'omic' studies related to
209 SARS-CoV-2. This compilation encompasses this study and 25 other functional genetic screens for
210 genes that influence SARS-CoV-2 infection [11-13, 15, 18, 19, 28, 31, 64-80], 24 human genetic
211 studies that correlate certain alleles with severe COVID-19 outcomes [5, 6, 8, 25, 26, 81-99], ten
212 publications detailing SARS-CoV-2 protein interactomes [100-109], six focusing on SARS-CoV-2
213 RNA interactomes [110-115], and one that examines proteins with altered phosphorylation states
214 in SARS-CoV-2-infected cells [116] **(Supp Tables 11-12 for the full, and summary tables,
215 respectively)**. This table highlights the depth of research in publications addressing SARS-CoV-2
216 infection: genes reported in several independent large-scale studies are more credible candidates
217 for biological relevance (**Supp Fig 3**). As expected, genes associated with the IFN pathway, such
218 as *IFNAR2*, *OAS1*, and *ZC3HAV1/ZAP*, frequently emerged as significant in SARS-CoV-2 studies.
219 The overlap of gene hits influencing SARS-CoV-2 between our arrayed screen and fifteen
220 published whole-genome pooled screens [19, 31, 64-67, 69-71, 74, 75, 77-80] was higher than
221 expected by chance (**Supp. Fig 4**). This finding indicates that genetic screens conducted with
222 different methods (e.g., CRISPR activation or CRISPR KO, pooled or arrayed format) and in various
223 cellular contexts (e.g., Huh-7.5, A549-ACE2, Calu-3, with or without IFN pretreatment) exhibit
224 both specificity and significant overlap. A pathway analysis of the hits from our arrayed screen,
225 alongside hits from pooled screens, is available in **Supp Table 13**.
226 We focused on 28 genes identified in both human genetic studies of COVID-19 patients
227 and in functional genetic screens in cell culture, including our own (**Fig 3**). These genes are likely
228 to have significant physiological relevance and to be well-suited for mechanistic studies in cell

229 culture. Among these, the ISG *PLSCR1* stood out, being identified as one of the most potent
230 antiviral genes in our screen (**Fig 1F**). *PLSCR1* variants have been linked to severe COVID-19 in a
231 recent GWAS (listed in **Table 1**)[25, 26]. This was attributed to a role of PLSCR1 in regulating the
232 IFN response in COVID-19 patients [26]. Indeed, a pioneering study showed that PLSCR1
233 potentiates the transcriptional response to IFN-β treatment in human ovarian carcinoma Hey1B
234 cells [24]. However, PLSCR1 surprisingly appeared as a potent SARS-CoV-2 antiviral even in the
235 absence of IFN in our screens, suggesting a cell intrinsic, IFN-independent function. In other
236 words, baseline levels of PLSCR1 may be sufficient to restrict SARS-CoV-2, and IFN pretreatment
237 could simply enhance this effect by elevating cellular PLSCR1 levels.
238

239 ### Intrinsic PLSCR1 restricts SARS-CoV-2 independently of the IFN pathway.

240 To better characterize the function of PLSCR1 during SARS-CoV-2 infection, we generated
241 and validated by western blot (WB) PLSCR1 KO bulk Huh-7.5 and A549-ACE2 lines (**Supp Fig 5A**).
242 As observed in the arrayed screen (**Supp Fig 2B**), PLSCR1 KO cells were viable (**Supp Fig 5B**).
243 PLSCR1 depletion increased susceptibility to SARS-CoV-2 independently of IFN pretreatment (**Fig**
244 **4A**). Cell treatment with a JAK-STAT inhibitor, which effectively abrogated IFN signaling, confirmed
245 that intrinsic PLSCR1 limits SARS-CoV-2 infection independently of the IFN signaling pathway (**Fig**
246 **4A**). SARS-CoV-2 susceptibility of PLSCR1 KO cells was reversed by the ectopic expression of
247 PLSCR1 (**Fig 4B, Supp Fig 5C**). Interestingly, while PLSCR1 tagged with an N-terminal FLAG tag
248 could rescue, PLSCR1 tagged with a C-terminal FLAG tag could not. The C-terminus of the protein
249 is extracellular, and previous research suggests that this region is important for the protein's
250 scramblase activity and Ca^{2+} binding [117]. It is possible that the addition of this FLAG-tag
251 impaired Ca^{2+} binding, affected PLSCR1's localization at the plasma membrane, or otherwise
252 disrupted the structure of this region, thereby abolishing PLSCR1's antiviral ability. We co-cultured
253 PLSCR1 reconstituted cells and PLSCR1 KO cells in the same well and infected them with SARS-
254 CoV-2. A higher proportion of PLSCR1 KO than PLSCR1 reconstituted cells were positive for SARS-
255 CoV-2 indicating that PLSCR1 acts in a cell autonomous manner (**Fig 4C**). Overall, our data indicate
256 that intrinsic PLSCR1 restricts SARS-CoV-2 in cell culture, even in the absence of IFN. Given that

257 PLSCR1 mRNA is constitutively expressed in SARS-CoV-2 target cells (**Supp Fig 5D**) [118], its
258 intrinsic antiviral function may also be effective *in vivo*.
259

260 ## IFN signaling is unaffected by the loss of PLSCR1 in A549-ACE2 and Huh-7.5 cells.

261 PLSCR1 has been shown to potentiate ISG transcription in IFN-treated Hey1B cells [24].
262 We thus hypothesized PLSCR1 might enhance the type I IFN response in A549-ACE2 and Huh-7.5
263 cells. We investigated PLSCR1's role in the IFN response by infecting Huh-7.5 cells with
264 chikungunya virus (CHIKV), which is unaffected by PLSCR1 KO without IFN (**Supp Fig 6A**). PLSCR1
265 depletion did not functionally affect the antiviral effects of IFN treatment (**Supp Fig 6B**).
266 Furthermore, IFN treatment induced *OAS1* and *IFI6*, two ISGs known to restrict SARS-CoV-2 [11,
267 13, 18, 95, 96, 98, 99], to a similar extent in both WT and PLSCR1 KO cells, indicating that the IFN
268 signaling pathway was unaffected by PLSCR1 depletion (**Supp Fig 6C-J**). Finally, PLSCR1 depletion
269 did not alter basal ISG transcription in the absence of IFN (**Supp Fig 7, Supp Tables 14 and 15**).
270 These findings indicate that PLSCR1 limits SARS-CoV-2 infection independently of the IFN
271 signaling pathway in A549-ACE2 and Huh-7.5 cells.
272

273 ## PLSCR1 restricts SARS-CoV-2 entry.

274 We hypothesized that PLSCR1 directly targets and inhibits a specific step of the SARS-CoV-
275 2 life cycle. PLSCR1 primarily localized at the plasma membrane in Huh-7.5 cells (**Fig 5A**).
276 Furthermore, PLSCR1 depletion led to increased SARS-CoV-2 foci formation (**Fig 5B,C**), and PLSCR1
277 KO cells did not show increased susceptibility to a SARS-CoV-2 replicon system that bypasses entry
278 (**Fig 5D**) [119]. In contrast, a single-cycle, replication-defective human immunodeficiency virus
279 type-1 (HIV-1) particles pseudo-typed with SARS-CoV-2 spike showed enhanced entry in PLSCR1
280 depleted cells (**Fig 5E, F**) [120]. This data indicates that PLSCR1 restricts SARS-CoV-2 spike-
281 mediated virion entry. Over-expression of TMPRSS2 lifted the PLSCR1-mediated restriction of
282 authentic SARS-CoV-2 (**Fig 5G-I**) and of SARS-CoV-2 spike pseudo-typed particles (**Fig 5J-M**),
283 indicating that PLSCR1 primarily restricts the endosomal entry route.
284 Other ISG products have been described to restrict SARS-CoV-2 entry (**Supp Fig 1**) [1],
285 notably: CH25H promotes cholesterol sequestration in lipid droplets, decreasing the pool of

286 accessible cholesterol required for virus-cell membrane fusion [28,29]; LY6E blocks virus-cell
287 membrane fusion via currently undetermined mechanisms [121]; nuclear receptor coactivator 7
288 (NCOA7) over-acidifies the lysosome, leading to viral antigen degradation by lysosomal proteases
289 [31,32]; and interferon induced transmembrane protein 2 (IFITM2) blocks pH- and cathepsin-
290 dependent SARS-CoV-2 virus-cell membrane fusion in the endosome [122]. The aforementioned
291 ISGs were not hits in our CRISPR KO screen for antiviral genes in IFN-treated cells. This may be
292 due to functional redundancies among them. We found that over-expression of any of the
293 aforementioned ISGs restricted SARS-CoV-2 in PLSCR1 KO cells, indicating that they do not need
294 PLSCR1 for their antiviral activity (**Supp Fig 8A**). PLSCR1 is unlikely to require CH25H, LY6E, or
295 IFITM2 for its function as these are expressed at minimal levels in Huh-7.5 cells without IFN pre-
296 treatment (**Supp Fig 8B,C, Supp Tables 4, 5, 16, and 17**). We cannot exclude an association
297 between PLSCR1 and NCOA7, although the latter was not hit in our screen.

298 In addition to SARS-CoV-2, we also evaluated the antiviral activity of PLSCR1 against ten
299 viruses that utilize endosomal entry: CHIKV, human parainfluenza virus (hPIV), herpes simplex
300 virus 1 (HSV-1), influenza A virus (IAV), human coronavirus OC43 (hCoV-OC43), human
301 coronavirus NL63 (hCoV-NL63), human coronavirus 229E (hCoV-229E), Sindbis virus (SINV),
302 Venezuelan equine encephalitis virus (VEEV), and vesicular stomatitis virus (VSV). Only SARS-CoV-
303 2 showed a notable susceptibility to PLSCR1's inhibitory effects (**Supp Fig 9**).

304 One hypothesis for PLSCR1's specificity for SARS-CoV-2 is that it alters the surface levels
305 of its receptor, ACE2. However, flow cytometry on live cells did not show a significant effect of
306 PLSCR1 on ACE2 surface levels in A549-ACE2 cells (**Supp Fig 10**). The precise mechanism of action
307 of PLSCR1 remains undetermined.

308

309 ## Recent variants of SARS-CoV-2 are less restricted by PLSCR1

310 During the COVID-19 pandemic, SARS-CoV-2 variants evolved from the initial strain,
311 showing increased immune evasion and transmissibility [123-125]. To examine if these variants
312 could circumvent the antiviral action of PLSCR1, we infected WT and PLSCR1 KO Huh-7.5 cells with
313 an early strain isolated in July 2020 (NY-RU-NY1, subsequently referred to as "parental") and the
314 Beta (B.1.352), Delta (B.1.617.2), Omicron (BA.5), and Omicron (XBB.1.5) variants. PLSCR1

315 continued to restrict these later variants when examining the percentage of infected cells 24
316 hours post-infection (**Figs 6A-E**).

317 To determine if the magnitude of PLSCR1 restriction was the same for the parental SARS-
318 CoV-2 strain and recent variants, we plotted the percentage of infection data from **Figs 6A-E** as a
319 ratio of PLSCR1 WT to KO (**Fig 6F**). Recent SARS-CoV-2 variants showed reduced differences in
320 infection rates between PLSCR1 WT and KO cells than the parental SARS-CoV-2 strain. The
321 diminished difference in sensitivity between PLSCR1 WT and KO cells was most pronounced with
322 Omicron BA.5 and its descendant, XBB.1.5 (**Fig 6F**).

323 To examine this further, we infected PLSCR1 WT and KO Huh-7.5 cells with approximately
324 50 focus-forming units (FFU) per well for different SARS-CoV-2 strains (**Figs 6G and 6H**). In line
325 with **Fig 6F,** the data indicate that the difference in virus susceptibility between PLSCR1 WT and
326 KO cells is lower for more recent variants such as Beta (B.1.352) and especially Omicron (XBB.1.5)
327 compared with the parental strain (**Fig 6H**).

328 Finally, we quantified virus production over an infectious time course for the parental
329 SARS-CoV-2 strain versus Omicron (XBB.1.5) in Huh-7.5 PLSCR1 WT and KO cells (**Figs 6I and J**). As
330 expected, parental SARS-CoV-2 replicated with faster kinetics upon PLSCR1 depletion. In contrast,
331 Omicron (XBB.1.5) replication was not affected by PLSCR1 depletion. Our data suggest that
332 PLSCR1 restricts newer SARS-CoV-2 variants less efficiently in Huh-7.5 cells. This could be due to
333 adaptation of the recent variants to directly antagonize PLSCR1 and/or utilize an alternative entry
334 route in Huh-7.5 cells that is TMPRSS2-independent and invulnerable to PLSCR1.

335

336 Association between PLSCR1 variants and severe COVID-19

337 PLSCR1 encodes a 318 amino acid protein containing a palmitoylation motif and a
338 transmembrane domain which regulate its plasma membrane localization, and a nuclear
339 localization signal (NLS) and transcriptional activation domain thought to be important for its
340 nuclear functions (**Fig 7A**)[22, 126-131].

341 A recent GWAS has identified an association between PLSCR1 variants and severe COVID-
342 19 outcomes, reporting an odds ratio of approximately 1.2 and a p-value of approximately 10^{-8}

343 (**Table 1**)[25, 26]. In other words, the GWAS suggests that PLSCR1 has a small, but significant effect
344 on severe COVID-19 risks.

345 GWAS typically identify variants associated with increased odds of a disease, but these
346 variants are not necessarily causative. Among the PLSCR1 variants identified in the COVID-19
347 GWAS cited above, only p.His262Tyr (rs343320) results in a protein-coding change, located in the
348 NLS (**Fig 7A**, **Table 1**). This raises the hypothesis that p.His262Tyr might alter PLSCR1's antiviral
349 function. However, we cannot dismiss the possibility that (i) some non-coding variants identified
350 in the GWAS could influence the regulation of PLSCR1 mRNA, potentially leading to functional
351 outcomes, and (ii) the GWAS might have missed other nonsynonymous variants besides
352 p.His262Tyr that could potentially impact PLSCR1 function.

353 To assess the relative importance of the p.His262Tyr variant in humans, we examined the
354 full collection of PLSCR1 variants reported in gnomAD, a human population reference database
355 (**Fig. 7B**) [132, 133]. The p.His262Tyr variant is the most common nonsynonymous variant in this
356 gene, with a minor allele frequency (MAF) of 0.07, MAFmax of 0.1, and 4,348 homozygous
357 individuals in gnomAD. Another variant, resulting in a frameshift mutation, p.Ile110fs
358 (rs749938276), is the most common predicted loss-of-function (pLOF) of PLSCR1 in gnomAD (MAF
359 of 0.0003, MAFmax of 0.01, 1 homozygous individual), indicating that PLSCR1 is not essential.

360 We aimed to investigate the functional effects of the p.His262Tyr and p.Ile110fs variants
361 in cell culture, along with two other relatively common nonsynonymous variants, p.Gly20Val
362 (rs79551579, MAF of 0.002, MAFmax of 0.04) and p.Ala29Thr (rs41267859, MAF of 0.01, MAFmax
363 of 0.04). For this, we stably and ectopically expressed the PLSCR1 variants of interest in PLSCR1
364 KO A549-ACE2 cells using a lentiviral vector [134]. The variant p.Ile110fs did not rescue PLSCR1
365 KO, confirming it as a loss-of-function mutation (**Fig 7C**). The p.His262Tyr variant, expressed at
366 similar levels to WT PLSCR1 in this system (**Supp Fig. 11A**), behaved as a hypomorphic allele,
367 providing only partial rescue of PLSCR1 antiviral function (**Figs. 7C and D**). Additionally,
368 introducing PLSCR1 p.His262Tyr into PLSCR1 WT A549-ACE2 cells increased their susceptibility to
369 SARS-CoV-2 infection (**Fig 7D**), suggesting a dominant effect. However, this effect might be
370 attributed to the overexpression of PLSCR1 p.His262Tyr from the transgene, compared to the
371 natural expression levels of PLSCR1 WT from the endogenous locus. To counter this, we examined

372 patient-derived SV40-immortalized fibroblasts expressing ACE2 that were heterozygous for
373 p.His262Tyr. These cells were already present in our collection, originating from a female
374 tuberculosis patient from Turkey (JL0192) and a female herpes simplex encephalitis patient from
375 France (JL0480). The origin of these cells is serendipitous; our goal was not to link these diseases
376 to PLSCR1 but rather to infect cells carrying the His262Tyr variant with SARS-CoV-2. Cells
377 heterozygous for p.His262Tyr were hyper-susceptible to SARS-CoV-2 infection compared to
378 PLSCR1 WT control SV40-fibroblasts (**Fig 7E**), further suggesting that p.His262Tyr is dominant. We
379 cannot formally rule out that the examined SV40-fibroblasts may carry other mutations
380 influencing SARS-CoV-2 infection.

381 Since the p.His262Tyr mutation is located in the NLS region, we hypothesized that it could
382 impair PLSCR1's nuclear localization. However, PLSCR1 WT was primarily localized in the
383 cytoplasm in untreated A549-ACE2 cells (**Fig 5A**), in IFN-treated cells (**Supp Fig 11B**), and in SARS-
384 CoV-2 infected cells (**Supp Fig 11C**). Similarly, PLSCR1 His262Tyr was also enriched in the
385 cytoplasm (**Supp Fig 12**). This suggests that the palmitoylation motif, known to be dominant over
386 the NLS [129], dictates the cytoplasmic localization of PLSCR1. Therefore, we propose that the
387 p.His262Tyr mutation affects PLSCR1 through a mechanism other than altering its nuclear
388 localization.

389 Our data collectively highlight PLSCR1's function in restricting SARS-CoV-2 entry in cell
390 culture, thereby clarifying the association between PLSCR1 variants and severe COVID-19
391 outcomes [25, 26]. Future human genetic studies are crucial for determining if certain PLSCR1
392 variants in the population cause increased risks of severe COVID-19. Our results highlight the
393 variant p.His262Tyr as a potential causative candidate, as it caused increased SARS-CoV-2
394 infection in cell culture.

395 Discussion

396 Here, we conducted an unbiased arrayed CRISPR KO screen on Huh-7.5 cells infected with
397 SARS-CoV-2. The screen revealed novel aspects of SARS-CoV-2 and IFN biology while also
398 confirming previously known facets. Pathways related to mRNA transcription and maturation
399 were identified as antiviral. This observation may stem from the conflict between the host cell

400 and SARS-CoV-2, where the host attempts to export mRNAs from the nucleus to facilitate antiviral
401 responses while the virus replicates in the cytoplasm, impeding nuclear export [135-138]. RNA
402 Pol III transcription was specifically essential for the IFN-mediated antiviral response, through
403 mechanisms that are yet to be determined. Interestingly, inborn errors in POLR3A and POLR3C
404 have been previously described in patients with severe varicella zoster virus infections [139].
405 Cellular respiration was identified as a key IFN-independent antiviral pathway. Furthermore,
406 mitophagy was identified as proviral. This may indicate the infected cell's increased demand for
407 energy and ATP to combat the virus. Alternatively, cellular respiration may have other, yet-to-be-
408 identified, IFN-independent antiviral roles. Conversely, translation and cholesterol homeostasis
409 emerged as the foremost proviral pathways. These findings underscore the complex, dualistic
410 nature of the interactions between SARS-CoV-2 and host cells.

411 Our screen notably identified the ISG zinc-finger antiviral protein (*ZC3HAV1*/*ZAP*) as a
412 proviral factor in IFN-treated cells. Initially, ZC3HAV1/ZAP gained attention as an antiviral factor
413 that targets the SARS-CoV-2 RNA genome [115] and prevents programmed ribosomal
414 frameshifting [140]. Yet, a recent study demonstrated that ZC3HAV1/ZAP also promotes the
415 formation of SARS-CoV-2 non-structural proteins 3 and 4-induced double-membrane vesicles,
416 essential for virus replication [72]. SARS-CoV-2 may have adapted to exploit certain ISG products,
417 such as ZC3HAV1/ZAP, within the cellular environment it encounters. It is still unclear if the
418 seemingly contradictory roles of ZC3HAV1/ZAP – both proviral and antiviral – are caused by
419 distinct isoforms.

420 Many other ISG products influenced SARS-CoV-2 infection, PLSCR1 being the most potent
421 restriction factor. PLSCR1 did not influence ISG induction as previously reported [24], but rather
422 inhibited spike-mediated SARS-CoV-2 entry through the endocytic route. Our results corroborate
423 a recent study from Xu et al [19] and provide an explanation for the enrichment for PLSCR1 SNPs
424 observed in a GWAS on severe COVID-19 [25, 26].

425 The molecular mechanisms of PLSCR1-mediated restriction of SARS-CoV-2 entry remain
426 to be elucidated. PLSCR1 could be altering the lipid composition at the contact site between the
427 virus and endosomal membranes, akin to the ISG interferon induced transmembrane protein 3
428 (IFITM3) for influenza A virus [141-144]. PLSCR1 was first identified as a Ca^{2+}-dependent

429 phospholipid scramblase [23], but it is unclear whether PLSCR1 depletion affects the bidirectional
430 movement of phospholipids *in vivo* [145-147]. A C-terminal FLAG-tag abolished the antiviral
431 ability of reconstituted PLSCR1, possibly by interfering with the function of the Ca^{2+} binding
432 domain. In contrast, inhibiting PLSCR1's phospholipid scramblase activity did not alleviate SARS-
433 CoV-2 restriction [19].

434 PLSCR1 is one of a few ISGs known to restrict SARS-CoV-2 entry (**Supp Fig 1A**)[1, 148], with
435 possibly more yet to be discovered. Future research should investigate the associations and
436 combinatorial effects between antiviral ISGs, which could lead to key mechanistic insights into
437 their mode of action.

438 Intriguingly, PLSCR1 specifically restricted SARS-CoV-2 in Huh-7.5 and A549-ACE2 cells but
439 it did not show similar inhibitory effects on other viruses that enter cells via endocytosis. Future
440 studies will investigate the mechanisms behind this specificity. PLSCR1 has been described to
441 inhibit a range of viruses in various cell lines, such as encephalomyocarditis virus, vesicular
442 stomatitis virus, Epstein-Barr virus, hepatitis B virus, hepatitis C virus, human cytomegalovirus,
443 human immunodeficiency virus 1, human T-cell lymphotropic virus type 1, and influenza A virus
444 [24, 149-155]. It has been proposed that PLSCR1 directly binds viral proteins and impairs their
445 functions to restrict the non-coronaviruses cited above, reviewed in [156]. However, it seems
446 unlikely that PLSCR1 has evolved to interact directly with such a diverse set of viral proteins. An
447 alternative explanation is that diverse viral proteins convergently evolved to bind PLSCR1 as a
448 mechanism of immune evasion. For example, by altering PLSCR1's subcellular localization.
449 Meanwhile, overexpressing PLSCR1 in cell culture could act *like a sponge*, absorbing these viral
450 proteins and thereby hindering viral function. We searched for PLSCR1 interactions in ten SARS-
451 CoV-2 proteins interactome studies, relying on ectopic expression of individual viral proteins [100-
452 102, 104-109, 157], and no interaction was reported in two or more independent studies. Two
453 interactions were reported in a single study: (i) PLSCR1-ORF7b [102], and (ii) PLSCR1-ORF8 [105],
454 both by proximity biotinylation, which was less stringent compared to affinity purification-mass
455 spectrometry (AP-MS) and yeast two-hybrid (Y2H) techniques (**Supp Fig 13**). To date, there is no
456 strong evidence of a direct interaction between a SARS-CoV-2 protein and PLSCR1, although we

457 cannot rule out that such interactions may occur or even appear in the future as SARS-CoV-2
458 evolves.

459 Previous research suggests that Omicron has developed increased resistance to IFN [158,
460 159], a trait associated with its highly-mutated spike protein [160]. Here, we show that recent
461 SARS-CoV-2 variants, including Omicron BA.5 and XBB.1.5, exhibit reduced sensitivity to PLSCR1-
462 mediated restriction compared to the New York 2020 strain, which served as a reference in our
463 study (**Fig 6**). Evasion from PLSCR1 may thus have contributed to Omicron's increased resistance
464 to IFN.

465 The original SARS-CoV-2 strain can enter cells through both TMPRSS2-dependent fusion
466 near the cell surface and clathrin-mediated endocytosis, with a preference for the former *in vivo*
467 [38]. ISGs that primarily restrict SARS-CoV-2 endocytosis, such as NCOA7, which perturbs
468 lysosome acidification [161, 162], and PLSCR1, may play a role in constraining the original strain
469 to TMPRSS2-dependent entry. Interestingly, the more recent Omicron variant shows both
470 increased evasion from PLSCR1 restriction **(Fig 6)** and an acquired preference for TMPRSS2-
471 independent entry. This occurs either via endocytosis or TMPRSS2-independent fusion near the
472 cell surface, utilizing metalloproteases to cleave the spike protein [160, 163, 164]. We postulate
473 that Omicron evolved its entry pathway to evade PLSCR1-mediated restriction while shifting its
474 cell tropism to the upper airways and away from TMPRSS2-expressing cells [163, 165-169].

475 Future research should investigate: (i) mechanism(s) by which Omicron evades PLSCR1
476 restriction and whether this evasion is primarily due to mutations in the spike protein, (ii) the
477 association between PLSCR1-mediated restriction and the distinct entry mechanisms utilized by
478 SARS-CoV-2 variants, (iii) how various intrinsic factors that restrict virus entry, such as PLSCR1,
479 have influenced SARS-CoV-2 entry routes, evolution, and cell tropism. Understanding these
480 aspects of PLSCR1 restriction could provide mechanistic insight into broad strategies of PLSCR1
481 evasion employed by both newer SARS-CoV-2 variants as well as viruses from other families that
482 were unaffected by PLSCR1 KO. Subversion of PLSCR1 restriction may serve as a useful immune
483 evasion strategy that could be shared by diverse viruses with longer evolutionary selection than
484 SARS-CoV-2.

485 Several PLSCR1 variants were enriched in a GWAS on severe COVID-19, with a relatively
486 low odds ratio of approximately 1.2 [25, 26]. This modest odds ratio likely reflects the complex
487 redundancies within antiviral defenses, from innate immunity featuring multiple effector ISGs
488 that restrict SARS-CoV-2 [10-15, 18, 19], to adaptive immunity [170]. For example, we show that
489 the ISGs CH25H [28,29], IFITM2 [122], LY6E [121], and NCOA7 [31,32] still function to restrict
490 SARS-CoV-2 in PLSCR1-depleted cells (**Supp Fig 8**). However, for these very reasons, the
491 identification of PLSCR1 variants in the GWAS remains noteworthy. Of these enriched variants,
492 only PLSCR1 p.His262Tyr (rs343320) resulted in a protein-coding change. Our findings indicate
493 that p.His262Tyr exhibits a hypomorphic and dominant effect in cell culture, leading to increased
494 SARS-CoV-2 infection. Future research should aim to ascertain whether p.His262Tyr, or potentially
495 other PLSCR1 variants, are directly responsible for elevated risks of severe COVID-19 in patients.
496 Our findings show that baseline levels of PLSCR1 are effective in limiting SARS-CoV-2
497 infection. This is in line with other studies where ISGs like *DAXX* and *LY6E* were shown to inhibit
498 SARS-CoV-2 independently of IFN [18, 121, 171]. mRNA-seq analyses of Huh-7.5 cells and primary
499 human hepatocytes, as well as data from the GTEx consortium on various human tissues [49,
500 172], revealed that many ISGs are constitutively expressed, even without IFN stimulation (**Supp**
501 **Fig 14**). This supports the idea that the IFN-induced antiviral state results more from enhanced
502 expression of antiviral genes rather than a binary ON/OFF switch. In future studies, it will be
503 interesting to explore whether intrinsically expressed ISGs also carry out cellular functions beyond
504 pathogen defense.
505

506 # Materials and Methods

507 ## Plasmids, oligos, and primers

508 The plasmids, gene fragments, and primers used in this study are listed in **Supp Tables 18,**
509 **19, and 20**, respectively.
510

511 ## Cell Lines

512 Huh-7.5 (human hepatocellular carcinoma; *H. sapiens*; sex: male) [173], Huh-7.5-Cas9
513 [31], A549-ACE2 (human lung carcinoma; *H. sapiens*; sex: male; generously provided by the
514 laboratory of Brad R. Rosenberg) [11], A549-ACE2-TMPRSS2 [31], Lenti-X 293T (*H. sapiens*; sex:
515 female: Takara, cat. #632180), Caco2 (*H. sapiens*; sex: male; ATCC, cat. HTB-37), Vero E6
516 (*Chlorocebus sabaeus*; sex: female; kidney epithelial cells, ATCC cat. #CRL-1586), BHK-21
517 (*Mesocricetus auratus*; sex: unspecified; kidney fibroblasts) cells, and SV40-Fibroblasts were
518 cultured in Dulbecco's Modified Eagle Medium (DMEM, Fisher Scientific, cat. #11995065)
519 supplemented with 0.1 mM nonessential amino acids (NEAA, Fisher Scientific, cat. #11140076)
520 and 10% fetal bovine serum (FBS, HyClone Laboratories, Lot. #KTH31760) at 37°C and 5% CO2. All
521 cell lines tested negative for mycoplasma.

522

523 ## Virus stocks

524 **CHIKV-181/25-mKate2:** the infectious clone was a kind gift from Mark Heise (University
525 of North Carolina, USA) [not published yet]. 20 µg of infectious clone DNA was linearized with
526 NotI-HF at 37°C overnight. Complete digestion was confirmed by running a sample of the digested
527 DNA on a 1% agarose gel. After confirmation, linearized DNA was cleaned via phenol-chloroform
528 extraction, and then ethanol precipitated. The precipitated DNA was resuspended in 20 µL of
529 RNase-free H_2O and in vitro transcribed with an SP6 mMessage mMachine In Vitro Transcription
530 Kit (ThermoFisher, cat. AM1340). The generated RNA was electroporated into 1.2 x 10^7 BHK-21
531 cells, and the produced virus was harvested once approximately 80% of the electroporated cells
532 lifted or showed signs of cytopathic effects and 100% of the cells were positive for mKate2 signal.
533 The titer of the virus was 8.5 x 10^6 focus-forming units (FFU) on Huh-7.5 cells.

534 **hCoV-NL63:** was generously provided by Volker Thiel (University of Bern) and amplified at
535 33°C in Huh-7.5 cells as in [31].

536 **hCoV-OC43**: was obtained from ZeptoMetrix (cat. #0810024CF) and amplified at 33°C in
537 Huh-7.5 cells as in [31].

538 **hPIV3-GFP** [174]: stock (based on strain JS) grown in VeroE6 cells as in [175].

539 **HSV-1-GFP**: stock made by passage on VeroE6 cells. 2 x 10^7 cells seeded in a T175 flask
540 were infected at an MOI of 0.01 PFU/ml of HSV-1-GFP virus engineered and provided by Ian Mohr
541 [176]. After a one-hour incubation at 37°C, the inoculum was removed, and 20 ml of DMEM
542 supplemented to contain 10% FBS and NEAA was added. Cells were incubated at 37°C for 24 h or
543 until CPE was evident. Cell supernatant containing progeny virus was harvested and titrated on
544 Vero E6 cells (2.4% avicel, fix 2 dpi) at 2.4 x 10^8 PFU/ml.

545 **IAV WSN (H1N1):** was generated in MDCK cells. Cells were inoculated at MOI 0.01 in
546 DMEM supplemented with NEAA, 0.2% BSA, 0.1% FCS, 50 mM Hepes, and 1 µg/ml TPCK-trypsin.
547 Virus-containing culture supernatant was harvested at 52 h post-infection and cleared by
548 centrifugation.

549 **SARS-CoV-2:** unless otherwise stated, the isolate SARS-CoV-2/human/USA/NY-RU-
550 NY1/2020 was used in this study [177]. The virus was sourced from the saliva of a deidentified
551 patient in New York City, collected on July 28, 2020. Its sequence is publicly accessible (GenBank
552 OM345241). The virus isolate was amplified in Caco-2 cells. The passage 3 stock employed had a
553 titer of 3.4 × 10^6 PFU/ml, as measured on Vero E6 cells using a 1% methylcellulose overlay,
554 according to previously described methods [178]. The Beta (B.1.351), Delta (B.1.617.2), Omicron
555 BA.5, and Omicron XBB.1.5 variants were obtained from BEI resources (cat. # NR-54008, NR-
556 55611, NR-58616, and NR-59104, respectively), amplified in Vero E6 cells engineered to stably
557 express TMPRSS2, and titer was determined as described above.

558 **SINV Toto1101** [179]: expressing an nsP3-mScarletI fusion reporter was generated by
559 cloning the sequence encoding mScarletI in frame into a unique SpeI restriction site in the
560 pToto1101 infectious clone plasmid as previously described [180]. *In vitro* transcribed, capped
561 RNA was generated from the pToto1101-nsP3-mScarletI plasmid (Invitrogen mMessage
562 mMachine SP6 kit, AM1340) and electroporated into BHK-J cells, a derivative of BHK-21 cells
563 (ATCC, CCL-10) as previously described [180]. 24 hours post electroporation, centrifuge clarified
564 supernatants were aliquoted and stored at -80C. BHK-J cells were cultured and virus stocks
565 generated in MEM supplemented with 7.5% FBS.

566 **VEEV-dsEGFP** [16, 181]: the infectious clone plasmid was linearized (MluI) and transcribed
567 *in vitro* using an mMessage mMachine SP6 transcription kit (Ambion). BHK-21 cells were

568 electroporated with viral RNA, and supernatant containing progeny virus was harvested after
569 incubation at 37°C for 30 h or until CPE was evident. Virus was titrated by plaque assay on BHK-
570 21 cells (2.4% avicel, fix 2 dpi). BHK-21: 1.45 x 10^9 FPU/ml.
571 **VSV-GFP** [182]: grown in BHK-21 cells as in [175].
572 **YFV 17D:** was generated via transfection of Huh-7.5 with in vitro transcribed RNA from
573 pACNR-FLYF-17D plasmid as described in [175].
574

575 ## mRNA-seq

576 ### mRNA-seq on SARS-CoV-2-infected cells

577 **Cell culture and infection:** 75,500 Huh-7.5 cells or 150,000 Calu-3 cells were seeded in
578 each well of a 12-well plate with 1 mL media. Media: DMEM with 5% FBS and 1% NEAA for Huh-
579 7.5 cells or EMEM (ATCC, 30-2003) with 10% FBS for Calu-3 cells. The next day, cells were infected
580 by removing 500 µL of media and adding 500 µL of media with SARS-CoV-2 strain USA-WA1/2020
581 (BEI Resources, NR-52281) at 5,000 PFU/well (virus titer determined in Huh-7.5 cells). After one
582 day, the wells were washed with PBS and cells were harvested in 1 mL TRIzol (Invitrogen, cat.
583 15596-018). N = 3 replicates (separate wells) per sample.
584 **RNA extraction:** 2 ml MaXtract High Density tubes (Qiagen, 129056) were centrifugated
585 at 12,000–16,000 x g for 20-30 second centrifugation. A volume of 750 µL TRIzol-prepared sample
586 was combined with 150 µL chloroform in these tubes and hand-shaken vigorously. Phase
587 separation was accomplished by centrifugation at 1500 x g for 5 min at 4°C. The aqueous phase
588 was then mixed with 400 µL ethanol 95-100% in a separate tube. These preparations were then
589 transferred to Zymo Research RNA clean and concentrator-25 kit columns (Zymo Research, cat.
590 R1018) and subjected to multiple wash and centrifugation steps as recommended by the
591 manufacturer. An in-column DNase I treatment was performed using Qiagen DNase (Qiagen,
592 79254). Finally, RNA was eluted with 50 µL DNase/RNase-Free water and stored at -80°C.
593 **Sequencing:** Poly-A enriched libraries were made using the TruSeq stranded mRNA LT kit
594 (Illumina, Cat# 20020594) and sequenced on a NovaSeq SP with PE150 read length.
595

596 mRNA-seq on IFN-treated cells

597 **Cell culture and treatment: A549 cells**: 300,000 cells were seeded in each well of a 6-well
598 plate with 3 mL of DMEM supplemented with 10% FBS and 1% NEAA. The following day, the media
599 was aspirated and replaced with 2 mL of DMEM with or without 0.5 nM IFN-α2a (PBL, cat. 11101-
600 2), and the cells were incubated at 37°C. After 24 hours, the cells were harvested in 500 µL TRIzol.
601 N = 3 replicates (separate wells treated on the same day) per sample. **Calu-3 cells**: 200,000 cells
602 were seeded in each well of a 12-well plate with 1 mL media. Two days later, the media was
603 replaced with EMEM (ATCC, cat. 30-2003) with 10% FBS with 0.5 IFN-α2a (PBL, cat. 11101-2) and
604 incubated at 37ºC. 24 h later, cells were harvested in 500 µL TRIzol. N = 3 replicates (separate
605 wells treated on the same day) per sample. **Huh-7.5 cells**: 75,500 cells were seeded in each well
606 of a 12-well plate with 1 mL media. Two days later, the media was replaced with 1 mL of DMEM
607 with 5%FBS, 1% NEAA with 0.5 nM IFN-α2a (PBL, cat. 11101-2) and incubated at 37ºC. 24 h later,
608 cells were harvested in 500 µL TRIzol. N = 3 replicates (separate wells treated on the same day)
609 per sample.

610 **RNA extraction** as described above.

611 **Sequencing:** Poly A-enriched libraries were made using the NEBNext Ultra II RNA Library
612 Prep Kit for Illumina (NEB, cat. E7770) and sequenced on a NovaSeq SP with PE150 read length.

613

614 mRNA-seq on PLSCR1 KO cells

615 **Cell culture and CRISPR KO:** 30,000 Huh-7.5 cells were seeded in five wells of a 24-well
616 plate with 480 uL media. The cells were reverse transfected with 120 uL of a transfection mixture
617 composed of 250 nM of pooled anti-PLSCR1 or non-targeting Edit-R crRNAs from Horizon
618 Discovery (cat. CM-003729-01-0002, CM-003729-02-0002, CM-003729-03-0002, and CM-
619 003729-04-0002 or U-007501-01-05, U-007502-01-05, U-007503-01-05, and U-007504-01-05,
620 respectively) which had been resuspended with an equimolar amount of Edit-R tracrRNA
621 (Horizon, cat. U-002005-20) and a 1:200 dilution of Dharmafect 4 (Horizon, cat. T-2004-01). The
622 following day, the media was changed, and the cells were progressively scaled up to a 6-well plate
623 over the next 4 days. When the cells were confluent in the 6-well plate, the media was removed
624 from four of the wells. They were then washed with 1x PBS (cat. 14190-144) and lysed with 1 mL

625 TRIzol (Life Technologies, cat. 15596-018) for 5 minutes at room temperature before transferring
626 to an Eppendorf tube and freezing at -80°C to await RNA extraction. The remaining well was lysed
627 with 300 µL of RIPA buffer (Thermo cat. 89900) supplemented with 1x protease inhibitor (Thermo
628 cat. 87786) and 1x EDTA and prepared for western blot as described below, in the "Western Blots"
629 section.

630 **RNA extraction** as described above.

631 **Sequencing:** Poly A-enriched libraries were made using the NEBNext Ultra II RNA Library
632 Prep Kit for Illumina (NEB, cat. E7770) and sequenced on a NovaSeq SP with PE150 read length.

633

634 ### mRNA-seq analysis

635 mRNA-seq reads were first quality-filtered and adapter-trimmed using Trim Galore with
636 parameters -q 20 -e 0.1 --length 20 --paired and Cutadapt. Reads were then mapped to the human
637 genome GRCh38 or to a combined SARS-CoV-2 MN985325.1/human genome GRCh38 using STAR
638 [183] with settings including --runThreadN 8 --outFilterMultimapNmax 1 --twopassMode Basic.
639 Feature counting was performed using the featureCounts function from the Rsubread package
640 [184], with strandness specified depending on the sequencing and other parameters as default.
641 The resulting counts were imported into a DESeqDataSet object using the DESeq2 package [185]
642 with a design formula of ~Group. Size factors were estimated and normalized counts were
643 extracted and saved. Differential expression analysis was performed using DESeq with the created
644 DESeqDataSet object, contrasted by sample groups, cooksCutoff and independentFiltering
645 disabled, and otherwise default parameters.

646

647 ### TMPRSS2 western blot

648 Cell lysates were prepared in RIPA buffer (150 mM NaCl, 1% NP-40, 0.5% DOC, 0.1% SDS,
649 50 mM Tris-HCl [pH 7.4] with addition of Halt™ Protease and Phosphatase Inhibitor Cocktail
650 [ThermoFisher: 78440]) and incubated on ice for 30 min. Lysates were clarified by centrifugation
651 at 16,000 x g for 10 min at 4°C. Protein concentration was determined by bicinchoninic (BCA)
652 protein assay (Pierce BCA Protein Assay Kit, ThermoFisher Scientific: 23227) and samples were
653 resolved on NuPAGE 4%–12% Bis-Tris gels (Invitrogen) followed by transfer onto 0.4 µm

654 nitrocellulose membranes. Membranes were incubated in blocking buffer (TBS + 5% milk) and
655 incubated with primary antibody prepared in blocking buffer with 0.1% Tween-20. Membranes
656 were washed 3X with TBS + 0.1% Tween-20 and incubated with LI-COR (Lincoln, NE, USA) IRDye®
657 680RD or IRDye® 800CW secondary antibodies. Membranes were imaged using an Azure (Dublin,
658 CA, USA) 600 imaging system.
659

660 ## Unbiased arrayed CRISPR KO screening

661 ### Screen overview

662 The content of each gRNA 384-well plate constituting the whole-genome library (61
663 library plates total) was transfected to 16 assay 384-well plates (976 assay plates total). Positive
664 and negative control gene gRNAs were incorporated into vacant wells of each assay plate as
665 described below. Huh-7.5-Cas9 cells were subsequently seeded into these assay plates. The 16
666 assay plates served as replicates for three distinct experimental conditions: 4 replicates for mock
667 treatment followed by mock infection, 5 replicates for IFN-α2a treatment followed by SARS-CoV-
668 2 infection, and 7 replicates for mock treatment followed by SARS-CoV-2 infection. Each day, three
669 library 384-well plates were processed, along with their corresponding 48 assay plates. The full
670 gRNA library, distributed across 61 384-well plates, was completed over a span of 21 days. For
671 each set of plates, cell seeding was conducted on day 0, IFN-α2a treatment on day 4, SARS-CoV-
672 2 infection on day 5, and cell fixation on day 6.

673 ### gRNA library preparation

674 A 0.1 nmol Edit-R Human Whole Genome crRNA Library (Horizon, cat. GP-005005-01)
675 containing four crRNAs per gene and one gene per well (total 0.1 nmol crRNA/well) was
676 resuspended in 80 µL of a 1.25 µM tracrRNA (Horizon, cat. U-002005-1000) 10 mM Tris-HCL pH
677 7.4 solution to create a 1.25 µM gRNA solution. The library was then aliquoted in 10 mM Tris-HCL
678 pH 7.4 in several 96-well plate and 384-well plate copies using a Tecan Freedom EVO liquid
679 handler. A single-use library copy containing a 40 µL/well of a 312.5 nM gRNA solution in the 384-
680 well plate format was used in this study.

681 gRNA reverse transfection (day 0)

682 In each well of the 384-well assay plates, 40 µL of a transfection solution was prepared by
683 combining 2% DharmaFect-4 transfection reagent (Horizon, cat. GP-T-2004-07A) in Opti-MEM
684 (Gibco, cat. 31985070). This was added to 40 µL of a 312.5 nM gRNA library using a Thermofisher
685 Multidrop Reagent Dispenser, yielding an 80 µL/well transfection mixture. The mixture was left
686 to incubate at room temperature for 20 minutes. Simultaneously, assay plates were preloaded
687 with 11 µL/well of serum-free media, which was formulated from DMEM, 1X Antibiotic-
688 Antimycotic solution (Gibco, cat. 15240-062), and 1X NEAA, dispensed via a Thermofisher
689 Multidrop Reagent Dispenser. Subsequently, 4 µL/well of the transfection mixture was dispensed
690 into each of the assay plates (16 assay plates per library plate) using a Tecan Freedom EVO liquid
691 handler. During this time, Huh-7.5 cells were prepared in media containing 25% FBS, 1X Antibiotic-
692 Antimycotic solution, and 1X NEAA. A volume of 10 µL cells/well was added to the assay plates,
693 again using a Thermofisher Multidrop Reagent Dispenser. Ultimately, each well contained 1,250
694 cells in a 25 µL final volume, with a composition of 25 nM gRNA, 10% FBS, 0.8X Antibiotic-
695 Antimycotic, and 0.8X NEAA. Plates were then span at 200 g for 5 minutes. To minimize
696 evaporation, plates were sealed with Breathe-Easy sealing membranes (Sigma-Aldrich, cat.
697 Z380059) and placed in humid chambers constructed from a 245 mm x 245 mm dish containing
698 a paper towel moistened with 15 mL of 1X Antibiotic-Antimycotic solution. Four assay plates were
699 placed in each humid chamber and incubated at 37°C.

700 IFN-α2a treatment (day 1)

701 Each well received 5 µL of IFN-α2a (PBL, cat. 11101-2) in media (DMEM, 20% FBS, 1X
702 Antibiotic-Antimycotic solution, 1X NEAA), using a Thermofisher Multidrop Reagent Dispenser,
703 for a final concentration of 1 pM IFN-α2a in a final volume of 30 µL. Plates were then span at 200
704 g for 5 minutes and incubated at 37°C.

705 SARS-CoV-2 infection (day 5)

706 Each well received 212.5 PFU SARS-CoV-2 virus (titer determined on Vero E6 cells, see
707 Virus Stocks section above) diluted in 5 µL of media (DMEM, 20% FBS, 1X Antibiotic-Antimycotic
708 solution, 1X NEAA) for a final volume of 35 µL in the BSL3. Plates were then span at 200 g for 5
709 minutes and incubated at 37°C.

710 Fixing (day 6)

711 Each well received 50 µL of 20% neutral buffered formalin (Azer Scientific, cat. 20NBF-4-
712 G) and plates were incubated overnight. The formalin mixture was then removed and each well
713 received 50 µL of PBS.

714 IF staining

715 For IF staining of SARS-CoV-2 infected cells in the arrayed CRISPR KO screen (**Figs 1D-F)**, as
716 well as some focused experiments (**Fig 4**, **Fig 5G-I**, **Figs 7 C and E**, **Supp Fig 8**, **Supp Fig 9F**): the
717 following solutions were prepared for both 96-well plate (96-wp) and 384-well plate (384-wp):
718 PBS (Phosphate Buffered Saline), Perm Solution: Comprised of PBS with an added concentration
719 of 0.1% Triton X100, Blocking Solution: PBS was mixed with 1% BSA. This solution was prepared a
720 day in advance and filtered before use, PBST: PBS with 0.1% of Tween 20, Primary Antibody
721 Solution: Genetex anti SARS-CoV-2 N poly rabbit antibody (GTX135357) at a dilution of 1:3000,
722 Secondary Antibody Solution: AF647 anti-rabbit antibodies at a dilution of 1:3000 and Hoechst
723 33342 (10 mg/ml) at 1:10,000. Plates were stained on a Biotek EL406 Microplate Washer
724 Dispenser using the following steps: 1. Priming: The washer was primed with 200 ml of each
725 buffer: PBS, Perm Solution, Blocking Solution, and PBST. 2. First Washing Phase: Contents of the
726 plates were aspirated. Plates were then washed with 50 µL/well (384-wp) or 200 µL/well (96-wp)
727 of Perm Solution, followed by a slow shake for 3 seconds. 3. Permeabilization: A delay of
728 approximately 1 minute was implemented for permeabilization, in addition to the time required
729 to process all the plates (around 1 minute per plate). 4. Second Washing Phase: Plates were
730 washed with 50 µL/well (384-wp) or 200 µL/well (96-wp) of PBS. Subsequently, 50 µL/well (384-
731 wp) or 200 µL/well (96-wp) of Blocking Solution was added to the plates, followed by a slow shake
732 for 3 seconds. 5. Blocking, autoclean, and Primary Antibody Priming: The washer was set to
733 undergo an autoclean cycle with PBS for 30 minutes. Simultaneously, the syringe containing the
734 Primary Antibody Solution was primed with 16 ml. 6. Third Washing Phase and First Antibody
735 Dispensing: After aspirating the contents of the plates, 15 µL/well (384-wp) or 60 µL/well (96-wp)
736 from the Primary Antibody Solution was added, followed by a slow shake for 3 seconds. 7. Primary
737 Antibody Incubation, autoclean, and Secondary Antibody Priming: The washer was subjected to
738 another autoclean cycle using PBS for 2 hours and 5 minutes. The syringe containing the

Secondary Antibody Solution was primed with 16 ml during this period. 8. Fourth Washing Phase and Second Antibody Dispensing: Plates were washed with 50 µL/well (384-wp) or 200 µL/well (96-wp) of PBST, followed by a 2-second slow shake and aspiration. Then, 15 µL/well (384-wp) or 60 µL/well (96-wp) from the Secondary Antibody Solution was added, accompanied by a 3-second slow shake. 9. Secondary Antibody Incubation and autoclean: An autoclean cycle with PBS was initiated and lasted for 1 hour. 10. Final Washing Phase: Plates were washed with 50 µL/well (384-wp) or 200 µL/well (96-wp) of PBST. This was followed by two consecutive washes with 50 µL/well (384-wp) or 200 µL/well (96-wp) of PBS, incorporating a 2-second slow shake in each cycle. Finally, plates were left with 50 µL/well (384-wp) or 200 µL/well (96-wp) of PBS.

Imaging

Plates were imaged with a ImageXpress micro-XL and analyzed with MetaXpress (Molecular Devices).

Analysis

Analysis was conducted in R.

Data Omission: We excluded five library plates, constituting 8% of the total library, due to insufficient infection levels for accurate quantification.

Normalization: Two variables were subject to normalization—percentage of SARS-CoV-2 positive cells and the count of nuclei. The normalization steps were applied separately for the three screening conditions: mock treatment followed by mock infection, IFN-α2a treatment followed by SARS-CoV-2 infection, and mock treatment followed by SARS-CoV-2 infection. Data was first Z-scale normalized within assay plates:

$$Scale(x) = \frac{x - mean(x)}{sd(x)}$$

And then Z-scale normalized per row and per column to remove any spatial effects.

Statistics: a robust statistic accounting for technical and biological variability was applied using the below formula within the replicates of each gene**:**

$$Stat\ score(x) = \frac{mean(x)}{sd(x)}$$

765 This statistic was further standardized by Z-scaling across all genes to produce our final z-
766 score.
767 **Exclusion of genes influencing cell proliferation:** 224 genes with nuclei count z-score ≥ 2
768 and 388 genes with nuclei count z-score ≤ 2 in the mock treatment followed by mock infection
769 condition were deemed to influence cell proliferation and excluded from subsequent analyses.
770 **Exclusion of genes not expressed in cell lines of interest (A549, Calu-3, Huh-7.5 cells) and**
771 **in human lung cells.** Expression data from cell lines from [47, 48]. Expression data from tissues
772 from [49]. Genes were considered expressed if they had at least one read count within exons.
773

774 ## Gene set enrichment analysis

775 For the pathway analysis in **Supp Fig 2E**, we leveraged the FGSEA package [186] to perform
776 Gene Set Enrichment Analysis (GSEA) using gene sets found in the Molecular Signatures Database
777 (MSigDB) [187]: Reactome [188], KEGG [189], Wikipathways [190], Pathway Interaction Database
778 [191], and Biocarta [192]. The analysis was conducted separately for two conditions: IFN-α
779 pretreated SARS-CoV-2 infection and non-pretreated SARS-CoV-2 infection. We attributed a score
780 to each pathway for both conditions:

781 $$Score = -log10(padj) \times sign(Normalized\ Enrichment\ Score)$$

782 Each pathway was then attributed to one of nine quadrants (as in **Fig 1F**) based on its
783 score in the IFN-α pretreated condition (axis x) versus non-pretreated condition (axis y), using
784 padj ≤ 0.05 as a cutoff.
785

786 ## Compilation of published large-scale omic studies on SARS-CoV-2

787 As a rule, we listed the genes classified as 'hits' by the authors of the respective studies.
788 Below are some exceptions or clarifications:

789 ### Functional genetic screens

790 **Baggen, et al. [80]:** we used the “low stringency adjusted” analysis in Suppl Table 11.
791 Proviral: p_value_neg ≤ 0.05 and log2 FC ≥ 1. Antiviral: p_value_pos ≤ 0.05 and log2 FC ≤ -1. We
792 also used “High stringency” analysis in Suppl Table 7. Proviral: Gene is TMEM106B (log2 FC = 3.8
793 and p_value_neg = 0.08) or p_value_neg ≤ 0.05 and log2 FC ≥ 1 (no gene matched this criteria).

794 Antiviral: p_value_pos ≤ 0.05 and log2 FC ≤ -1 (no gene matched this criteria). **Biering, et al. [79]:**
795 in Supplementary Table 1, in Tab 1: LOF-enriched screen analysis, for proviral genes, we used FDR
796 ≤ 0.05. In Tab 2: GOF-depleted screen analysis, proviral: FDR ≤ 0.05. In Tab 3: GOF-enriched screen
797 analysis, for antiviral genes, we used FDR ≤ 0.05. **Chan, et al. [78]:** in Multimedia component 6,
798 for Vero E6 (T16); UM-UC-4 (T23); HEK293+A+T (T12); HuH-7 (T15) and Calu-3 (T43), we
799 considered gene as hits at FDR < 0.1 (as in Figure 4A). We listed the genes as proviral if differential
800 ≥ 0 or antiviral if differential ≤ 0. **Daniloski, et al. [77]:** we used Table S1. FDR MOI1 ≤ 0.05 or FDR
801 MOI3 ≤ 0.05. **Danziger, et al. [11]:** in S1 Table, we used the genes annotated as proviral or antiviral
802 by the authors. **Gordon, et al. [76]:** for A549 +ACE2 in Table S6 or Caco2 in Table S7, for proviral
803 genes, we used Averaged z-scores ≤ 2 and for antiviral genes, we used Averaged z-scores ≥ 2.
804 **Grodzki, et al. [75]:** for VeroE6 in additional file 4, tab 4, we used FDR <0.25. For HEK293T +Cas9
805 Study 1 in additional file 6, tab17, we used FDR <0.25. For HEK293T +Cas9 Study 1 in additional
806 file 7, tab7, we used FDR <0.25. **Hoffmann, et al. [28]:** for 37°C (Table S1E) and for 33°C (Table
807 S1C), we selected proviral genes if FDR ≤ 0.05 and z-score ≥ 0 and antiviral genes if FDR ≤ 0.05 and
808 z-score ≤ 0. **Hossain, et al. [69]:** in Figure 3E, we selected the top 15 genes in the spike-mNG axis
809 by negative log robust rank aggregation. **Israeli, et al. [74]:** we used Supplementary Data 1. **Kaur,**
810 **et al. [15]:** we used the genes labelled in Figure 1. **Le Pen et al. (this study):** we used z-score ≥ 2
811 for antiviral genes and ≤ 2 for proviral genes, see Unbiased arrayed CRISPR KO Screen analysis
812 section above for more details. **Loo, et al. [73]:** we used the genes labelled in Figure 2. **Mac Kain,**
813 **et al. [18]:** in Electronic Supplementary Material 5, for antiviral genes, we used the filter: pos|rank
814 ≤13, for proviral genes, we used neg|rank ≤13. **Martin-Sancho, et al. [12]:** we used Table S3,
815 "Lentivirus validated hits". **Pahmeier, et al. [72]:** we used the genes labelled in Figure 6.
816 **Rebendenne, et al. [71]:** for Calu3_Gattinara, we used for proviral genes: residual_z-score_avg ≥
817 2.5 and for antiviral genes: residual_z-score_avg ≤ 2.5 (no gene). For VeroE6, proviral: residual_z-
818 score_avg ≥ 2.5, and antiviral: residual_z-score_avg ≤ 2.5. For Caco2, proviral: residual_z-
819 score_avg ≥ 2.5 and antiviral: residual_z-score_avg ≤ 2.5. For Calu3_Calabrese, proviral:
820 residual_z-score_avg ≤ 2 and antiviral: residual_z-score_avg ≥ 2. **Rehfeld, et al. [70]:** In Table S1,
821 we considered genes as hits for PRF-1 top eGFP-mCh or PRF-1 bottom eGFP-mCh if FDR ≤ 0.05.
822 **Schneider, et al. [31]:** for both 37°C (Table_S1A) and 33°C (Table_S1B), we listed the gene as

823 proviral if FDR ≤ 0.05 and z-score ≥ 0 and antiviral if FDR ≤ 0.05 and z-score ≤ 0. **Wang, et al. [67]:**
824 we used Table S1. Proviral: Enrichment score ≤ 10^(-4). **Wei, et al. 2021 [66]:** we used Table S1.
825 For proviral genes, we used Cas9-v1 Avg. ≥ 2.5 & Cas9-v2 Avg. ≥ 2.5. Average between Cas9-v1
826 Avg. and Cas9-v2 Avg. is given in the table. For antiviral genes, we used Cas9-v1 Avg. ≤ -2.5 &
827 Cas9-v2 Avg. ≤ -2.5. Average between Cas9-v1 Avg. and Cas9-v2 Avg. is given in the table. **Wei, et**
828 **al. 2023 [65]:** in Table S1, for Day 7 or Day 14, we used fdr ≤ 0.05 for positive regulators of
829 ribosomal frameshifting or negative regulators of ribosomal frameshifting. **Wickenhagen, et al.**
830 **[13]:** we used the genes labelled in Figure 1B. **Xu, et al. [19]:** in Huh-7.5 or A549-ACE2 cells, in
831 untreated or in IFN-gamma treatment, we used Log10 p-value (mNG-High vs. mNG-Low
832 Enrichment) ≥ 3. **Zhu et al. [64]:** In Supplementary Data 1 , SARS-CoV-2 WT and 2 VOCs tested,
833 for proviral genes, we used pos.score_wt ≤ 0.0005 or pos.score_alpha ≤ 0.0005 or pos.score_beta
834 ≤ 0.0005.

835 ### Human genetic studies

836 **Degenhardt, et al. [90]:** we used Table 2 and added KANSL1 and TAC4, based on new
837 analysis by Pairo-Castineira et al. 2023 [25]. **Kousathanas, et al. [26]:** we used Table 1 from Pairo-
838 Castineira, et al. 2023 [25]. **Pairo-Castineira, et al. 2021 [98]**: we used Table 1 from Pairo-
839 Castineira, et al. 2023 [25]. **Pairo-Castineira, et al. 2023 [25]**: we only considered variants near
840 annotated genes (i.e., we excluded rs1073165). **Roberts, et al. [83]:** we used Figure 2. **Zhou, et**
841 **al. [95]**: we used Table 1 and the p-values from COVID-19 hospitalization (European ancestry
842 only).

843 ### SARS-CoV-2 protein interactomes

844 Davies, et al. [109], Laurent, et al. [102], Li, et al. [108], Samavarch-Tehrani, et al. [100],
845 St-Germain, et al. [103], Stukalov, et al. [107]: we used the Supplementay Table 3 from [27].
846 Gordon, et al. [101]: we used the genes listed in Table S2. Liu, et al. [104] and May, et al. [105]:
847 we used the genes listed in May, et al. [105] Table S5-new. Zhou, et al. [106]: we used the genes
848 listed in Table S1. "SARS-CoV-2-human protein-protein interactions identified in this study."

849 ### SARS-CoV-2 RNA interactomes

850 Flynn, et al. [114], Kamel, et al. [113], Labeau, et al. [112], Lee, et al. [115], Schmidt, et al.
851 2021 [111]: we used the Supplementay Table 3 from [27]. Schmidt, et al. 2023 [110]: we used

852 Table S2, "Huh-7 interactome comparison tab", genes listed in the following categories: "Huh-7
853 gRNA FDR5 HS" and "Huh-7 sgmRNA FDR5 HS".

854 ### Altered phosphorylation states in SARS-CoV-2-infected cells.

855 **Bouhaddou, et al. [116]:** for Vero E6 cells, we used Table S1, tab 1 "PhosphoDataFull" and
856 filtered for adj.pvalue ≤ 0.05 & log2FC ≥ 1 or adj.pvalue ≤ 0.05 & log2FC ≤ -1 in at least three
857 different time points.

858

859 ## Generation of PLSCR1 KO cells

860 ### CRISPR KO

861 KO Huh-7.5 and A549-ACE2 cells were generated using two anti-PLSCR1 Edit-R crRNAs
862 from Horizon Discovery (cat. CM-003729-02-0002 and CM-003729-04-0002) or non-targeting
863 controls (cat. U-007501-01-05 and U-007502-01-05) resuspended with an equimolar amount of
864 Edit-R tracrRNA (Horizon, cat. U-002005-20) to form sgRNAs. The sgRNAs were then co-
865 transfected with Cas9-mKate2 mRNA (Horizon, cat. CAS12218) according to the manufacturer's
866 protocol. 24 to 48 hours after transfection, cells were examined for mKate2 signal and FACS sorted
867 into bulk and single cell populations, gating on mKate2 signal. Bulk and single cell populations
868 were then assessed for PLSCR1 expression by western blot to confirm KO.

869 ### Amplicon sequencing

870 Genomic DNA was isolated from a frozen cell pellet using the Qiagen DNeasy kit (Qiagen,
871 cat. 69504) and treated with RNAse A in the optional RNA digestion step. The region of interest
872 was then amplified using Q5 2x mastermix (New England Biolabs, cat. M0492S), 500 ng of
873 template DNA, 0.5 µM of forward and reverse primers, and the following PCR conditions: 98°C
874 for 30 seconds, followed by 98°C for 5 seconds, 64°C for 15 seconds, and 72°C for 20 seconds,
875 repeating those steps 30 times before holding at 72°C for 2 minutes. The primers used when
876 amplifying PLSCR1 genomic DNA from WT and KO Huh-7.5 and A549+ACE2 cells were RU-O-
877 32687 (5' AACATAGAGGTGATTATGATTTCGTCT) and RU-O-32526 (5'
878 GGAGGAGCTTGGATTTCTATCTAC). PCR reactions were run on a 1% agarose gel to confirm
879 amplification. Amplicons were purified with a Zymo DNA clean and concentrator kit (Zymo, cat.
880 D4013) before sending to Genewiz for amplicon sequencing.

881 ## Western Blots

882 Cell pellets were collected and lysed in RIPA buffer (Thermo, catalog number 89900) with
883 1x Halt protease inhibitor cocktail and 1x EDTA (Thermo, catalog number 87786). Cell lysates were
884 spun down in a refrigerated centrifuge at 15,000 g at 4°C for 15 minutes to pellet any cell debris,
885 and the supernatant was collected and transferred to another tube. The collected samples were
886 quantified by BCA assay (Thermo Scientific, cat. #23225). Before loading into the gel, we added
887 sample buffer (Thermo, catalog number NP0007) with β-mercaptoethanol and heated the sample
888 at 95°C for 10 minutes. Samples were allowed to cool back to room temperature before loading
889 into 12% Bis-Tris 1.0 mm gels (Invitrogen, cat. #NP0321BOX). Proteins were electrophoretically
890 transferred onto nitrocellulose membranes. Membranes were blocked with 5% fat-free milk in 1X
891 TBS (Thermo, catalog number NP00061) and then incubated with primary antibody at 4°C
892 overnight in 5% fat-free milk in 1x TBS with 0.5% Tween-20 (TBST). Primary antibody: rabbit anti-
893 PLSCR1 polyclonal antibody (Proteintech, cat. #11582-1-AP) and mouse anti-β-actin antibody
894 (Millipore Sigma, cat. A5316-100UL) as a loading control. After incubation, membranes were
895 washed three times with 1x TBST and then incubated with fluorescently conjugated secondary
896 antibodies for 2 hours at room temperature. Secondary antibodies: LI-COR IRDye goat anti-rabbit
897 800 and goat anti-mouse 680 (LI-COR cat. 926-32211 and 926-68070, respectively). Membranes
898 were washed three times with 1X TBST, once with 1X TBS, then imaged on an Azure 600. For the
899 western blot in Supplementary Figure 4, this protocol was modified slightly: proteins were
900 electrophoretically transferred onto 0.22 µm polyvinylidene difluoride (PVDF) membranes,
901 incubated with a primary antibody solution of rabbit anti-PLSCR1 polyclonal antibody
902 (Proteintech, cat. #11582-1-AP) and polyclonal rabbit anti-RPS11 antibody (Abcam, cat.
903 ab157101), a secondary antibody solution of goat anti-rabbit HRP (Invitrogen, cat. 31462) and
904 visualized using a SuperSignal West Femto Maximum Sensitivity Substate kit (Thermo, cat.
905 #34096).

906

907 ## Cell viability assay

908 4,000 A549-ACE2 cells/well or 8,000 Huh-7.5 cells/well were seeded on day 0 in 100 µL
909 media (DMEM, 10% FBS, 1X NEAA, 1X Penicillin-Streptomycin) in a 96-well plate. The next day,

910 blasticidin selection was added as indicated in the figure to serve as a control for reduced cell
911 viability. On day 4, cell viability was assessed by resazurin assay (Abcam, cat. ab129732) according
912 to the manufacturer's protocol.
913

914 ### JAK-STAT inhibitor treatment

915 InSolution (Millipore, cat. 420097-500UG) was used according to the manufacturer's
916 instructions.
917

918 ### Titration of IFN-a2a in CHIKV-infected cells

919 6,000 Huh-7.5 cells/well were seeded in 100 µL media (DMEM, 10% FBS, 1X NEAA). The
920 following day, we treated cells with one of twelve concentrations of IFN-a2a (PBL, cat. 11101-2):
921 64 pM, 32 pM, 16 pM, 8 pM, 4 pM, 2 pM, 1 pM, 0.5 pM, 0.25 pM, 0.125 pM, 0.0625 pM, and 0
922 pM. The following day, the cells were infected with 2 µL of CHIKV-181/25-mKate2 (approximately
923 17,000 FFU per well, titer determined on Huh-7.5 cells) and fixed after 12 hours. Plates were
924 stained with a 1:1000 dilution of Hoechst for at least 10 minutes before washing with PBS and
925 imaging for mKate2 signal.
926

927 ### RT-qPCRs on ISGs

928 Huh-7.5 and A549-ACE2 cells were seeded at densities of 36,000 or 18,000 cells/well,
929 respectively, in 500 µL of media (DMEM, 10% FBS, 1X NEAA) in 24-well plates. The following day,
930 a dilution series of IFN-α2a (PBL, cat. 11101-2) or IFN-β (PBL, cat. #11415) was prepared (64 pM,
931 32 pM, 16 pM, 8 pM, 4 pM, 2 pM, 1 pM, 0.5 pM, 0.25 pM, 0.125 pM, 0.0625 pM, and 0 pM) and
932 50 µL of each dilution added to the cells in duplicate. After 24 hours, the media was removed and
933 the cells were washed with 1 mL of ice-cold PBS. 200 µL of RNA Lysis Buffer (Zymo Research, cat.
934 #R1060-1-100) was added to the cells, and the plates were frozen at -20°C before RNA isolation.
935 RNA was extracted using the Zymo Quick RNA 96-kit (Zymo Research, cat. R1052) including
936 DNaseI treatment, followed by cDNA synthesis using the SuperScript™ IV VILO™ Master Mix
937 (Invitrogen, cat. 11756050) according to manufacturers' instructions. qPCRs were conducted on

938 a QuantStudio 3 cycler using the Taqman Fast Advance master mix (Life Technologies Corporation,
939 cat. 4444965) and the following assays: *RPS11* (ThermoFisher 4331182; Hs01574200_gH), *IFI6*
940 (ThermoFisher 4331182; Hs00242571_m1), *OAS1* (ThermoFisher 4331182; Hs00973635_m1).
941 *IFI6* and *OAS1* were normalized to *RPS11* mRNA levels using the deltaCt method [193].
942

943 ## PLSCR1 subcellular localization

944 ### IF staining

945 A549-ACE2 cells were plated onto #1.5, 12mm glass coverslips (Fisher Scientific, cat.
946 #1254581) placed at the bottom of the wells of a 24-well plate. When confluent, the cells were
947 fixed, permeabilized with 1% Triton X-100 for 5 minutes and blocked for 1 hour at room
948 temperature with 1 mL of PBS-BGT (1x PBS with 0.5% bovine serum albumin, 0.1% glycine, 0.05%
949 Tween 20). Afterward, the cells were incubated in a 1:500 dilution of 4D2 mouse anti-PLSCR1
950 antibody (Millipore Sigma, cat. #MABS483) in PBS-BG (1x PBS with 0.5% bovine serum albumin
951 and 0.1% glycine) overnight at 4C with rocking. The cells were then washed twice with PBS-BGT
952 before incubation with a secondary antibody solution of 1:1000 anti-mouse 588 (ThermoFisher,
953 cat. #A-11001) and 1:1000 Hoechst dye (ThermoFisher, cat. #62249) in PBS-BG for two hours at
954 room temperature, followed by three washes with PBS-BGT. For those images where cells were
955 treated with IFN shown in **Supp Fig 11B**, A549-ACE2 cells were treated with 20 pM of IFN-α2a
956 (PBL, cat. 11101-2) for 48 hours before harvest, then fixed and stained as described above. For
957 those images where cells were infected with SARS-CoV-2 shown in **Supp Fig 11C**, A549-ACE2 cells
958 were infected with approximately 3,400,000 PFU of SARS-CoV-2 (titer determined on Vero E6
959 cells) diluted in 200 µL Opti-MEM to achieve almost 100% infection. After 24 hours, cells were
960 fixed and stained as described above, with slight modification to the antibody solutions. Primary
961 antibody solution: 1:500 4D2 mouse anti-PLSCR1 and 1:3000 rabbit anti-SARS-CoV-2 N (Genetex,
962 cat. GTX135357) in PBS-BG. Secondary antibody solution: 1:1000 goat anti-mouse 594, 1:1000
963 goat anti-rabbit 647, and 1:1000 Hoechst dye.

964 ### Imaging

965 The coverslips were mounted onto slides (Fisher Scientific, cat. #1255015) with Invitrogen
966 ProLong Gold Antifade Mountant (Fisher Scientific, cat. # P36930). The slides were allowed to

967 cure for 24 hours before the edges of the coverslips were sealed. For **Fig 5A**, the cells were imaged
968 by confocal microscopy. Confocal images were acquired using Zeiss Zen Blue (v3.5) software on a
969 LSM 980 point scanning confocal microscope (Zeiss) hooked to a Axio Observer.Z1 / 7 stand
970 equipped with C Plan-Apochromat 63X/1.40 oil (RI:1.518 at 23°C) objective lens (Zeiss). CW
971 excitation laser lines 405 nm and 488 nm were used to excite the fluorescence of DAPI and AF488
972 labeled samples. Emitted fluorescence were spectrally grated (410-483 nm for DAPI, 499-552 nm
973 for AF488) to avoid fluorescence bleed through and were detected in MA-PMT (DAPI), and GaAsP-
974 PMT (AF488). The confocal pinhole was set to 1AU for AF488, and the detector master gains were
975 set within the linear range of detection (550-750V). For the IFN-treated and SARS-CoV-2 infected
976 cells shown in **Supp Fig 11B,C**, these were mounted as described previously but imaged via
977 widefield imaging. Widefield imaging was performed in the Rockefeller University's Bio-Imaging
978 Resource Center, RRID:SCR_017791, on a DeltaVision Image Restoration Microscope (Applied
979 Precision, now Leica Microsystems) using inverted IX-70 stand (Olympus, Evident Scientific) and a
980 60X NA 1.42 oil immersion objective (Olympus), and filter sets for DAPI (Ex: 390 ± 18, Em: 435 ±
981 48), Alexa Fluor 594 (Ex: 575 ± 25, Em: 632 ± 60), Alexa Fluor 647 (Ex: 575 ± 25, Em: 676 ± 34).
982 Images were acquired on a pco.edge sCMOS camera, and were subsequently deconvolved using
983 the Deltavision image acquisition software (SoftWorx). Scanned images for both confocal and
984 widefield imaging were saved as .czi files.
985

986 ### Focus-forming assay on SARS-CoV-2-infected cells

987 In **Fig 5B**, Huh-7.5 and A549-ACE2 cells were cultured in media (DMEM with 5% FBS) and
988 seeded at densities of 2 x 10^5 and 1 x 10^5 cells per well, respectively, in collagen-coated 12-well
989 plates to reach 80-90% confluency by the day of infection. A 1:10 serial dilution of virus stock was
990 made in Opti-MEM in five separate tubes. Media was aspirated from the cells, and the wells were
991 washed with 1 ml of PBS before adding 200 µL of each virus dilution to the cells in triplicate. Plates
992 were incubated at 37°C with 5% CO2 for 1 hour, rocking every 15 minutes for even virus
993 distribution. A 1% methylcellulose overlay medium was prepared and mixed with complete
994 growth media at 37°C; 2 ml of this overlay was added to each well after removing the virus
995 inoculum. Plates were then incubated at 37°C with 5% CO2 for 48 for Huh-7.5 cells or 72 hours

996 for A549-ACE2 cells. Cells were then fixed in final 10% neutral buffered formalin and IF stained as
997 described in the Unbiased Arrayed CRISPR screen section. PLSCR1 KO and WT cells were
998 compared at similar virus dilutions.

999 In **Fig 6G**, the above protocol was followed to titer SARS-CoV-2 strains on Huh-7.5 PLSCR1
1000 KO cells. Then, Huh-7.5 WT and KO cells were seeded at 2 x 10^5 cells per well in 1 mL of media
1001 (DMEM, 10% FBS, 1X NEAA) in 12-well plates to reach 80-90% confluency the next day. Media
1002 was aspirated from the cells, the wells were washed with 1mL of PBS, and then the cells were
1003 infected with approximately 50 FFU of SARS-CoV-2 (for each strain) as determined on PLSCR1 KO
1004 Huh-7.5 cells diluted in 200 µL of Opti-MEM. Plates were then incubated, overlayed with
1005 methylcellulose, fixed, and stained as described above.

1006

1007 ### Transfection with SARS-CoV-2 replicon system

1008 The SARS-CoV-2 replicon and the method for electroporation has been described
1009 previously [119]. Briefly, 6 x 10^6 Huh-7.5 WT and PLSCR1 KO cells were electroporated at 710 V
1010 with 2 µg of SARS-CoV-2 N mRNA and 5 µg of replicon RNA. The cells rested for 10 minutes at
1011 room temperature before resuspending to a concentration of 300,000 cells/mL and plating 100
1012 µL of cells into each well of a 96-well plate. After 24 hours, supernatant was collected from the
1013 replicon-transfected cells and assayed for *Renilla* luciferase activity according to kit instructions
1014 (Promega, cat. E2810).

1015

1016 ### Transduction with SARS-CoV-2 spike/VSV-G-pseudotyped, single-cycle, replication-
1017 defective HIV-1 viruses.

1018 #### Virus preparation

1019 SARS-CoV-2 spike/VSV-G-pseudotyped, single-cycle, replication-defective HIV-1 viruses
1020 (pCCNanoLuc/GFP) were prepared as in [120]. Plasmids were a kind gift of Theodora Hatziioannou
1021 and Paul D. Bieniasz (The Rockefeller University, NY, USA) [120, 194, 195]. One day before the
1022 transfection, 4 x 10^6 293T cells were seeded in a 10 cm dish. One hour prior to transfection, the
1023 growth media in the dish was replaced with 9 mL of fresh media containing 2% serum. A 1,000

1024 µL transfection mixture was prepared, comprising the diluent (a 150 mM NaCl solution prepared
1025 with sterile cell culture water), 5 µg of HIV GP plasmid, 5 µg of pCLG plasmid, and either 2.5 µg of
1026 SARS-CoV-2 spike Δ19 or 1 µg of pHCMV.G plasmid, ensuring the total plasmid content did not
1027 exceed 12.5 µg. After brief vortexing, 50 µL of PEI (1 mg/mL, Polysciences cat. 23966) was added
1028 to achieve a 1:4 DNA/PEI ratio. The mixture was vortexed for 5 seconds and then allowed to sit
1029 for 20 minutes in a hooded environment. Following gentle mixing by pipetting, 1 mL of the
1030 transfection mixture was added to the 10 cm dish. Media was changed 12 hours post-transfection,
1031 and the supernatant was harvested and filtered through a 0.2-micron filter 48 hours post-
1032 transfection, then stored at -80°C.

1033 ### Transduction of PLSCR1 KO or WT A549-ACE2 cells

1034 Seeded in 96-well plates, 6,000 A549-ACE2 cells per well were cultured in 100 µL of media.
1035 After two days, either 10 µL of SARS-CoV-2 spike pseudotyped virus or 0.01 µL of VSV-G
1036 pseudotyped virus were diluted in a final volume of 100 µL of media and added to the wells to
1037 yield comparable NanoLuc signals. Plates were then spun at 200 g for 5 minutes and incubated at
1038 37°C. Two days post-infection, the media was aspirated and replaced with 50 µL of NanoGlo
1039 solution, sourced from the Promega Nano-Glo Luciferase Assay kit (Promega, N1110), with a
1040 substrate to buffer ratio of 1:100. NanoLuc signal was subsequently quantified using a Fluostar
1041 Omega plate reader.

1042 ### Transduction of siRNA-treated HEK293T cells

1043 Seeded in 96-well plates, 1,600 HEK293T, HEK293T-ACE2, or HEK293T-ACE2-TMPRSS2 cells
1044 were cultured in 80 µL of media. The next day, a 20 µL transfection mixture made of Opti-MEM,
1045 1% DharmaFECT1 (Horizon, T-2001-03), and 250 nM siRNA, PLSCR1 ON-TARGETplus SMARTpool
1046 siRNA (Horizon, cat. L-003729-00-0005) or non-targeting control (Horizon, cat. D-001810-10-05)
1047 was added to the cells. The final concentration of siRNAs was 25 nM. After two days, either 2 µL
1048 of SARS-CoV-2 spike pseudotyped virus or 0.2 µL of VSV-G pseudotyped virus were diluted in a
1049 final volume of 100 µL of media and added to the wells to yield comparable NanoLuc signals.
1050 Plates were then span at 200 g for 5 minutes and incubated at 37°C. Two days after infection,
1051 NanoLuc signal was quantified as described in the “Infection of PLSCR1 KO or WT cells” section.
1052

1053 ### Infection of siRNA-treated A549 cells with SARS-CoV-2

1054 Seeded in 96-well plates, 1,000 A549, A549-ACE2, or A549-ACE2-TMPRSS2 cells were
1055 cultured in 80 µL of media. On the same day, a 20 µL transfection mixture made of Opti-MEM, 1%
1056 DharmaFECT1 (Horizon, T-2001-03), and 250 nM siRNA, PLSCR1 ON-TARGETplus SMARTpool
1057 siRNA (Horizon, cat. L-003729-00-0005) or non-targeting control (Horizon, cat. D-001810-10-05)
1058 was added to the cells. The final concentration of siRNAs was 25 nM. Three days after
1059 transfection, the cells were infected by adding 34,000 PFU of SARS-CoV-2 (titer determined on
1060 Vero E6 cells) diluted in 10 µL media to each well. Plates were then spun at 200 g for 5 minutes
1061 and incubated at 37°C. Staining and readout as described above in the "Unbiased arrayed CRISPR
1062 KO screening" section.

1063

1064 ### Pan-virus infection of PLSCR1 KO cells

1065 A549-ACE2 cells were seeded at a density of 6,000 cells/well in 96-well plates in 90 µL
1066 media. The following day, 10 µL diluted virus was added to each well. Virus concentrations as
1067 follow: CHIKV-mKate, 0.05 µL virus stock per well (titer 8.5 x 10^6 PFU/mL determined in Huh-7.5
1068 cells); hCoV-NL63, 10 µL virus stock per well (titer 1.4 x 10^5 PFU/mL); hCoV-OC43, 10 µL virus stock
1069 per well (titer 1.06 x 10^7 PFU/mL); hPIV-GFP, 0.05 µL virus stock per well; HSV1-GFP, 0.5 µL virus
1070 stock per well (titer 2.4 x 10^8 PFU/mL determined on Vero E6 cells); IAV WSN, 0.5 µL virus stock
1071 per well; SARS-CoV-2, 0.5 µL virus stock per well (titer 3.4 x 10^6 PFU/mL determined on Vero E6
1072 cells); SINV-Toto1101-mScarletI, 10 µL virus stock per well; VEEV-EGFP, 0.005 µL virus stock per
1073 well (titer 1.45 x 10^9 PFU/mL determined on BHK-21); VSV-GFP, 0.05 µL virus stock per well;
1074 YFV_17D, 5 µL virus stock per well. The cells were fixed, stained and imaged as described in the
1075 *Unbiased arrayed CRISPR KO screen* section. Fluorescent viruses were not stained: the fluorescent
1076 signal was used as a reporter. We used the following primary antibodies when applicable: anti-
1077 dsRNA (J2) mouse (Nordic MUbio, cat. 10010200) diluted 1:500 was used for hCoV-NL63 and
1078 hCoV-OC43, anti-IAV mouse (Millipore, cat. MAB8257) diluted 1:3000, anti-YFV mouse (Santa
1079 Cruz Biotechnology, cat# sc-58083) diluted 1:500, anti-SARS2-S rabbit (Genetex, cat. GTX135357)
1080 diluted 1:3000.

1081 Huh-7.5 cells were transfected with a 1:200 dilution of Dharmafect 4 (Horizon, cat. T-2004-
1082 01) and 25 nM ON-TARGETplus SMARTpool siRNAs (Horizon Discovery) in 96-well plates. The cells
1083 were infected three days after siRNA transfection with hCoV-NL63 or hCoV-OC43 or four days
1084 after siRNA transfection with SARS-CoV-2 or hCoV-229E. IF and imaging as described above.
1085

1086 ### Measuring extracellular ACE2 expression using flow cytometry

1087 A549-ACE2 cells were detached from the wells using Accutase (Innovative Cell
1088 Technologies, Inc., Cat: AT-104) for 5 minutes at 37°C. Following detachment, cells were rinsed
1089 once with PBS and stained with LIVE/DEAD Fixable Aqua (Invitrogen, Cat: L34966, diluted 1:1000
1090 in PBS) for 15 minutes at room temperature in the dark. After staining, cells were rinsed once
1091 more with PBS. Then, cells were incubated with FcR blocking reagent (Miltenyi Biotec, 1:50) and
1092 ACE2-AF488 (Sino Biological, Cat: 10108-MM37-F-100, 1:30) in FACS buffer (2% FBS in PBS) for 30
1093 min at 4°C in the dark. Following incubation, cells were washed twice with FACS buffer and
1094 subjected to flow cytometry analysis. Samples were acquired on an LSRII flow cytometer (BD
1095 Biosciences), and the results were analyzed with FlowJo software (Tree Star). Before analyzing cell
1096 surface ACE2 expression, gating procedures were implemented to exclude dead cells and
1097 doublets from the analysis.
1098

1099 ### SARS-CoV-2 variant infections

1100 For **Figure 6A-E**, Huh-7.5 cells were plated at 7,500 cells/well in 100 µL of media (DMEM,
1101 10% FBS, 1X NEAA) in 96-well plates. The next day, cells were infected with quantities of virus that
1102 yielded comparable percent infections in the WT cells, then spun at 200 g for 5 minutes and
1103 incubated at 33°C. The quantities of virus used were as follows: 0.1 µL/well for parental, 0.05
1104 µL/well for beta, 1 µL/well for delta, 0.5 µL/well for Omicron BA.5, and 0.05 µL/well for Omicron
1105 XBB.1.5. The infected cells were fixed after 24 hours and stained as described previously.
1106

1107 ### Growth curves using the parental SARS-CoV-2 strain and Omicron (XBB.1.5)

1108 Huh-7.5 WT and PLSCR1 KO cells were plated at 100,000 cells/well in 1mL media (DMEM,
1109 10% FBS, 1X NEAA) in a 24-well plate. The following day, cells were infected at MOI 0.01 (as titered

1110 on PLSCR1 KO Huh-7.5 cells) with the New York 2020 isolate of SARS-CoV-2 ("parental") and SARS-
1111 CoV-2 Omicron XBB.1.5. Plates were incubated for 1hr at 37°C. Inoculum was removed and saved
1112 as the 0hr timepoint. Cells were washed twice with PBS. Fresh media was added, then collected
1113 as the 1hr timepoint. Fresh media was added again, and the cells were incubated at 33°C. All
1114 supernatant was collected from the cells again at 24 hours, 48 hours, and 72 hours, and was
1115 replaced with fresh media. Collected supernatant was frozen at -80°C until titering. Supernatants
1116 were titered by plaque assay as follows: Vero E6 cells were plated at 200,000 cells/well in 12-well
1117 plates. The following day, collected supernatant was tenfold serially diluted, the media removed
1118 from the plates, and 300 µL diluted virus added. Each sample of supernatant was titered in
1119 duplicate. Cells were incubated with virus for 1 hour at 37°C, then inoculum was removed and
1120 1mL of 1% methylcellulose (supplemented with 5% FBS). Plates were incubated for 3 days at 37°C,
1121 then fixed with 2mL of 7% formaldehyde and stained with crystal violet before being rinsed with
1122 water, left to dry overnight, and the plaques counted.
1123

1124 Generating and infecting cells overexpressing ISGs (Including PLSCR1)

1125 Plasmid sources

1126 WT PLSCR1, IFITM2, and LY6E over-expression lentiviral plasmids originated from the
1127 SCRPSY library [196]. CH25H originated from the Thermo Scientific Precision LentiORF Collection.
1128 RRL.sin.cPPT.CMV/Flag-NCOA7 variant 6.IRES-puro.WPRE (CG494) was a gift from Caroline Goujon
1129 (Addgene plasmid # 139447) [161].

1130 Plasmid cloning

1131 N-terminal 3x FLAG-tagged PLSCR1, C-terminal 3x FLAG-tagged PLSCR1, and PLSCR1
1132 H262Y in the SCRPSY vector, used in **Figs 4B and 7D**, were generated by designing and ordering
1133 large dsDNA gene blocks of PLSCR1 that contained the desired mutations from IDT. These gene
1134 blocks were cloned into the PLSCR1-SCRPSY vector [196] and confirmed by sequencing using
1135 Plasmidsaurus (see **Supp Table 18** for sequences).

1136 PLSCR1 variants of interest (**Fig 7C and Supp Fig 12**) were cloned by site directed
1137 mutagenesis using the NEB Quick Protocol for Q5® Site-Directed Mutagenesis Kit (cat. E0552)
1138 according to the manufacturer's instructions. For G20V (rs79551579), we used the primers

1139 JLP621-O-01/02; for A29T (rs41267859), we used the primers JLP621-O-03/04; for I110fs
1140 rs749938276, we used the primers JLP621-O-07/08; and for H262Y (rs343320), we used the
1141 primers JLP621-O-09/10. Primer sequences are listed in **Supp Table 20**.

1142 ### Lentivirus production

1143 Lentivirus were generated in Lenti-X 293T cells by transfecting 200 ng VSV-G plasmid, 700
1144 ng Gag-Pol plasmid, and 1100 ng plasmid of interest with lipofectamine 2000 in DMEM
1145 supplemented with 5% FBS. Media was changed 4-6 hours later, and lentivirus harvested at 24
1146 and 48 hours. Lentivirus-containing supernatants from both timepoints were pooled, then filtered
1147 through a 0.45 µM filter before aliquoting into 2 mL tubes and freezing at -80°C until use.

1148 ### Cell transduction

1149 0.3 million cells were transduced in suspension in a 12-well plate using a serial dilution of
1150 each lentivirus in DMEM (Fisher Scientific, cat. #11995065) supplemented with 5% FBS (HyClone
1151 Laboratories, Lot. #KTH31760) and 4 µg/mL polybrene (Millipore, cat. #TR-1003-G). The cells
1152 were then spinoculated at 37°C for 1 hour at 1000 x g. The following day, the cells were split into
1153 two 6-well plates. After 24 hours, one of the duplicates was treated with 2 µg/mL puromycin to
1154 select for transduced cells. Further experiments were carried out using the cells that had
1155 approximately 30% transduction before selection.

1156 ### SARS-CoV-2 infection

1157 In **Fig 7D**, Huh-7.5 and A549+ACE2 cells were plated at 6,000 cells/well and 3,000
1158 cells/well, respectively, in 100 µL of media (DMEM, 10% FBS, 1X NEAA) in 96-well plates. The
1159 following day, cells were treated with IFN (10pM for Huh-7.5 cells and 20pM for A549+ACE2 cells).
1160 On the third day, the Huh-7.5 cells were infected by adding 10 µL of media containing 0.1 µL of
1161 virus (titer of 3.4 × 106 PFU/ml, as measured on Vero E6 cells) to each well and the A549+ACE2
1162 cells were infected by adding 10 µL of media containing 1 µL of virus to each well. After adding
1163 the virus, the plates were spun at 200 g for 5 minutes and incubated at 37°C. Plates were
1164 harvested the next day by fixing and staining as described above

1165 In **Fig 7C** and **Supp Figs 8A and 12**, A549+ACE2 cells were plated at 7,000 cells/well in 100
1166 µL of media (DMEM, 10% FBS, 1X NEAA) in 96-well plates. The following day, cells were infected

1167 by adding 10 µL of media containing 1 µL of virus (titer of 3.4 × 106 PFU/ml, as measured on Vero
1168 E6 cells) to each well as described above.

1169 ### IF staining and imaging

1170 In **Figs 7C-E and Supp Figs 8A and 12**, cells were stained for IF as described in the *Unbiased*
1171 *arrayed CRISPR KO screening* section, with different primary and secondary antibody solutions.
1172 The primary antibody solution was a 1:3000 dilution of rabbit anti-SARS-CoV-2 nucleocapsid
1173 polyclonal antibody (Genetex, cat. #GTX135357) and a 1:500 dilution of 4D2 mouse anti-PLSCR1
1174 antibody (Millipore Sigma, cat. #MABS483) in PBS, and the secondary antibody solution was
1175 1:1000 goat anti-rabbit 594 (ThermoFisher, cat. #A-11012) or 1:1000 goat anti-rabbit Alexa
1176 Fluor™v 647 (ThermoFisher, cat. #A-21245), 1:1000 goat anti-mouse Alexa Fluor™ 488
1177 (Thermofisher, cat. #A-11001), and 1:1000 Hoechst dye (ThermoFisher, cat. #62249) in PBST.

1178

1179 ## SARS-CoV-2 infection of human SV40-fibroblasts-ACE2

1180 ### Patients

1181 Written informed consent was obtained in the country of residence of the patients, in
1182 accordance with local regulations, and with institutional review board (IRB) approval.
1183 Experiments were conducted in the United States in accordance with local regulations and with
1184 the approval of the IRB. Approval was obtained from the Rockefeller University Institutional
1185 Review Board in New York, USA (protocol no. JCA-0700).

1186 PLSCR1 H262Y was genotyped using the primers JLP616-O-1-4 listed in **Supp Table 20**.

1187 ### Generation of human SV40-fibroblasts ACE2 stable cell lines

1188 *ACE2* cDNA was inserted with In-Fusion cloning kit (Takara Bio) and using the XhoI and
1189 BamHI restriction sites into linearized pTRIP-SFFV-CD271-P2A in accordance with the
1190 manufacturers' instructions. We checked the entire sequence of the *ACE2* cDNA in the plasmid
1191 by Sanger sequencing. Then, HEK293T cells were dispensed into a six-well plate at a density of
1192 8 x10^5 cells per well. On the next day, cells were transfected with pCMV-VSV-G (0.2 µg), pHXB2-
1193 env (0.2 µg; NIH-AIDS Reagent Program; 1069), psPAX2 (1 µg; Addgene plasmid no. 12260) and
1194 pTRIP-SFFV-CD271-P2A-ACE2 (1.6 µg) in Opti-MEM (Gibco; 300 µL) containing X-tremeGene-9

1195 (Sigma Aldrich; 10 µL) according to the manufacturers' protocol. After transfection for 6 h, the
1196 medium was replaced with 3 mL fresh culture medium, and the cells were incubated for a further
1197 24 h for the production of lentiviral particles. The viral supernatant was collected and passed
1198 through a syringe filter with 0.2 µm pores (Pall) to remove debris. Protamine sulfate (Sigma;
1199 10 µg/mL) was added to the supernatant, which was then used immediately or stored at −80 °C
1200 until use.

1201 For the transduction of SV40-fibroblasts with ACE2, 5 x10^5 cells per well were seeded in
1202 six-well plates. Viral supernatant was added (500 µL per well). The cells were then further
1203 incubated for 48 h at 37 °C. Cells were keep in culture and after 8 days, transduction efficiency
1204 was evaluated by CD271 surface staining with CD271 AlexaFluor 647, 1:200 dilution (BD
1205 Pharmigen 560326). MACS-sorting was performed with CD271 positive selection beads (Miltenyi
1206 Biotec) if the proportion of CD271-positive cells was below 80% [8, 177].

1207 ### Infection

1208 5,000 cells per well were seeded in a 96-well plate and infected the next day with SARS-
1209 CoV-2 at MOI = 0.05, using a titer determined on Vero E6 cells. Cells were fixed at 2 dpi, stained
1210 and imaged as described in the *Unbiased arrayed CRISPR KO screen* section.

1211

1212 Acknowledgments

1213 We thank Georgia McClain for reading and editing this manuscript. We thank the staff at
1214 the Laboratory of Virology and Infectious Disease: Ellen Castillo, Michela De Santis, Arnella Norris,
1215 Aileen O'Connell, Santa Maria Pecoraro Di Vittorio, Glen Santiago, and Sonia Shirley. Ching-Wen
1216 Chang and Lihong Liu (Columbia University, NY, USA), and Theodora Hatziioannou, Viren Baharani
1217 and Paul D. Bieniasz (The Rockefeller University, NY, USA) generously provided plasmids,
1218 instructions to generate SARS-CoV-2 spike-pseudotyped, single-cycle, replication-defective HIV-1
1219 viruses [120, 194, 195], and assisted us with data interpretation. Oded Danziger and Brad R.
1220 Rosenberg (Department of Microbiology at the Icahn School of Medicine at Mount Sinai, NY, USA)
1221 kindly provided the A549-ACE2 cells [11] used in this study. FACS was conducted at the Flow
1222 Cytometry Resource Center at Rockefeller University. mRNA-seq was performed by the Genomics

1223 Resource Center at The Rockefeller University and by Novogene. Confocal microscopy was
1224 performed in the Rockefeller University's Bio-Imaging Resource Center, RRID:SCR_017791. We
1225 thank Ankit Patel, Sales Manager at Horizon Discovery.
1226 Trim Galore was developed at The Babraham Institute by @FelixKrueger, now part of Altos
1227 Labs. The Genotype-Tissue Expression (GTEx) Project [49] was supported by the Common Fund of
1228 the Office of the Director of the National Institutes of Health, and by NCI, NHGRI, NHLBI, NIDA,
1229 NIMH, and NINDS. The data used for the analyses described in this manuscript were obtained
1230 from the EMBL-European Bioinformatics Institute portal,
1231 "https://www.ebi.ac.uk/gxa/experiments/E-MTAB-5214/Results", on October 1st, 2020.
1232 Work in the Laboratory of Virology and Infectious Disease was supported by NIH grants
1233 P01AI138398-S1, 2U19AI111825, R01AI091707-10S1, and R01AI161444; a George Mason
1234 University Fast Grant; the G. Harold and Leila Y. Mathers Charitable Foundation; the Meyer
1235 Foundation; the Pilot Project Robertson Therapeutic Development Fund at The Rockefeller
1236 University; and the Bawd Foundation. The Laboratory of Human Genetics of Infectious Diseases
1237 is supported by the Howard Hughes Medical Institute, the St. Giles Foundation, NIH
1238 (R01AI163029, UL1TR001866), the French National Research Agency (ANR) under the
1239 "Investments for the Future" program (ANR-10-IAHU-01), the Integrative Biology of Emerging
1240 Infectious Diseases Laboratory of Excellence (ANR-10-LABX-62-IBEID), the French Foundation for
1241 Medical Research (FRM) (EQU201903007798), ANR GENVIR (ANR-20-CE93-003) project, the ANR-
1242 RHU COVIFERON Program (ANR-21-RHUS-08), the French Foundation for Medical Research (FRM)
1243 (EQU201903007798), the European Union's Horizon 2020 research and innovation program
1244 under grant agreement No. 824110 (EASI-genomics), the HORIZON-HLTH-2021-DISEASE-04
1245 program under grant agreement 01057100 (UNDINE), the Square Foundation, William E. Ford,
1246 General Atlantic's Chairman and Chief Executive Officer, Gabriel Caillaux, General Atlantic's Co-
1247 President, Managing Director and Head of Business at EMEA, and the General Atlantic
1248 Foundation. J.L.P. was supported by the Francois Wallace Monahan Postdoctoral Fellowship at
1249 The Rockefeller University and the European Molecular Biology Organization Long-Term
1250 Fellowship (ALTF 380-2018). G.P. was supported by the James H. Gilliam Fellowship for Advanced
1251 Study from the Howard Hughes Medical Institute and the Graduate Research Fellowship Program

from the National Science Foundation (FAIN 1946429). M.B. was supported by a Swiss National Science Foundation fellowship (P500PB_203007).

Financial Disclosure

The funders had no role in study design, data collection and analysis, decision to publish, or preparation of the manuscript.

Data and code availability

mRNA-seq data is available on the Sequence Read Archive (SRA), hosted by the National Center for Biotechnology Information (NCBI), under BioProject PRJNA1138251 and BioSamples SAMN42689767-SAMN42689770 corresponding to **Supp Tables 2 and 3**, BioSamples SAMN42689771- SAMN42689774 corresponding to **Supp Tables 4 and 5**, BioSamples SAMN42689775- SAMN42689776 corresponding to **Supp Tables 14 and 15**, BioSamples SAMN42689777- SAMN42689778 corresponding to **Supp Tables 16 and 17**.

Code and Supporting Information are available on Dryad (DOI: 10.5061/dryad.6q573n65k).

Tables

Table 1. PLSCR1 variants associated with severe COVID-19 in a GWAS [25, 26]

GWAS p-value	**rsID**	**Genomic Coordinate (GRCh38)**	**Nucleotide Change**	**Gene**	**Functional Consequence**
7.52E-07	rs116553931	chr3:146430956	C:T	PLSCR2	intron variant
1.08E-07	rs454645	chr3:146514682	C:T	PLSCR1	Downstream

							transcript variant
5.43E-08	20	rs3433	17122	chr3:14651	G:A	PLSCR1	His262Tyr
8.21E-08	18	rs3433	18204	chr3:14651	T:C	PLSCR1	intron variant
1.52E-07	17	rs3433	18374	chr3:14651	A:G	PLSCR1	intron variant
1.00E-07	10	rs1869	20241	chr3:14651	A:G	PLSCR1	intron variant
1.13E-07	50	rs1731	20256	chr3:14651	A:T	PLSCR1	intron variant
1.35E-07	2408	rs7130	20389	chr3:14651	T:C	PLSCR1	intron variant
7.06E-08	16	rs3433	21151	chr3:14651	A:G	PLSCR1	intron variant
4.64E-08	14	rs3433	22652	chr3:14651	C:T	PLSCR1	intron variant
7.46E-08	12	rs3433	22970	chr3:14651	G:A	PLSCR1	intron variant

Figure Legends

Figure 1. An unbiased arrayed CRISPR KO screen identifies IFN-dependent and IFN-independent genes influencing SARS-CoV-2 infection.

A. mRNA-seq comparison between Huh-7.5 and Calu-3 cells, focusing on a subset of 224 ISGs, in response to 24 h SARS-CoV-2 infection MOI 0.03. Red diamond, PLSCR1 RNA level. Viral RNA levels were comparable in both cell lines (not shown). ****, $p \leq 0.0001$; two-tailed t-test.

1279 B. Cells were treated with 0.5 nM IFN-α2a for 24 h. mRNA-seq analysis as in **(A)**.
1280 C. Huh-7.5-Cas9 cells were pretreated with different amounts of IFN-α2a, then infected with
1281 SARS-CoV-2 for 24 h followed by IF staining for SARS-CoV-2 N protein; n = 6 separate wells
1282 infected on the same day; error bars represent SEM; ****, $p \leq 0.0001$; two-tailed t-test.
1283 D. Diagram of the arrayed CRISPR KO screen method.
1284 E. Median SARS-CoV-2 positive cell percentages determined by IF staining for the indicated
1285 control genes. The control genes were distributed across 28 separate wells (without IFN
1286 pretreatment) or across 20 separate wells (with IFN pretreatment) for each screened
1287 library plate. NTC: non-targeting control.
1288 F. The virus level (percentage of infected cells normalized and z-score calculated) is plotted
1289 for 24 h 0 pM (y axis) or 1 pM (x axis) IFN-α2a pretreatment followed by 24 h infection (n
1290 ≥ 5). The genes were categorized as ISG or other based on mRNA-seq of IFN-α2a-treated
1291 cells as in **(B)**. ISGs were defined by a fold change ≥ 2 and padj ≤ 0.05 in the IFN-treatment
1292 versus untreated pairwise comparison.
1293 The data underlying this Figure can be found in **Supp Table 1**.
1294
1295

1296 ## Figure 2. Cellular pathways influencing SARS-CoV-2 infection.

1297 GSEA was performed on the screen data (**Supp Table 10**). The individual genes for some
1298 of the top pathways are shown here. The full names of the plotted pathways are as
1299 follows: translation initiation, "REACTOME EUKARYOTIC TRANSLATION INITIATION";
1300 negative rRNA regulation, "REACTOME NEGATIVE EPIGENETIC REGULATION OF RRNA
1301 EXPRESSION"; cholesterol biosynthesis, "REACTOME REGULATION OF CHOLESTEROL
1302 BIOSYNTHESIS BY SREBP SREBF"; pre-mRNA processing, "REACTOME PROCESSING OF
1303 CAPPED INTRON CONTAINING PRE MRNA"; cellular respiration, "WP ELECTRON
1304 TRANSPORT CHAIN OXPHOS SYSTEM IN MITOCHONDRIA"; RNA Pol III transcription,
1305 "REACTOME RNA POLYMERASE III TRANSCRIPTION INITIATION FROM TYPE 3 PROMOTER."
1306 Pathways are from the Reactome [188] and Wikipathways [190] databases.
1307 The data underlying this Figure can be found in **Supp Table 1**.

1308

1309 Figure 3. Human genes significant in human genetics studies on COVID-19 patients
1310 and in functional genetic screens in cell culture

1311 Overlap between genes considered significant by human genetics studies on COVID-19
1312 patients [5, 6, 8, 25, 26, 81-99] and functional genetic screens for genes influencing SARS-
1313 CoV-2 infection in cell culture [11-13, 15, 18, 19, 28, 31, 64-80]. The full list of genes is
1314 available in **Supp Table 11**, and a summary is in **Supp Table 12**. Please note that not all
1315 genes represented here will influence COVID-19 outcomes. We apologize to the many
1316 colleagues whose work was not cited and discussed.

1317

1318 Figure 4. PLSCR1 is a highly effective anti-SARS-CoV-2 effector ISG contributing to
1319 intrinsic immunity in the absence of IFN.

1320 A. Cells were pretreated with a JAK-STAT inhibitor (InSolution 1 µM) for 2 h, followed by IFN-
1321 α2a (10 pM Huh-7.5 or 20 µM A549-ACE2) for 24 h and were infected with SARS-CoV-2 for
1322 24 h followed by IF staining for viral N protein. Huh-7.5 infection using an MOI of 0.5 (titer
1323 determined by focus forming assay on Huh-7.5 WT cells). A549-ACE2 infection using an
1324 MOI of 0.01 (titer determined by focus forming assay on A549-ACE2 WT cells). The
1325 percentage of SARS-CoV-2 positive cells is plotted. n = 4 separate wells infected on the
1326 same day.

1327 B. Cells were reconstituted with the indicated proteins by stable transduction with
1328 lentiviruses, then infected as in **(A)**. n = 4 separate wells infected on the same day.

1329 C. Cells were co-cultured as indicated (50:50 mix), then infected as in **(A)** and the % infection
1330 of each cell type was determined. n = 4 separate wells infected on the same day; ****, p
1331 ≤ 0.0001; two-tailed t-test.

1332 The data underlying this Figure can be found in **Supp Table 1**.

1333

1334 Figure 5. PLSCR1 restricts spike-mediated SARS-CoV-2 entry.

1335 A. A549-ACE2 cells were IF stained using an anti-PLSCR1 antibody (white) and Hoechst
1336 33342 nuclear staining (blue) and imaged at 63 X magnification on a confocal
1337 microscope.

1338 B. Focus forming assays: SARS-CoV-2 N IF (red) and Hoechst 33342 nuclear staining (blue)
1339 on similarly infected WT or PLSCR1 KO Huh-7.5 and A549-ACE2 cells after 2 and 3 d,
1340 respectively.

1341 C. Quantification of **(B)**.

1342 D. Huh-7.5 WT and PLSCR1 KO cells electroporated with SARS-CoV-2 replicon which
1343 produces a secreted luciferase. Luciferase activity assayed 24 hours after
1344 electroporation. n = 36 separate wells from a single electroporation event. Error bars
1345 represent sd; ns = non-significant; two-tailed t-test.

1346 E-F. Transduction of A549-ACE2 cells with an HIV-based replicon expressing the
1347 nanoluciferase pseudotyped with VSV-G or SARS-CoV-2 spike, respectively. n = 5
1348 separate wells transduced on the same day. Nanoluciferase signal measured 2 dpi. Error
1349 bars represent sd; ns, non-significant; **, $p \leq 0.01$; two-tailed t-test.

1350 G-I. A549 cells WT, expressing ACE2, or expressing ACE2-TMPRSS2 as indicated were
1351 transfected with PLSCR1 or non-template control (NTC) siRNAs as indicated for 3 d and
1352 infected with SARS-CoV-2 for 1 d. SARS-CoV-2 N was stained by IF and the percentage of
1353 positive cells was determined by imaging. n = 6 separate wells infected on the same day.
1354 Error bars represent sd; ns, non-significant; **, $p \leq 0.01$; ***, $p \leq 0.001$; two-tailed t-
1355 test.

1356 J-M. HEK293T cells expressing ACE2 or ACE2-TMPRSS2, as indicated, were transfected with
1357 siRNA knockdown of PLSCR1 or non-template control (NTC), as indicated, for 3 d and
1358 transduced with an HIV-based replicon expressing the nanoluciferase pseudotyped with
1359 VSV-G or SARS-CoV-2 spike, as indicated for 2 d. n = 3 separate wells transduced on the
1360 same day. Error bars represent sd; ns, non-significant; **, $p \leq 0.01$; two-tailed t-test.

1361 The data underlying this Figure can be found in **Supp Table 1**.

1362

1363 Figure 6. Newer variants of SARS-CoV-2 are less restricted by PLSCR1

1364 A-E. Infection of Huh-7.5 cells with SARS-CoV-2 (parental) or its descendant variants, Beta,
1365 Delta, Omicron BA.5, and Omicron XBB.1.5 for 24 hours. SARS-CoV-2 N was stained by
1366 IF and the percentage of positive cells determined by imaging. n = 10 separate wells
1367 infected on the same day. Error bars represent sd; ****, $p < 0.0001$; two-tailed t-test.

1368 F. Ratio of WT/KO percent infection from A-E. Error bars represent sd. ns, non-significant;
1369 ***, $p \leq 0.001$; ****, $p \leq 0.0001$; one-way ANOVA.

1370 G. Focus forming assay on Huh-7.5 WT and PLSCR1 KO cells infected with approximately 50
1371 FFU of SARS-CoV-2 variants as indicated. FFUs were determined on PLSCR1 KO Huh-7.5
1372 cells. Representative images.

1373 H. Foci from (**G**) were counted, and then a ratio of WT-to-KO plotted for each SARS-CoV-2
1374 variant. n = 6 separate wells infected on the same day. Error bars represent sd. **, $p \leq$
1375 0.01; one-way ANOVA.

1376 I. Virus production over an infectious time course (growth curve) for the parental SARS-
1377 CoV-2 strain. n = 2 to 3 separate wells infected on the same day. Error bars represent
1378 sd. ns, non-significant, *, $p \leq 0.05$, ***, $p \leq 0.001$, two-tailed t-test on the log10-
1379 transformed values.

1380 J. As in (**I**) with the Omicron (XBB.1.5) strain.

1381 The data underlying this Figure can be found in **Supp Table 1**.

1382

1383 Figure 7. PLSCR1 p.His262Tyr, which associates with severe COVID-19, leads to
1384 higher SARS-CoV-2 infection in cell culture.

1385 A. Protein diagram of PLSCR1. Domain coordinates from UniProt [197].

1386 B. CADD MAF plot showing the common variants of the PLSCR1 gene reported in gnomAD
1387 [132, 133]. The plot displays the Combined Annotation Dependent Depletion (CADD)
1388 scores, indicating the predicted deleteriousness of each variant, against the Minor Allele
1389 Frequency (MAF). Fs, frameshift.

1390 C. A549-ACE2 PLSCR1 KO cells were transduced to stably and ectopically express the
1391 indicated PLSCR1 variants. The cells were then infected for 24 h with SARS-CoV-2. SARS-

1392 CoV-2 N was stained by IF and the percentage of positive cells determined by imaging. n
1393 = 4 separate wells infected on the same day. Error bars represent sd; **, $p \leq 0.01$; ****, p
1394 < 0.0001; one-way ANOVA. Fs, frameshift.

1395 D. A549-ACE2 cells, WT and PLSCR1 KO, stably expressing N-terminal FLAG-tagged Firefly
1396 Luciferase (Fluc), N-terminal FLAG-tagged PLSCR1, or N-terminal FLAG-tagged PLSCR1
1397 H262Y mutant and infected with SARS-CoV-2 for 24 hours. SARS-CoV-2 N was stained by
1398 IF and the percentage of positive cells determined by imaging. n = 15 separate wells
1399 infected on the same day. Error bars represent sd; ****, $p \leq 0.0001$; two-tailed t-test.

1400 E. SV40-Fibroblast-ACE2 cells, genotype as indicated, infected for 24 hours with SARS-CoV-2.
1401 n = 8 separate wells infected on the same day. ns, non-significant; *, $p \leq 0.05$; **, $p \leq 0.01$;
1402 ****, $p \leq 0.0001$; one-way ANOVA.

1403 The data underlying this Figure can be found in **Supp Table 1**.

1404

1405 Supplementary Figure Legends

1406 Supplementary Figure 1.

1407 A. A schematic of SARS-CoV-2 entry and the sites where known ISG entry restriction factors
1408 function is shown, adapted from [1]. CD74 suppresses endolysosomal cathepsins, enzymes
1409 that process certain viral glycoproteins to make them fusion-competent [148, 198]. CH25H
1410 facilitates the sequestration of accessible cholesterol, which results in decreased virus-cell
1411 membrane fusion and viral entry [14, 63]. NCOA7 accelerates the acidification of the
1412 lysosome, leading to the degradation of viral antigens [161, 162]. The role of IFITM1-3
1413 proteins in SARS-CoV-2 entry has been the subject of numerous studies, which have
1414 sometimes yielded varying conclusions [1, 122, 199-205]. However, it appears that (i)
1415 IFITM2 restricts WT SARS-CoV-2 endosomal entry [122], (ii) recent SARS-CoV-2 variants
1416 may evade IFITM2 [199], and (iii) IFITM3 KO mice are hyper-susceptible to WT SARS-CoV-2
1417 [206]. LY6E and PLSCR1 restrict virus-cell membrane fusion at the endosome through
1418 unknown mechanisms, see [19, 121] and this study.

1419 B. TMPRSS2 western blot in Huh-7.5-Cas9 cells, both WT and TMPRSS2 KO, conducted as in
1420 the whole-genome arrayed screen (**Fig 1**), and in A549-ACE2 (A549 + A) and A549-ACE2-
1421 TMPRSS2 (A549 + A/T) cells.
1422

1423 ## Supplementary Figure 2.

1424 A. Model of protein levels of the gene product over time after complete KO, considering the
1425 Huh-7.5 cell division rate (1.7 times per day) and protein half-lives in hepatocytes from
1426 [207].
1427 B. Nuclei count (z-score) in arrayed genetic screen without SARS-CoV-2 infection. Examples
1428 of VCP (essential gene) and PLSCR1 (SARS-CoV-2 antiviral hit) are plotted.
1429 C. Volcano plot of Huh-7.5 cells mRNA-seq treated with 0.5 nM IFN-α2a for 24 h as in **Fig 1B**.
1430 D. Gene set enrichment analysis conducted on the arrayed CRISPR KO screens data
1431 represented in **Figs 1 and 2**. Description of the top pathways ranked by p-value for each
1432 quadrant. Databases: [1]Reactome; [2]WikiPathways; [3]Pathway Interaction Database; [4]KEGG;
1433 [5]Biocarta.
1434 The data underlying this Figure can be found in **Supp Table 1**.
1435

1436 ## Supplementary Figure 3

1437 A. Occurrence of human genes interacting with SARS-CoV-2 drawn from a selection of 67
1438 large-scale studies. The occurrence reflects the number of independent studies finding
1439 each gene as significant.
1440 B. Upset plot on data as in **(A)**, showing the overlap in significant genes in large-scale SARS-
1441 CoV-2 studies by category.
1442

1443 ## Supplementary Figure 4.

1444 Cross comparison between proviral and antiviral hits reported in this study and fifteen
1445 published whole-genome pooled screens [19, 31, 64-67, 69-71, 74, 75, 77-80]. P-value:
1446 Fisher's exact test.

1447

1448 ## Supplementary Figure 5.

1449 A. Western blot on PLSCR1 KO cells against PLSCR1 (green) and ß-actin (red).

1450 B. Cells as indicated were seeded at similar density, treated or not with Blasticidin (used here
1451 as a control to decrease cell viability), and cultured for 4 days before resazurin cell viability
1452 assay. n = 4 independent wells.

1453 C. Western blot on PLSCR1 WT and KO A549-ACE2 cells against PLSCR1 (green) and ß-actin
1454 (red).

1455 D. Single-cell RNA-seq data from [118], showing the *PLSCR1* mRNA expression in some SARS-
1456 CoV-2 target cells.

1457 The data underlying this Figure can be found in **Supp Table 1**.

1458

1459 ## Supplementary Figure 6.

1460 A. Huh-7.5 WT and PLSCR1 KO cells were infected with 17,000 FFU of CHIKV 181/25 mKate2
1461 for 12 or 24 hours, then fixed, IF stained for nuclei, and the percentage of positive cells
1462 determined by imaging for mKate2 reporter signal. n = 12 separate wells infected on the
1463 same day. Error bars represent sd. ns, non-significant; two-way ANOVA.

1464 B. Huh-7.5 cells, PLSCR1 KO as indicated, were pretreated with different amounts of IFN-α2a,
1465 then infected with 17,000 FFU of CHIKV-mKate for 12 h; n = 7 separate wells infected on
1466 the same day; error bars represent sd.

1467 C-J. Cells were treated for 24 h by IFN, as indicated, followed by RT-qPCRs on ISGs.

1468 The data underlying this Figure can be found in **Supp Table 1**.

1469

1470 ## Supplementary Figure 7.

1471 A. Western blot against PLSCR1 and RPS11. Cas-9-expressing Huh-7.5 cells were transfected
1472 with 4-gRNA pools targeting PLSCR1 or non-template control (as indicated) and cells were
1473 in culture for 7 d.

1474 B. Quantification of bands intensity in **(A)**.

1475 C. mRNA-seq on PLSCR1 KO Huh-7.5 cells as in **(A,B)**.

1476 The data underlying this Figure can be found in **Supp Table 1**.

1477

1478 ## Supplementary Figure 8.

1479 A. A549-ACE2 PLSCR1 KO cells were transduced to stably and ectopically express the
1480 indicated genes. The cells were then infected for 24 h with parental SARS-CoV-2. SARS-
1481 CoV-2 N was stained by IF and the percentage of positive cells determined by imaging. n
1482 = 4 separate wells infected on the same day. Error bars represent sd; **, $p \leq 0.01$; ****, p
1483 < 0.0001; one-way ANOVA.

1484 B. Normalised reads count from mRNA-seq on A549 cells treated or not with 0.5 nM IFN-α2a
1485 for 24 h.

1486 C. Normalised reads count from mRNA-seq on Huh-7.5 cells treated or not with 0.5 nM IFN-
1487 α2a for 24 h.

1488 The data underlying this Figure can be found in **Supp Table 1**.

1489

1490 ## Supplementary Figure 9.

1491 A-I. Infection of A549-ACE2 cells with viruses as indicated. IF staining was used for IAV WSN,
1492 hCoV-OC43 and SARS-CoV-2, otherwise a fluorescent reporter was used. Percentage of
1493 virus positive cells was determined by imaging. n = six separate wells infected on the
1494 same day, error bars represent SD; ns, non-significant; **, $p \leq 0.01$; ***, $p \leq 0.001$; ****,
1495 $p \leq 0.0001$; ****, $p \leq 0.0001$; two-tailed t-test.

1496 J-M. Infection of Huh-7.5 cells with viruses as indicated. siRNA knockdown of PLSCR1 vs non-
1497 template control (NTC). n = four to sixteen separate wells infected on the same day; ns,
1498 non-significant; ****, $p \leq 0.0001$; two-tailed t-test.

1499 The data underlying this Figure can be found in **Supp Table 1**.

1500

1501

1502 Supplementary Figure 10.

1503 Flow cytometry measuring ACE2 surface levels in live A549-ACE2 cells.

1504

1505 Supplementary Figure 11.

1506 A. Western Blot against PLSCR1 and β-actin (loading control). A549-ACE2 PLSCR1 KO cells
1507 were stably transduced with FLAG-tagged Fluc, FLAG-tagged PLSCR1, or FLAG-tagged
1508 PLSCR1 H262Y.

1509 B. Representative confocal images of A549-ACE2 cells treated with IFN-α2a for 48 h.

1510 C. Representative confocal images of A549-ACE2 cells infected with SARS-CoV-2 for 24 h.

1511

1512 Supplementary Figure 12.

1513 Representative images from the experiment shown in **Fig 7C**. A549-ACE2 PLSCR1 KO cells
1514 were transduced to stably and ectopically express the indicated PLSCR1 variants. The cells were
1515 then infected for 24 h with SARS-CoV-2 (**A**) or mock (**B**). SARS-CoV-2 N and PLSCR1 were stained
1516 and imaged

1517

1518 Supplementary Figure 13.

1519 Comparison between selected SARS-CoV-2 protein interactome studies [100-102, 104-
1520 109, 157].

1521

1522 Supplementary Figure 14.

1523 Comparison between the relative mRNA levels of 97 hallmark IFN-α-stimulated genes and
1524 the remaining transcriptome in cell lines as indicated. Red diamond, *PLSCR1* RNA level. For Huh-
1525 7.5 cells mRNA-seq, cells treated with 0.5 nM IFN-α2a for 24 h as in **Fig 2B**. For primary human
1526 hepatocytes, cells were treated with 0.1 nM IFN-α2a for 24 h (full data and methods to be
1527 released elsewhere). For the human tissues, data from [49].

1528 The data underlying this Figure can be found in **Supp Table 1**.

1529

1530 ## Supplementary Tables

1531 Available on Dryad (DOI: 10.5061/dryad.6q573n65k).

1532

1533 ### Supplementary Table 1.

1534 Data underlying Figures 1ABCEF, 2, 4ABC, 5CDEFGHIJKLM, 6ABCDEFHIJ, 7BCDE, S2ABC,
1535 S5BD, S6ABCDEFGHIJ, S7BC, S8ABC, S9ABCDEFGHIJKLM, S14

1536

1537 ### Supplementary Table 2.

1538 mRNA-seq on SARS-CoV-2 infected Calu-3 and Huh-7.5 cells, Normalized reads, related to
1539 **Fig 1A**.

1540

1541 ### Supplementary Table 3.

1542 mRNA-seq on SARS-CoV-2 infected Calu-3 and Huh-7.5 cells, Differential Gene Expression.

1543

1544 ### Supplementary Table 4.

1545 mRNA-seq on IFN-treated Calu-3 and Huh-7.5 cells, Normalized reads, related to **Fig 1B**,
1546 and **Supp Figs 8C and 13.**

1547

1548 ### Supplementary Table 5.

1549 mRNA-seq on IFN-treated Calu-3 and Huh-7.5 cells, Differential Gene Expression, related
1550 to **Fig 1F** and **Supp Fig 2C**.

1551

1552 ### Supplementary Table 6.

1553 Genes expressed in three cell lines relevant for SARS-CoV-2 research (A549, Calu-3, Huh-
1554 7.5 cells) and human lung cells [47-49].

1555

1556 Supplementary Table 7.

1557 Arrayed CRISPR KO screen, raw data.

1558

1559 Supplementary Table 8.

1560 Arrayed CRISPR KO screen, analyzed data. Related to **Fig. 1F** and **Supp Fig 2B**. Columns are
1561 as follow: *Stat.W1_SARS2_IFN_0pM*: cell growth z-score determined by nuclear staining in
1562 samples with no interferon pretreatment and with SARS-CoV-2 infection.
1563 *Stat.W1_SARS2_IFN_1pM*: cell growth z-score determined by nuclear staining in samples with
1564 interferon pretreatment and with SARS-CoV-2 infection. *Stat.W1_Uninfected_IFN_0pM*: cell
1565 growth z-score determined by nuclear staining in samples with no interferon pretreatment and
1566 no SARS-CoV-2 infection. *Stat.W2_SARS2_IFN_0pM*: SARS-CoV-2 infection z-score in samples with
1567 no interferon pretreatment and with SARS-CoV-2 infection. *Stat.W2_SARS2_IFN_1pM*: SARS-CoV-
1568 2 infection z-score in samples with interferon pretreatment and with SARS-CoV-2 infection.
1569 *Stat.W2_Uninfected_IFN_0pM*: SARS-CoV-2 infection z-score in samples with no interferon
1570 pretreatment and no SARS-CoV-2 infection. Index: random index used for plotting. RNAseq:
1571 classification of the gene as an interferon-stimulated gene ("ISG") or not ("NS") based on the
1572 accompanying mRNA-seq data.

1573

1574 Supplementary Table 9.

1575 Arrayed CRISPR KO screen, summary table.

1576

1577 Supplementary Table 10.

1578 GSEA on arrayed CRISPR KO screen. Related to **Supp Fig 2D**.

1579

1580 Supplementary Table 11.

1581 Consolidated list of human genes classified as hits in selected SARS-CoV-2 studies, full
1582 table. Related to **Fig 3** and **Supp Fig 3.**

1583

1584 Supplementary Table 12.

1585 Consolidated list of human genes classified as hits in selected SARS-CoV-2 studies,
1586 summary table. Related to **Fig 3** and **Supp Fig 3.**

1587

1588 Supplementary Table 13.

1589 Pathway analysis of hits from our arrayed screen alongside fifteen unbiased pooled
1590 screens [19, 31, 64-67, 69-71, 74, 75, 77-80] using the STRING database [208]. Related to **Supp**
1591 **Fig 4**.

1592

1593 Supplementary Table 14.

1594 mRNA-seq on PLSCR1 KO Huh-7.5 cells, Normalized reads, related to **Supp Fig 7C**.

1595

1596 Supplementary Table 15.

1597 mRNA-seq on PLSCR1 KO Huh-7.5 cells, Differential Gene Expression, related to **Supp Fig**
1598 **7C**.

1599

1600 Supplementary Table 16.

1601 mRNA-seq on IFN-treated A549 cells, Normalized reads, related to **Supp Fig 8B**.

1602

1603 Supplementary Table 17.

1604 mRNA-seq on IFN-treated A549 cells, Differential Gene Expression, related to **Supp Fig 8B**.

1605

1606 Supplementary Table 18.

1607 Plasmids used in this study.

1608

1609 Supplementary Table 19.

1610 Gene fragments used in this study.

1611

Supplementary Table 20.

Primers used in this study.

Supporting Information

Available on Dryad (DOI: 10.5061/dryad.6q573n65k).

Supporting Information 1

Raw images, related to **Supp Figs 1B, 5AC, 7A, 11**.

Supporting Information 2

Flow cytometry gating strategy, related to **Supp Fig 10**.

Supporting Information 3

Flow cytometry raw data, related to **Supp Fig 10**.

Supporting Information 4

mRNA-seq raw reads, related to **Supp Tables 2, 3, 4, 5, 14, 15, 16, 17**.

References

1. Le Pen J, Rice CM. The antiviral state of the cell: lessons from SARS-CoV-2. Curr Opin Immunol. 2024;87:102426. Epub 20240523. doi: 10.1016/j.coi.2024.102426. PubMed PMID: 38795501.
2. Bastard P, Zhang Q, Zhang SY, Jouanguy E, Casanova JL. Type I interferons and SARS-CoV-2: from cells to organisms. Curr Opin Immunol. 2022;74:172-82. Epub 20220125. doi: 10.1016/j.coi.2022.01.003. PubMed PMID: 35149239; PubMed Central PMCID: PMCPMC8786610.
3. Bastard P, Gervais A, Le Voyer T, Rosain J, Philippot Q, Manry J, et al. Autoantibodies neutralizing type I IFNs are present in ~4% of uninfected individuals over 70 years old and account for ~20% of COVID-19 deaths. Sci Immunol. 2021;6(62). Epub 2021/08/21. doi: 10.1126/sciimmunol.abl4340. PubMed PMID: 34413139.

1642 4. Lopez J, Mommert M, Mouton W, Pizzorno A, Brengel-Pesce K, Mezidi M, et al. Early nasal
1643 type I IFN immunity against SARS-CoV-2 is compromised in patients with autoantibodies against
1644 type I IFNs. J Exp Med. 2021;218(10). Epub 20210806. doi: 10.1084/jem.20211211. PubMed
1645 PMID: 34357402; PubMed Central PMCID: PMCPMC8352718.
1646 5. Asano T, Boisson B, Onodi F, Matuozzo D, Moncada-Velez M, Maglorius Renkilaraj MRL, et
1647 al. X-linked recessive TLR7 deficiency in ~1% of men under 60 years old with life-threatening
1648 COVID-19. Sci Immunol. 2021;6(62). doi: 10.1126/sciimmunol.abl4348. PubMed PMID:
1649 34413140; PubMed Central PMCID: PMCPMC8532080.
1650 6. Zhang Q, Bastard P, Liu Z, Le Pen J, Moncada-Velez M, Chen J, et al. Inborn errors of type I
1651 IFN immunity in patients with life-threatening COVID-19. Science. 2020;370(6515). Epub
1652 20200924. doi: 10.1126/science.abd4570. PubMed PMID: 32972995; PubMed Central PMCID:
1653 PMCPMC7857407.
1654 7. Bastard P, Rosen LB, Zhang Q, Michailidis E, Hoffmann HH, Zhang Y, et al. Autoantibodies
1655 against type I IFNs in patients with life-threatening COVID-19. Science. 2020;370(6515). Epub
1656 20200924. doi: 10.1126/science.abd4585. PubMed PMID: 32972996; PubMed Central PMCID:
1657 PMCPMC7857397.
1658 8. Zhang Q, Matuozzo D, Le Pen J, Lee D, Moens L, Asano T, et al. Recessive inborn errors of
1659 type I IFN immunity in children with COVID-19 pneumonia. J Exp Med. 2022;219(8). Epub
1660 20220616. doi: 10.1084/jem.20220131. PubMed PMID: 35708626; PubMed Central PMCID:
1661 PMCPMC9206114.
1662 9. Zhou P, Yang XL, Wang XG, Hu B, Zhang L, Zhang W, et al. A pneumonia outbreak associated
1663 with a new coronavirus of probable bat origin. Nature. 2020;579(7798):270-3. Epub 20200203.
1664 doi: 10.1038/s41586-020-2012-7. PubMed PMID: 32015507; PubMed Central PMCID:
1665 PMCPMC7095418.
1666 10. Savan R, Gale M, Jr. Innate immunity and interferon in SARS-CoV-2 infection outcome.
1667 Immunity. 2023;56(7):1443-50. doi: 10.1016/j.immuni.2023.06.018. PubMed PMID: 37437537;
1668 PubMed Central PMCID: PMCPMC10361255.
1669 11. Danziger O, Patel RS, DeGrace EJ, Rosen MR, Rosenberg BR. Inducible CRISPR activation
1670 screen for interferon-stimulated genes identifies OAS1 as a SARS-CoV-2 restriction factor. PLoS
1671 Pathog. 2022;18(4):e1010464. Epub 20220414. doi: 10.1371/journal.ppat.1010464. PubMed
1672 PMID: 35421191; PubMed Central PMCID: PMCPMC9041830.
1673 12. Martin-Sancho L, Lewinski MK, Pache L, Stoneham CA, Yin X, Becker ME, et al. Functional
1674 landscape of SARS-CoV-2 cellular restriction. Mol Cell. 2021;81(12):2656-68 e8. Epub 20210413.
1675 doi: 10.1016/j.molcel.2021.04.008. PubMed PMID: 33930332; PubMed Central PMCID:
1676 PMCPMC8043580.
1677 13. Wickenhagen A, Sugrue E, Lytras S, Kuchi S, Noerenberg M, Turnbull ML, et al. A prenylated
1678 dsRNA sensor protects against severe COVID-19. Science. 2021;374(6567):eabj3624. Epub
1679 20211029. doi: 10.1126/science.abj3624. PubMed PMID: 34581622.
1680 14. Zang R, Case JB, Yutuc E, Ma X, Shen S, Gomez Castro MF, et al. Cholesterol 25-hydroxylase
1681 suppresses SARS-CoV-2 replication by blocking membrane fusion. Proc Natl Acad Sci U S A.
1682 2020;117(50):32105-13. Epub 20201125. doi: 10.1073/pnas.2012197117. PubMed PMID:
1683 33239446; PubMed Central PMCID: PMCPMC7749331.

1684 15. Kaur R, Tada T, Landau NR. Restriction of SARS-CoV-2 replication by receptor transporter
1685 protein 4 (RTP4). mBio. 2023;14(4):e0109023. Epub 20230629. doi: 10.1128/mbio.01090-23.
1686 PubMed PMID: 37382452; PubMed Central PMCID: PMCPMC10470548.
1687 16. Schoggins JW, Wilson SJ, Panis M, Murphy MY, Jones CT, Bieniasz P, et al. A diverse range
1688 of gene products are effectors of the type I interferon antiviral response. Nature.
1689 2011;472(7344):481-5. Epub 20110410. doi: 10.1038/nature09907. PubMed PMID: 21478870;
1690 PubMed Central PMCID: PMCPMC3409588.
1691 17. Schoggins JW. Interferon-Stimulated Genes: What Do They All Do? Annu Rev Virol.
1692 2019;6(1):567-84. Epub 2019/07/10. doi: 10.1146/annurev-virology-092818-015756. PubMed
1693 PMID: 31283436.
1694 18. Mac Kain A, Maarifi G, Aicher SM, Arhel N, Baidaliuk A, Munier S, et al. Identification of
1695 DAXX as a restriction factor of SARS-CoV-2 through a CRISPR/Cas9 screen. Nat Commun.
1696 2022;13(1):2442. Epub 20220504. doi: 10.1038/s41467-022-30134-9. PubMed PMID: 35508460;
1697 PubMed Central PMCID: PMCPMC9068693.
1698 19. Xu D, Jiang W, Wu L, Gaudet RG, Park ES, Su M, et al. PLSCR1 is a cell-autonomous defence
1699 factor against SARS-CoV-2 infection. Nature. 2023;619(7971):819-27. Epub 20230712. doi:
1700 10.1038/s41586-023-06322-y. PubMed PMID: 37438530; PubMed Central PMCID:
1701 PMCPMC10371867.
1702 20. Kim HS, Lee K, Kim SJ, Cho S, Shin HJ, Kim C, et al. Arrayed CRISPR screen with image-based
1703 assay reliably uncovers host genes required for coxsackievirus infection. Genome Res.
1704 2018;28(6):859-68. Epub 20180430. doi: 10.1101/gr.230250.117. PubMed PMID: 29712754;
1705 PubMed Central PMCID: PMCPMC5991512.
1706 21. Cross BC, Lawo S, Archer CR, Hunt JR, Yarker JL, Riccombeni A, et al. Increasing the
1707 performance of pooled CRISPR-Cas9 drop-out screening. Sci Rep. 2016;6:31782. Epub 20160822.
1708 doi: 10.1038/srep31782. PubMed PMID: 27545104; PubMed Central PMCID: PMCPMC4992892.
1709 22. Kodigepalli KM, Bowers K, Sharp A, Nanjundan M. Roles and regulation of phospholipid
1710 scramblases. FEBS Lett. 2015;589(1):3-14. Epub 20141203. doi: 10.1016/j.febslet.2014.11.036.
1711 PubMed PMID: 25479087.
1712 23. Zhou Q, Zhao J, Stout JG, Luhm RA, Wiedmer T, Sims PJ. Molecular cloning of human
1713 plasma membrane phospholipid scramblase. A protein mediating transbilayer movement of
1714 plasma membrane phospholipids. J Biol Chem. 1997;272(29):18240-4. doi:
1715 10.1074/jbc.272.29.18240. PubMed PMID: 9218461.
1716 24. Dong B, Zhou Q, Zhao J, Zhou A, Harty RN, Bose S, et al. Phospholipid scramblase 1
1717 potentiates the antiviral activity of interferon. J Virol. 2004;78(17):8983-93. doi:
1718 10.1128/JVI.78.17.8983-8993.2004. PubMed PMID: 15308695; PubMed Central PMCID:
1719 PMCPMC506946.
1720 25. Pairo-Castineira E, Rawlik K, Bretherick AD, Qi T, Wu Y, Nassiri I, et al. GWAS and meta-
1721 analysis identifies 49 genetic variants underlying critical COVID-19. Nature. 2023;617(7962):764-
1722 8. Epub 20230517. doi: 10.1038/s41586-023-06034-3. PubMed PMID: 37198478; PubMed
1723 Central PMCID: PMCPMC10208981.
1724 26. Kousathanas A, Pairo-Castineira E, Rawlik K, Stuckey A, Odhams CA, Walker S, et al. Whole-
1725 genome sequencing reveals host factors underlying critical COVID-19. Nature.

2022;607(7917):97-103. Epub 20220307. doi: 10.1038/s41586-022-04576-6. PubMed PMID: 35255492; PubMed Central PMCID: PMCPMC9259496.

27. Baggen J, Vanstreels E, Jansen S, Daelemans D. Cellular host factors for SARS-CoV-2 infection. Nat Microbiol. 2021;6(10):1219-32. Epub 20210901. doi: 10.1038/s41564-021-00958-0. PubMed PMID: 34471255.

28. Hoffmann HH, Sanchez-Rivera FJ, Schneider WM, Luna JM, Soto-Feliciano YM, Ashbrook AW, et al. Functional interrogation of a SARS-CoV-2 host protein interactome identifies unique and shared coronavirus host factors. Cell Host Microbe. 2021;29(2):267-80 e5. Epub 20201216. doi: 10.1016/j.chom.2020.12.009. PubMed PMID: 33357464; PubMed Central PMCID: PMCPMC7833927.

29. Li Q, Wu J, Nie J, Zhang L, Hao H, Liu S, et al. The Impact of Mutations in SARS-CoV-2 Spike on Viral Infectivity and Antigenicity. Cell. 2020;182(5):1284-94 e9. Epub 20200717. doi: 10.1016/j.cell.2020.07.012. PubMed PMID: 32730807; PubMed Central PMCID: PMCPMC7366990.

30. Riva L, Yuan S, Yin X, Martin-Sancho L, Matsunaga N, Pache L, et al. Discovery of SARS-CoV-2 antiviral drugs through large-scale compound repurposing. Nature. 2020;586(7827):113-9. Epub 20200724. doi: 10.1038/s41586-020-2577-1. PubMed PMID: 32707573; PubMed Central PMCID: PMCPMC7603405.

31. Schneider WM, Luna JM, Hoffmann HH, Sanchez-Rivera FJ, Leal AA, Ashbrook AW, et al. Genome-Scale Identification of SARS-CoV-2 and Pan-coronavirus Host Factor Networks. Cell. 2021;184(1):120-32 e14. Epub 20201209. doi: 10.1016/j.cell.2020.12.006. PubMed PMID: 33382968; PubMed Central PMCID: PMCPMC7796900.

32. Xia S, Lan Q, Su S, Wang X, Xu W, Liu Z, et al. The role of furin cleavage site in SARS-CoV-2 spike protein-mediated membrane fusion in the presence or absence of trypsin. Signal Transduct Target Ther. 2020;5(1):92. Epub 20200612. doi: 10.1038/s41392-020-0184-0. PubMed PMID: 32532959; PubMed Central PMCID: PMCPMC7289711.

33. Xia S, Liu M, Wang C, Xu W, Lan Q, Feng S, et al. Inhibition of SARS-CoV-2 (previously 2019-nCoV) infection by a highly potent pan-coronavirus fusion inhibitor targeting its spike protein that harbors a high capacity to mediate membrane fusion. Cell Res. 2020;30(4):343-55. Epub 20200330. doi: 10.1038/s41422-020-0305-x. PubMed PMID: 32231345; PubMed Central PMCID: PMCPMC7104723.

34. Yan Y, Chang L, Wang L. Laboratory testing of SARS-CoV, MERS-CoV, and SARS-CoV-2 (2019-nCoV): Current status, challenges, and countermeasures. Rev Med Virol. 2020;30(3):e2106. Epub 20200417. doi: 10.1002/rmv.2106. PubMed PMID: 32302058; PubMed Central PMCID: PMCPMC7235496.

35. Sumpter R, Jr., Loo YM, Foy E, Li K, Yoneyama M, Fujita T, et al. Regulating intracellular antiviral defense and permissiveness to hepatitis C virus RNA replication through a cellular RNA helicase, RIG-I. J Virol. 2005;79(5):2689-99. doi: 10.1128/JVI.79.5.2689-2699.2005. PubMed PMID: 15708988; PubMed Central PMCID: PMCPMC548482.

36. Matsuyama S, Nao N, Shirato K, Kawase M, Saito S, Takayama I, et al. Enhanced isolation of SARS-CoV-2 by TMPRSS2-expressing cells. Proc Natl Acad Sci U S A. 2020;117(13):7001-3. Epub 20200312. doi: 10.1073/pnas.2002589117. PubMed PMID: 32165541; PubMed Central PMCID: PMCPMC7132130.

1769 37. Hoffmann M, Kleine-Weber H, Schroeder S, Kruger N, Herrler T, Erichsen S, et al. SARS-
1770 CoV-2 Cell Entry Depends on ACE2 and TMPRSS2 and Is Blocked by a Clinically Proven Protease
1771 Inhibitor. Cell. 2020;181(2):271-80 e8. Epub 20200305. doi: 10.1016/j.cell.2020.02.052. PubMed
1772 PMID: 32142651; PubMed Central PMCID: PMCPMC7102627.
1773 38. Jackson CB, Farzan M, Chen B, Choe H. Mechanisms of SARS-CoV-2 entry into cells. Nat
1774 Rev Mol Cell Biol. 2022;23(1):3-20. Epub 20211005. doi: 10.1038/s41580-021-00418-x. PubMed
1775 PMID: 34611326; PubMed Central PMCID: PMCPMC8491763.
1776 39. de Weerd NA, Samarajiwa SA, Hertzog PJ. Type I interferon receptors: biochemistry and
1777 biological functions. J Biol Chem. 2007;282(28):20053-7. Epub 20070514. doi:
1778 10.1074/jbc.R700006200. PubMed PMID: 17502368.
1779 40. de Weerd NA, Nguyen T. The interferons and their receptors--distribution and regulation.
1780 Immunol Cell Biol. 2012;90(5):483-91. Epub 20120313. doi: 10.1038/icb.2012.9. PubMed PMID:
1781 22410872; PubMed Central PMCID: PMCPMC7165917.
1782 41. Uze G, Schreiber G, Piehler J, Pellegrini S. The receptor of the type I interferon family. Curr
1783 Top Microbiol Immunol. 2007;316:71-95. doi: 10.1007/978-3-540-71329-6_5. PubMed PMID:
1784 17969444.
1785 42. Perng YC, Lenschow DJ. ISG15 in antiviral immunity and beyond. Nat Rev Microbiol.
1786 2018;16(7):423-39. doi: 10.1038/s41579-018-0020-5. PubMed PMID: 29769653; PubMed Central
1787 PMCID: PMCPMC7097117.
1788 43. Speer SD, Li Z, Buta S, Payelle-Brogard B, Qian L, Vigant F, et al. ISG15 deficiency and
1789 increased viral resistance in humans but not mice. Nat Commun. 2016;7:11496. Epub 20160519.
1790 doi: 10.1038/ncomms11496. PubMed PMID: 27193971; PubMed Central PMCID:
1791 PMCPMC4873964.
1792 44. Zhang X, Bogunovic D, Payelle-Brogard B, Francois-Newton V, Speer SD, Yuan C, et al.
1793 Human intracellular ISG15 prevents interferon-alpha/beta over-amplification and auto-
1794 inflammation. Nature. 2015;517(7532):89-93. Epub 20141012. doi: 10.1038/nature13801.
1795 PubMed PMID: 25307056; PubMed Central PMCID: PMCPMC4303590.
1796 45. Malakhova OA, Kim KI, Luo JK, Zou W, Kumar KG, Fuchs SY, et al. UBP43 is a novel regulator
1797 of interferon signaling independent of its ISG15 isopeptidase activity. EMBO J. 2006;25(11):2358-
1798 67. Epub 20060518. doi: 10.1038/sj.emboj.7601149. PubMed PMID: 16710296; PubMed Central
1799 PMCID: PMCPMC1478183.
1800 46. Francois-Newton V, Magno de Freitas Almeida G, Payelle-Brogard B, Monneron D, Pichard-
1801 Garcia L, Piehler J, et al. USP18-based negative feedback control is induced by type I and type III
1802 interferons and specifically inactivates interferon alpha response. PLoS One. 2011;6(7):e22200.
1803 Epub 20110714. doi: 10.1371/journal.pone.0022200. PubMed PMID: 21779393; PubMed Central
1804 PMCID: PMCPMC3136508.
1805 47. Barretina J, Caponigro G, Stransky N, Venkatesan K, Margolin AA, Kim S, et al. The Cancer
1806 Cell Line Encyclopedia enables predictive modelling of anticancer drug sensitivity. Nature.
1807 2012;483(7391):603-7. Epub 20120328. doi: 10.1038/nature11003. PubMed PMID: 22460905;
1808 PubMed Central PMCID: PMCPMC3320027.
1809 48. Klijn C, Durinck S, Stawiski EW, Haverty PM, Jiang Z, Liu H, et al. A comprehensive
1810 transcriptional portrait of human cancer cell lines. Nat Biotechnol. 2015;33(3):306-12. Epub
1811 20141208. doi: 10.1038/nbt.3080. PubMed PMID: 25485619.

1812 49. Consortium GT. Human genomics. The Genotype-Tissue Expression (GTEx) pilot analysis:
1813 multitissue gene regulation in humans. Science. 2015;348(6235):648-60. Epub 20150507. doi:
1814 10.1126/science.1262110. PubMed PMID: 25954001; PubMed Central PMCID:
1815 PMCPMC4547484.
1816 50. Horvath CM, Stark GR, Kerr IM, Darnell JE, Jr. Interactions between STAT and non-STAT
1817 proteins in the interferon-stimulated gene factor 3 transcription complex. Mol Cell Biol.
1818 1996;16(12):6957-64. doi: 10.1128/MCB.16.12.6957. PubMed PMID: 8943351; PubMed Central
1819 PMCID: PMCPMC231699.
1820 51. Veals SA, Schindler C, Leonard D, Fu XY, Aebersold R, Darnell JE, Jr., et al. Subunit of an
1821 alpha-interferon-responsive transcription factor is related to interferon regulatory factor and Myb
1822 families of DNA-binding proteins. Mol Cell Biol. 1992;12(8):3315-24. doi:
1823 10.1128/mcb.12.8.3315-3324.1992. PubMed PMID: 1630447; PubMed Central PMCID:
1824 PMCPMC364572.
1825 52. Darnell JE, Jr., Kerr IM, Stark GR. Jak-STAT pathways and transcriptional activation in
1826 response to IFNs and other extracellular signaling proteins. Science. 1994;264(5164):1415-21.
1827 doi: 10.1126/science.8197455. PubMed PMID: 8197455.
1828 53. Schindler C, Strehlow I. Cytokines and STAT signaling. Adv Pharmacol. 2000;47:113-74.
1829 doi: 10.1016/s1054-3589(08)60111-8. PubMed PMID: 10582086.
1830 54. Levy DE, Darnell JE, Jr. Stats: transcriptional control and biological impact. Nat Rev Mol
1831 Cell Biol. 2002;3(9):651-62. doi: 10.1038/nrm909. PubMed PMID: 12209125.
1832 55. Naka T, Narazaki M, Hirata M, Matsumoto T, Minamoto S, Aono A, et al. Structure and
1833 function of a new STAT-induced STAT inhibitor. Nature. 1997;387(6636):924-9. doi:
1834 10.1038/43219. PubMed PMID: 9202127.
1835 56. Ziegler CGK, Allon SJ, Nyquist SK, Mbano IM, Miao VN, Tzouanas CN, et al. SARS-CoV-2
1836 Receptor ACE2 Is an Interferon-Stimulated Gene in Human Airway Epithelial Cells and Is Detected
1837 in Specific Cell Subsets across Tissues. Cell. 2020;181(5):1016-35 e19. Epub 20200427. doi:
1838 10.1016/j.cell.2020.04.035. PubMed PMID: 32413319; PubMed Central PMCID:
1839 PMCPMC7252096.
1840 57. Onabajo OO, Banday AR, Stanifer ML, Yan W, Obajemu A, Santer DM, et al. Interferons and
1841 viruses induce a novel truncated ACE2 isoform and not the full-length SARS-CoV-2 receptor. Nat
1842 Genet. 2020;52(12):1283-93. Epub 20201019. doi: 10.1038/s41588-020-00731-9. PubMed PMID:
1843 33077916; PubMed Central PMCID: PMCPMC9377523.
1844 58. Zhao MM, Yang WL, Yang FY, Zhang L, Huang WJ, Hou W, et al. Cathepsin L plays a key role
1845 in SARS-CoV-2 infection in humans and humanized mice and is a promising target for new drug
1846 development. Signal Transduct Target Ther. 2021;6(1):134. Epub 20210327. doi: 10.1038/s41392-
1847 021-00558-8. PubMed PMID: 33774649; PubMed Central PMCID: PMCPMC7997800.
1848 59. Shang J, Wan Y, Luo C, Ye G, Geng Q, Auerbach A, et al. Cell entry mechanisms of SARS-
1849 CoV-2. Proc Natl Acad Sci U S A. 2020;117(21):11727-34. Epub 20200506. doi:
1850 10.1073/pnas.2003138117. PubMed PMID: 32376634; PubMed Central PMCID:
1851 PMCPMC7260975.
1852 60. Liu T, Luo S, Libby P, Shi GP. Cathepsin L-selective inhibitors: A potentially promising
1853 treatment for COVID-19 patients. Pharmacol Ther. 2020;213:107587. Epub 20200526. doi:

10.1016/j.pharmthera.2020.107587. PubMed PMID: 32470470; PubMed Central PMCID: PMCPMC7255230.

61. Pellegrini S, John J, Shearer M, Kerr IM, Stark GR. Use of a selectable marker regulated by alpha interferon to obtain mutations in the signaling pathway. Mol Cell Biol. 1989;9(11):4605-12. doi: 10.1128/mcb.9.11.4605-4612.1989. PubMed PMID: 2513475; PubMed Central PMCID: PMCPMC363606.

62. Velazquez L, Fellous M, Stark GR, Pellegrini S. A protein tyrosine kinase in the interferon alpha/beta signaling pathway. Cell. 1992;70(2):313-22. doi: 10.1016/0092-8674(92)90105-l. PubMed PMID: 1386289.

63. Wang S, Li W, Hui H, Tiwari SK, Zhang Q, Croker BA, et al. Cholesterol 25-Hydroxylase inhibits SARS-CoV-2 and other coronaviruses by depleting membrane cholesterol. EMBO J. 2020;39(21):e106057. Epub 20201005. doi: 10.15252/embj.2020106057. PubMed PMID: 32944968; PubMed Central PMCID: PMCPMC7537045.

64. Zhu Y, Feng F, Hu G, Wang Y, Yu Y, Zhu Y, et al. A genome-wide CRISPR screen identifies host factors that regulate SARS-CoV-2 entry. Nat Commun. 2021;12(1):961. Epub 20210211. doi: 10.1038/s41467-021-21213-4. PubMed PMID: 33574281; PubMed Central PMCID: PMCPMC7878750.

65. Wei LH, Sun Y, Guo JU. Genome-wide CRISPR screens identify noncanonical translation factor eIF2A as an enhancer of SARS-CoV-2 programmed -1 ribosomal frameshifting. Cell Rep. 2023;42(8):112987. Epub 20230814. doi: 10.1016/j.celrep.2023.112987. PubMed PMID: 37581984.

66. Wei J, Alfajaro MM, DeWeirdt PC, Hanna RE, Lu-Culligan WJ, Cai WL, et al. Genome-wide CRISPR Screens Reveal Host Factors Critical for SARS-CoV-2 Infection. Cell. 2021;184(1):76-91 e13. Epub 20201020. doi: 10.1016/j.cell.2020.10.028. PubMed PMID: 33147444; PubMed Central PMCID: PMCPMC7574718.

67. Wang R, Simoneau CR, Kulsuptrakul J, Bouhaddou M, Travisano KA, Hayashi JM, et al. Genetic Screens Identify Host Factors for SARS-CoV-2 and Common Cold Coronaviruses. Cell. 2021;184(1):106-19 e14. Epub 20201209. doi: 10.1016/j.cell.2020.12.004. PubMed PMID: 33333024; PubMed Central PMCID: PMCPMC7723770.

68. Song J, Chow RD, Pena-Hernandez MA, Zhang L, Loeb SA, So EY, et al. LRRC15 inhibits SARS-CoV-2 cellular entry in trans. PLoS Biol. 2022;20(10):e3001805. Epub 20221013. doi: 10.1371/journal.pbio.3001805. PubMed PMID: 36228039; PubMed Central PMCID: PMCPMC9595563.

69. Hossain MS, Kerkvliet JG, Hoppe AD. Whole genome CRISPR screening strategy to identify genes contributing to SARS-CoV-2 spike and VSV-G mediated entry. J Med Virol. 2023;95(9):e29087. doi: 10.1002/jmv.29087. PubMed PMID: 37707319.

70. Rehfeld F, Eitson JL, Ohlson MB, Chang TC, Schoggins JW, Mendell JT. CRISPR screening reveals a dependency on ribosome recycling for efficient SARS-CoV-2 programmed ribosomal frameshifting and viral replication. Cell Rep. 2023;42(2):112076. Epub 20230130. doi: 10.1016/j.celrep.2023.112076. PubMed PMID: 36753415; PubMed Central PMCID: PMCPMC9884621.

71. Rebendenne A, Roy P, Bonaventure B, Chaves Valadao AL, Desmarets L, Arnaud-Arnould M, et al. Bidirectional genome-wide CRISPR screens reveal host factors regulating SARS-CoV-2,

1897 MERS-CoV and seasonal HCoVs. Nat Genet. 2022;54(8):1090-102. Epub 20220725. doi:
1898 10.1038/s41588-022-01110-2. PubMed PMID: 35879413.
1899 72. Pahmeier F, Lavacca TM, Goellner S, Neufeldt CJ, Prasad V, Cerikan B, et al. Identification
1900 of host dependency factors involved in SARS-CoV-2 replication organelle formation through
1901 proteomics and ultrastructural analysis. J Virol. 2023:e0087823. Epub 20231031. doi:
1902 10.1128/jvi.00878-23. PubMed PMID: 37905840.
1903 73. Loo L, Waller MA, Moreno CL, Cole AJ, Stella AO, Pop OT, et al. Fibroblast-expressed
1904 LRRC15 is a receptor for SARS-CoV-2 spike and controls antiviral and antifibrotic transcriptional
1905 programs. PLoS Biol. 2023;21(2):e3001967. Epub 20230209. doi: 10.1371/journal.pbio.3001967.
1906 PubMed PMID: 36757924; PubMed Central PMCID: PMCPMC9910744.
1907 74. Israeli M, Finkel Y, Yahalom-Ronen Y, Paran N, Chitlaru T, Israeli O, et al. Genome-wide
1908 CRISPR screens identify GATA6 as a proviral host factor for SARS-CoV-2 via modulation of ACE2.
1909 Nat Commun. 2022;13(1):2237. Epub 20220425. doi: 10.1038/s41467-022-29896-z. PubMed
1910 PMID: 35469023; PubMed Central PMCID: PMCPMC9039069.
1911 75. Grodzki M, Bluhm AP, Schaefer M, Tagmount A, Russo M, Sobh A, et al. Genome-scale
1912 CRISPR screens identify host factors that promote human coronavirus infection. Genome Med.
1913 2022;14(1):10. Epub 20220127. doi: 10.1186/s13073-022-01013-1. PubMed PMID: 35086559;
1914 PubMed Central PMCID: PMCPMC8792531.
1915 76. Gordon DE, Hiatt J, Bouhaddou M, Rezelj VV, Ulferts S, Braberg H, et al. Comparative host-
1916 coronavirus protein interaction networks reveal pan-viral disease mechanisms. Science.
1917 2020;370(6521). Epub 20201015. doi: 10.1126/science.abe9403. PubMed PMID: 33060197;
1918 PubMed Central PMCID: PMCPMC7808408.
1919 77. Daniloski Z, Jordan TX, Wessels HH, Hoagland DA, Kasela S, Legut M, et al. Identification
1920 of Required Host Factors for SARS-CoV-2 Infection in Human Cells. Cell. 2021;184(1):92-105 e16.
1921 Epub 20201024. doi: 10.1016/j.cell.2020.10.030. PubMed PMID: 33147445; PubMed Central
1922 PMCID: PMCPMC7584921.
1923 78. Chan K, Farias AG, Lee H, Guvenc F, Mero P, Brown KR, et al. Survival-based CRISPR genetic
1924 screens across a panel of permissive cell lines identify common and cell-specific SARS-CoV-2 host
1925 factors. Heliyon. 2023;9(1):e12744. Epub 20221230. doi: 10.1016/j.heliyon.2022.e12744.
1926 PubMed PMID: 36597481; PubMed Central PMCID: PMCPMC9800021.
1927 79. Biering SB, Sarnik SA, Wang E, Zengel JR, Leist SR, Schafer A, et al. Genome-wide
1928 bidirectional CRISPR screens identify mucins as host factors modulating SARS-CoV-2 infection. Nat
1929 Genet. 2022;54(8):1078-89. Epub 20220725. doi: 10.1038/s41588-022-01131-x. PubMed PMID:
1930 35879412; PubMed Central PMCID: PMCPMC9355872.
1931 80. Baggen J, Persoons L, Vanstreels E, Jansen S, Van Looveren D, Boeckx B, et al. Genome-
1932 wide CRISPR screening identifies TMEM106B as a proviral host factor for SARS-CoV-2. Nat Genet.
1933 2021;53(4):435-44. Epub 20210308. doi: 10.1038/s41588-021-00805-2. PubMed PMID:
1934 33686287.
1935 81. van der Made CI, Simons A, Schuurs-Hoeijmakers J, van den Heuvel G, Mantere T, Kersten
1936 S, et al. Presence of Genetic Variants Among Young Men With Severe COVID-19. JAMA.
1937 2020;324(7):663-73. doi: 10.1001/jama.2020.13719. PubMed PMID: 32706371; PubMed Central
1938 PMCID: PMCPMC7382021.

82. Shelton JF, Shastri AJ, Ye C, Weldon CH, Filshtein-Sonmez T, Coker D, et al. Trans-ancestry analysis reveals genetic and nongenetic associations with COVID-19 susceptibility and severity. Nat Genet. 2021;53(6):801-8. Epub 20210422. doi: 10.1038/s41588-021-00854-7. PubMed PMID: 33888907.

83. Roberts GHL, Partha R, Rhead B, Knight SC, Park DS, Coignet MV, et al. Expanded COVID-19 phenotype definitions reveal distinct patterns of genetic association and protective effects. Nat Genet. 2022;54(4):374-81. Epub 20220411. doi: 10.1038/s41588-022-01042-x. PubMed PMID: 35410379.

84. Pietzner M, Chua RL, Wheeler E, Jechow K, Willett JDS, Radbruch H, et al. ELF5 is a potential respiratory epithelial cell-specific risk gene for severe COVID-19. Nat Commun. 2022;13(1):4484. Epub 20220815. doi: 10.1038/s41467-022-31999-6. PubMed PMID: 35970849; PubMed Central PMCID: PMCPMC9378714.

85. Latini A, Agolini E, Novelli A, Borgiani P, Giannini R, Gravina P, et al. COVID-19 and Genetic Variants of Protein Involved in the SARS-CoV-2 Entry into the Host Cells. Genes (Basel). 2020;11(9). Epub 20200827. doi: 10.3390/genes11091010. PubMed PMID: 32867305; PubMed Central PMCID: PMCPMC7565048.

86. Horowitz JE, Kosmicki JA, Damask A, Sharma D, Roberts GHL, Justice AE, et al. Genome-wide analysis provides genetic evidence that ACE2 influences COVID-19 risk and yields risk scores associated with severe disease. Nat Genet. 2022;54(4):382-92. Epub 20220303. doi: 10.1038/s41588-021-01006-7. PubMed PMID: 35241825; PubMed Central PMCID: PMCPMC9005345.

87. Garcia-Garcia A, Perez de Diego R, Flores C, Rinchai D, Sole-Violan J, Deya-Martinez A, et al. Humans with inherited MyD88 and IRAK-4 deficiencies are predisposed to hypoxemic COVID-19 pneumonia. J Exp Med. 2023;220(5). Epub 20230303. doi: 10.1084/jem.20220170. PubMed PMID: 36880831; PubMed Central PMCID: PMCPMC9998661.

88. Fallerini C, Daga S, Mantovani S, Benetti E, Picchiotti N, Francisci D, et al. Association of Toll-like receptor 7 variants with life-threatening COVID-19 disease in males: findings from a nested case-control study. Elife. 2021;10. Epub 20210302. doi: 10.7554/eLife.67569. PubMed PMID: 33650967; PubMed Central PMCID: PMCPMC7987337.

89. Severe Covid GG, Ellinghaus D, Degenhardt F, Bujanda L, Buti M, Albillos A, et al. Genomewide Association Study of Severe Covid-19 with Respiratory Failure. N Engl J Med. 2020;383(16):1522-34. Epub 20200617. doi: 10.1056/NEJMoa2020283. PubMed PMID: 32558485; PubMed Central PMCID: PMCPMC7315890.

90. Degenhardt F, Ellinghaus D, Juzenas S, Lerga-Jaso J, Wendorff M, Maya-Miles D, et al. Detailed stratified GWAS analysis for severe COVID-19 in four European populations. Hum Mol Genet. 2022;31(23):3945-66. doi: 10.1093/hmg/ddac158. PubMed PMID: 35848942; PubMed Central PMCID: PMCPMC9703941.

91. D'Antonio M, Nguyen JP, Arthur TD, Matsui H, Initiative C-HG, D'Antonio-Chronowska A, et al. SARS-CoV-2 susceptibility and COVID-19 disease severity are associated with genetic variants affecting gene expression in a variety of tissues. Cell Rep. 2021;37(7):110020. Epub 20211103. doi: 10.1016/j.celrep.2021.110020. PubMed PMID: 34762851; PubMed Central PMCID: PMCPMC8563343.

1981 92. Cruz R, Diz-de Almeida S, Lopez de Heredia M, Quintela I, Ceballos FC, Pita G, et al. Novel
1982 genes and sex differences in COVID-19 severity. Hum Mol Genet. 2022;31(22):3789-806. doi:
1983 10.1093/hmg/ddac132. PubMed PMID: 35708486; PubMed Central PMCID: PMCPMC9652109.
1984 93. Initiative C-HG. A first update on mapping the human genetic architecture of COVID-19.
1985 Nature. 2022;608(7921):E1-E10. Epub 20220803. doi: 10.1038/s41586-022-04826-7. PubMed
1986 PMID: 35922517; PubMed Central PMCID: PMCPMC9352569.
1987 94. Andolfo I, Russo R, Lasorsa VA, Cantalupo S, Rosato BE, Bonfiglio F, et al. Common variants
1988 at 21q22.3 locus influence MX1 and TMPRSS2 gene expression and susceptibility to severe COVID-
1989 19. iScience. 2021;24(4):102322. Epub 20210317. doi: 10.1016/j.isci.2021.102322. PubMed
1990 PMID: 33748697; PubMed Central PMCID: PMCPMC7968217.
1991 95. Zhou S, Butler-Laporte G, Nakanishi T, Morrison DR, Afilalo J, Afilalo M, et al. A
1992 Neanderthal OAS1 isoform protects individuals of European ancestry against COVID-19
1993 susceptibility and severity. Nat Med. 2021;27(4):659-67. Epub 20210225. doi: 10.1038/s41591-
1994 021-01281-1. PubMed PMID: 33633408.
1995 96. Huffman JE, Butler-Laporte G, Khan A, Pairo-Castineira E, Drivas TG, Peloso GM, et al.
1996 Multi-ancestry fine mapping implicates OAS1 splicing in risk of severe COVID-19. Nat Genet.
1997 2022;54(2):125-7. Epub 20220113. doi: 10.1038/s41588-021-00996-8. PubMed PMID: 35027740;
1998 PubMed Central PMCID: PMCPMC8837537.
1999 97. Initiative C-HG. Mapping the human genetic architecture of COVID-19. Nature.
2000 2021;600(7889):472-7. Epub 20210708. doi: 10.1038/s41586-021-03767-x. PubMed PMID:
2001 34237774; PubMed Central PMCID: PMCPMC8674144.
2002 98. Pairo-Castineira E, Clohisey S, Klaric L, Bretherick AD, Rawlik K, Pasko D, et al. Genetic
2003 mechanisms of critical illness in COVID-19. Nature. 2021;591(7848):92-8. Epub 20201211. doi:
2004 10.1038/s41586-020-03065-y. PubMed PMID: 33307546.
2005 99. Banday AR, Stanifer ML, Florez-Vargas O, Onabajo OO, Papenberg BW, Zahoor MA, et al.
2006 Genetic regulation of OAS1 nonsense-mediated decay underlies association with COVID-19
2007 hospitalization in patients of European and African ancestries. Nat Genet. 2022;54(8):1103-16.
2008 Epub 20220714. doi: 10.1038/s41588-022-01113-z. PubMed PMID: 35835913; PubMed Central
2009 PMCID: PMCPMC9355882.
2010 100. Payman S-T, Hala A, James DRK, Audrey A, Reuben S, Zhen-Yuan L, et al. A SARS-CoV-2 –
2011 host proximity interactome. bioRxiv. 2020:2020.09.03.282103. doi: 10.1101/2020.09.03.282103.
2012 101. Gordon DE, Jang GM, Bouhaddou M, Xu J, Obernier K, White KM, et al. A SARS-CoV-2
2013 protein interaction map reveals targets for drug repurposing. Nature. 2020;583(7816):459-68.
2014 Epub 20200430. doi: 10.1038/s41586-020-2286-9. PubMed PMID: 32353859; PubMed Central
2015 PMCID: PMCPMC7431030.
2016 102. Estelle MNL, Yorgos S, Anastassia K, Jean-Pascal G, Payman Samavarchi T, Dae-Kyum K, et
2017 al. Global BioID-based SARS-CoV-2 proteins proximal interactome unveils novel ties between viral
2018 polypeptides and host factors involved in multiple COVID19-associated mechanisms. bioRxiv.
2019 2020:2020.08.28.272955. doi: 10.1101/2020.08.28.272955.
2020 103. St-Germain JR, Astori A, Samavarchi-Tehrani P, Abdouni H, Macwan V, Kim D-K, et al. A
2021 SARS-CoV-2 BioID-based virus-host membrane protein interactome and virus peptide
2022 compendium: new proteomics resources for COVID-19 research. bioRxiv.
2023 2020:2020.08.28.269175. doi: 10.1101/2020.08.28.269175.

2024 104. Liu X, Huuskonen S, Laitinen T, Redchuk T, Bogacheva M, Salokas K, et al. SARS-CoV-2-host
2025 proteome interactions for antiviral drug discovery. Mol Syst Biol. 2021;17(11):e10396. doi:
2026 10.15252/msb.202110396. PubMed PMID: 34709727; PubMed Central PMCID:
2027 PMCPMC8552907.
2028 105. May DG, Martin-Sancho L, Anschau V, Liu S, Chrisopulos RJ, Scott KL, et al. A BioID-Derived
2029 Proximity Interactome for SARS-CoV-2 Proteins. Viruses. 2022;14(3). Epub 20220315. doi:
2030 10.3390/v14030611. PubMed PMID: 35337019; PubMed Central PMCID: PMCPMC8951556.
2031 106. Zhou Y, Liu Y, Gupta S, Paramo MI, Hou Y, Mao C, et al. A comprehensive SARS-CoV-2-
2032 human protein-protein interactome reveals COVID-19 pathobiology and potential host
2033 therapeutic targets. Nat Biotechnol. 2023;41(1):128-39. Epub 20221010. doi: 10.1038/s41587-
2034 022-01474-0. PubMed PMID: 36217030; PubMed Central PMCID: PMCPMC9851973.
2035 107. Stukalov A, Girault V, Grass V, Karayel O, Bergant V, Urban C, et al. Multilevel proteomics
2036 reveals host perturbations by SARS-CoV-2 and SARS-CoV. Nature. 2021;594(7862):246-52. Epub
2037 20210412. doi: 10.1038/s41586-021-03493-4. PubMed PMID: 33845483.
2038 108. Li J, Guo M, Tian X, Wang X, Yang X, Wu P, et al. Virus-Host Interactome and Proteomic
2039 Survey Reveal Potential Virulence Factors Influencing SARS-CoV-2 Pathogenesis. Med.
2040 2021;2(1):99-112 e7. Epub 20200721. doi: 10.1016/j.medj.2020.07.002. PubMed PMID:
2041 32838362; PubMed Central PMCID: PMCPMC7373048.
2042 109. Davies JP, Almasy KM, McDonald EF, Plate L. Comparative Multiplexed Interactomics of
2043 SARS-CoV-2 and Homologous Coronavirus Nonstructural Proteins Identifies Unique and Shared
2044 Host-Cell Dependencies. ACS Infect Dis. 2020;6(12):3174-89. Epub 20201202. doi:
2045 10.1021/acsinfecdis.0c00500. PubMed PMID: 33263384; PubMed Central PMCID:
2046 PMCPMC7724760.
2047 110. Schmidt N, Ganskih S, Wei Y, Gabel A, Zielinski S, Keshishian H, et al. SND1 binds SARS-
2048 CoV-2 negative-sense RNA and promotes viral RNA synthesis through NSP9. Cell.
2049 2023;186(22):4834-50 e23. Epub 20231003. doi: 10.1016/j.cell.2023.09.002. PubMed PMID:
2050 37794589; PubMed Central PMCID: PMCPMC10617981.
2051 111. Schmidt N, Lareau CA, Keshishian H, Ganskih S, Schneider C, Hennig T, et al. The SARS-CoV-
2052 2 RNA-protein interactome in infected human cells. Nat Microbiol. 2021;6(3):339-53. Epub
2053 20201221. doi: 10.1038/s41564-020-00846-z. PubMed PMID: 33349665; PubMed Central
2054 PMCID: PMCPMC7906908.
2055 112. Labeau A, Fery-Simonian L, Lefevre-Utile A, Pourcelot M, Bonnet-Madin L, Soumelis V, et
2056 al. Characterization and functional interrogation of the SARS-CoV-2 RNA interactome. Cell Rep.
2057 2022;39(4):110744. doi: 10.1016/j.celrep.2022.110744. PubMed PMID: 35477000; PubMed
2058 Central PMCID: PMCPMC9040432.
2059 113. Kamel W, Noerenberg M, Cerikan B, Chen H, Jarvelin AI, Kammoun M, et al. Global analysis
2060 of protein-RNA interactions in SARS-CoV-2-infected cells reveals key regulators of infection. Mol
2061 Cell. 2021;81(13):2851-67 e7. Epub 20210524. doi: 10.1016/j.molcel.2021.05.023. PubMed
2062 PMID: 34118193; PubMed Central PMCID: PMCPMC8142890.
2063 114. Flynn RA, Belk JA, Qi Y, Yasumoto Y, Wei J, Alfajaro MM, et al. Discovery and functional
2064 interrogation of SARS-CoV-2 RNA-host protein interactions. Cell. 2021;184(9):2394-411 e16. Epub
2065 20210311. doi: 10.1016/j.cell.2021.03.012. PubMed PMID: 33743211; PubMed Central PMCID:
2066 PMCPMC7951565.

115. Lee S, Lee YS, Choi Y, Son A, Park Y, Lee KM, et al. The SARS-CoV-2 RNA interactome. Mol Cell. 2021;81(13):2838-50 e6. Epub 20210427. doi: 10.1016/j.molcel.2021.04.022. PubMed PMID: 33989516; PubMed Central PMCID: PMCPMC8075806.
116. Bouhaddou M, Memon D, Meyer B, White KM, Rezelj VV, Correa Marrero M, et al. The Global Phosphorylation Landscape of SARS-CoV-2 Infection. Cell. 2020;182(3):685-712 e19. Epub 20200628. doi: 10.1016/j.cell.2020.06.034. PubMed PMID: 32645325; PubMed Central PMCID: PMCPMC7321036.
117. Sanchez-Magraner L, Posada IM, Andraka N, Contreras FX, Viguera AR, Guerin DM, et al. The C-terminal transmembrane domain of human phospholipid scramblase 1 is essential for the protein flip-flop activity and Ca(2)(+)-binding. J Membr Biol. 2014;247(2):155-65. Epub 20131217. doi: 10.1007/s00232-013-9619-7. PubMed PMID: 24343571.
118. Abdulla S, Aevermann B, Assis P, Badajoz S, Bell SM, Bezzi E, et al. CZ CELL×GENE Discover: A single-cell data platform for scalable exploration, analysis and modeling of aggregated data. bioRxiv. 2023:2023.10.30.563174. doi: 10.1101/2023.10.30.563174.
119. Ricardo-Lax I, Luna JM, Thao TTN, Le Pen J, Yu Y, Hoffmann HH, et al. Replication and single-cycle delivery of SARS-CoV-2 replicons. Science. 2021;374(6571):1099-106. Epub 20211014. doi: 10.1126/science.abj8430. PubMed PMID: 34648371; PubMed Central PMCID: PMCPMC9007107.
120. Schmidt F, Weisblum Y, Muecksch F, Hoffmann HH, Michailidis E, Lorenzi JCC, et al. Measuring SARS-CoV-2 neutralizing antibody activity using pseudotyped and chimeric viruses. J Exp Med. 2020;217(11). doi: 10.1084/jem.20201181. PubMed PMID: 32692348; PubMed Central PMCID: PMCPMC7372514.
121. Pfaender S, Mar KB, Michailidis E, Kratzel A, Boys IN, V'Kovski P, et al. LY6E impairs coronavirus fusion and confers immune control of viral disease. Nat Microbiol. 2020;5(11):1330-9. Epub 20200723. doi: 10.1038/s41564-020-0769-y. PubMed PMID: 32704094; PubMed Central PMCID: PMCPMC7916999.
122. Winstone H, Lista MJ, Reid AC, Bouton C, Pickering S, Galao RP, et al. The Polybasic Cleavage Site in SARS-CoV-2 Spike Modulates Viral Sensitivity to Type I Interferon and IFITM2. J Virol. 2021;95(9). Epub 20210412. doi: 10.1128/JVI.02422-20. PubMed PMID: 33563656; PubMed Central PMCID: PMCPMC8104117.
123. Thorne LG, Bouhaddou M, Reuschl AK, Zuliani-Alvarez L, Polacco B, Pelin A, et al. Evolution of enhanced innate immune evasion by SARS-CoV-2. Nature. 2022;602(7897):487-95. Epub 20211223. doi: 10.1038/s41586-021-04352-y. PubMed PMID: 34942634; PubMed Central PMCID: PMCPMC8850198.
124. Markov PV, Ghafari M, Beer M, Lythgoe K, Simmonds P, Stilianakis NI, et al. The evolution of SARS-CoV-2. Nature Reviews Microbiology. 2023;21(6):361-79. doi: 10.1038/s41579-023-00878-2.
125. Carabelli AM, Peacock TP, Thorne LG, Harvey WT, Hughes J, de Silva TI, et al. SARS-CoV-2 variant biology: immune escape, transmission and fitness. Nature Reviews Microbiology. 2023;21(3):162-77. doi: 10.1038/s41579-022-00841-7.
126. Huang P, Liao R, Chen X, Wu X, Li X, Wang Y, et al. Nuclear translocation of PLSCR1 activates STAT1 signaling in basal-like breast cancer. Theranostics. 2020;10(10):4644-58. Epub 20200325. doi: 10.7150/thno.43150. PubMed PMID: 32292520; PubMed Central PMCID: PMCPMC7150476.

127. Nanjundan M, Sun J, Zhao J, Zhou Q, Sims PJ, Wiedmer T. Plasma membrane phospholipid scramblase 1 promotes EGF-dependent activation of c-Src through the epidermal growth factor receptor. J Biol Chem. 2003;278(39):37413-8. Epub 20030718. doi: 10.1074/jbc.M306182200. PubMed PMID: 12871937.
128. Ben-Efraim I, Zhou Q, Wiedmer T, Gerace L, Sims PJ. Phospholipid scramblase 1 is imported into the nucleus by a receptor-mediated pathway and interacts with DNA. Biochemistry. 2004;43(12):3518-26. doi: 10.1021/bi0356911. PubMed PMID: 15035622.
129. Chen MH, Ben-Efraim I, Mitrousis G, Walker-Kopp N, Sims PJ, Cingolani G. Phospholipid scramblase 1 contains a nonclassical nuclear localization signal with unique binding site in importin alpha. J Biol Chem. 2005;280(11):10599-606. Epub 20041217. doi: 10.1074/jbc.M413194200. PubMed PMID: 15611084.
130. Wiedmer T, Zhao J, Nanjundan M, Sims PJ. Palmitoylation of phospholipid scramblase 1 controls its distribution between nucleus and plasma membrane. Biochemistry. 2003;42(5):1227-33. doi: 10.1021/bi026679w. PubMed PMID: 12564925.
131. Zhao J, Zhou Q, Wiedmer T, Sims PJ. Palmitoylation of phospholipid scramblase is required for normal function in promoting Ca2+-activated transbilayer movement of membrane phospholipids. Biochemistry. 1998;37(18):6361-6. doi: 10.1021/bi980218m. PubMed PMID: 9572851.
132. Chen S, Francioli LC, Goodrich JK, Collins RL, Kanai M, Wang Q, et al. A genomic mutational constraint map using variation in 76,156 human genomes. Nature. 2024;625(7993):92-100. doi: 10.1038/s41586-023-06045-0.
133. Zhang P, Bigio B, Rapaport F, Zhang SY, Casanova JL, Abel L, et al. PopViz: a webserver for visualizing minor allele frequencies and damage prediction scores of human genetic variations. Bioinformatics. 2018;34(24):4307-9. doi: 10.1093/bioinformatics/bty536. PubMed PMID: 30535305; PubMed Central PMCID: PMCPMC6289133.
134. Dittmann M, Hoffmann HH, Scull MA, Gilmore RH, Bell KL, Ciancanelli M, et al. A serpin shapes the extracellular environment to prevent influenza A virus maturation. Cell. 2015;160(4):631-43. doi: 10.1016/j.cell.2015.01.040. PubMed PMID: 25679759; PubMed Central PMCID: PMCPMC4328142.
135. Burke JM, St Clair LA, Perera R, Parker R. SARS-CoV-2 infection triggers widespread host mRNA decay leading to an mRNA export block. RNA. 2021;27(11):1318-29. Epub 20210727. doi: 10.1261/rna.078923.121. PubMed PMID: 34315815; PubMed Central PMCID: PMCPMC8522697.
136. Zhang K, Miorin L, Makio T, Dehghan I, Gao S, Xie Y, et al. Nsp1 protein of SARS-CoV-2 disrupts the mRNA export machinery to inhibit host gene expression. Sci Adv. 2021;7(6). Epub 20210205. doi: 10.1126/sciadv.abe7386. PubMed PMID: 33547084; PubMed Central PMCID: PMCPMC7864571.
137. Kimura I, Konno Y, Uriu K, Hopfensperger K, Sauter D, Nakagawa S, et al. Sarbecovirus ORF6 proteins hamper induction of interferon signaling. Cell Rep. 2021;34(13):108916. Epub 20210312. doi: 10.1016/j.celrep.2021.108916. PubMed PMID: 33765414; PubMed Central PMCID: PMCPMC7953434.
138. Setaro AC, Gaglia MM. All hands on deck: SARS-CoV-2 proteins that block early anti-viral interferon responses. Curr Res Virol Sci. 2021;2:100015. Epub 20211112. doi:

2151 10.1016/j.crviro.2021.100015. PubMed PMID: 34786565; PubMed Central PMCID:
2152 PMCPMC8588586.
2153 139. Ogunjimi B, Zhang SY, Sorensen KB, Skipper KA, Carter-Timofte M, Kerner G, et al. Inborn
2154 errors in RNA polymerase III underlie severe varicella zoster virus infections. J Clin Invest.
2155 2017;127(9):3543-56. Epub 20170807. doi: 10.1172/JCI92280. PubMed PMID: 28783042;
2156 PubMed Central PMCID: PMCPMC5669568.
2157 140. Zimmer MM, Kibe A, Rand U, Pekarek L, Ye L, Buck S, et al. The short isoform of the host
2158 antiviral protein ZAP acts as an inhibitor of SARS-CoV-2 programmed ribosomal frameshifting. Nat
2159 Commun. 2021;12(1):7193. Epub 20211210. doi: 10.1038/s41467-021-27431-0. PubMed PMID:
2160 34893599; PubMed Central PMCID: PMCPMC8664833.
2161 141. Klein S, Golani G, Lolicato F, Lahr C, Beyer D, Herrmann A, et al. IFITM3 blocks influenza
2162 virus entry by sorting lipids and stabilizing hemifusion. Cell Host Microbe. 2023. Epub 20230329.
2163 doi: 10.1016/j.chom.2023.03.005. PubMed PMID: 37003257.
2164 142. Guo X, Steinkuhler J, Marin M, Li X, Lu W, Dimova R, et al. Interferon-Induced
2165 Transmembrane Protein 3 Blocks Fusion of Diverse Enveloped Viruses by Altering Mechanical
2166 Properties of Cell Membranes. ACS Nano. 2021;15(5):8155-70. Epub 20210303. doi:
2167 10.1021/acsnano.0c10567. PubMed PMID: 33656312; PubMed Central PMCID:
2168 PMCPMC8159881.
2169 143. Suddala KC, Lee CC, Meraner P, Marin M, Markosyan RM, Desai TM, et al. Interferon-
2170 induced transmembrane protein 3 blocks fusion of sensitive but not resistant viruses by
2171 partitioning into virus-carrying endosomes. PLoS Pathog. 2019;15(1):e1007532. Epub 20190114.
2172 doi: 10.1371/journal.ppat.1007532. PubMed PMID: 30640957; PubMed Central PMCID:
2173 PMCPMC6347298.
2174 144. Desai TM, Marin M, Chin CR, Savidis G, Brass AL, Melikyan GB. IFITM3 restricts influenza
2175 A virus entry by blocking the formation of fusion pores following virus-endosome hemifusion.
2176 PLoS Pathog. 2014;10(4):e1004048. Epub 20140403. doi: 10.1371/journal.ppat.1004048.
2177 PubMed PMID: 24699674; PubMed Central PMCID: PMCPMC3974867.
2178 145. Fadeel B, Gleiss B, Hogstrand K, Chandra J, Wiedmer T, Sims PJ, et al. Phosphatidylserine
2179 exposure during apoptosis is a cell-type-specific event and does not correlate with plasma
2180 membrane phospholipid scramblase expression. Biochem Biophys Res Commun.
2181 1999;266(2):504-11. doi: 10.1006/bbrc.1999.1820. PubMed PMID: 10600532.
2182 146. Zhou Q, Zhao J, Al-Zoghaibi F, Zhou A, Wiedmer T, Silverman RH, et al. Transcriptional
2183 control of the human plasma membrane phospholipid scramblase 1 gene is mediated by
2184 interferon-alpha. Blood. 2000;95(8):2593-9. PubMed PMID: 10753839.
2185 147. Zhou Q, Zhao J, Wiedmer T, Sims PJ. Normal hemostasis but defective hematopoietic
2186 response to growth factors in mice deficient in phospholipid scramblase 1. Blood.
2187 2002;99(11):4030-8. doi: 10.1182/blood-2001-12-0271. PubMed PMID: 12010804.
2188 148. Majdoul S, Compton AA. Lessons in self-defence: inhibition of virus entry by intrinsic
2189 immunity. Nat Rev Immunol. 2022;22(6):339-52. Epub 20211013. doi: 10.1038/s41577-021-
2190 00626-8. PubMed PMID: 34646033; PubMed Central PMCID: PMCPMC8511856.
2191 149. Kusano S, Eizuru Y. Human phospholipid scramblase 1 interacts with and regulates
2192 transactivation of HTLV-1 Tax. Virology. 2012;432(2):343-52. Epub 20120711. doi:
2193 10.1016/j.virol.2012.06.019. PubMed PMID: 22789739.

150. Kusano S, Eizuru Y. Interaction of the phospholipid scramblase 1 with HIV-1 Tat results in the repression of Tat-dependent transcription. Biochem Biophys Res Commun. 2013;433(4):438-44. Epub 20130315. doi: 10.1016/j.bbrc.2013.02.098. PubMed PMID: 23501106.
151. Sadanari H, Takemoto M, Ishida T, Otagiri H, Daikoku T, Murayama T, et al. The Interferon-Inducible Human PLSCR1 Protein Is a Restriction Factor of Human Cytomegalovirus. Microbiol Spectr. 2022;10(1):e0134221. Epub 2022/02/10. doi: 10.1128/spectrum.01342-21. PubMed PMID: 35138119; PubMed Central PMCID: PMCPMC8826943.
152. Metz P, Dazert E, Ruggieri A, Mazur J, Kaderali L, Kaul A, et al. Identification of type I and type II interferon-induced effectors controlling hepatitis C virus replication. Hepatology. 2012;56(6):2082-93. Epub 20121014. doi: 10.1002/hep.25908. PubMed PMID: 22711689.
153. Yang J, Zhu X, Liu J, Ding X, Han M, Hu W, et al. Inhibition of Hepatitis B virus replication by phospholipid scramblase 1 in vitro and in vivo. Antiviral Res. 2012;94(1):9-17. Epub 20120209. doi: 10.1016/j.antiviral.2012.01.010. PubMed PMID: 22342889.
154. Kusano S, Ikeda M. Interaction of phospholipid scramblase 1 with the Epstein-Barr virus protein BZLF1 represses BZLF1-mediated lytic gene transcription. J Biol Chem. 2019;294(41):15104-16. Epub 2019/08/23. doi: 10.1074/jbc.RA119.008193. PubMed PMID: 31434743; PubMed Central PMCID: PMCPMC6791327.
155. Luo W, Zhang J, Liang L, Wang G, Li Q, Zhu P, et al. Phospholipid scramblase 1 interacts with influenza A virus NP, impairing its nuclear import and thereby suppressing virus replication. PLoS Pathog. 2018;14(1):e1006851. Epub 20180119. doi: 10.1371/journal.ppat.1006851. PubMed PMID: 29352288; PubMed Central PMCID: PMCPMC5792031.
156. Dal Col J, Lamberti MJ, Nigro A, Casolaro V, Fratta E, Steffan A, et al. Phospholipid scramblase 1: a protein with multiple functions via multiple molecular interactors. Cell Commun Signal. 2022;20(1):78. Epub 2022/06/02. doi: 10.1186/s12964-022-00895-3. PubMed PMID: 35650588.
157. Jonathan RS-G, Audrey A, Payman S-T, Hala A, Vinitha M, Dae-Kyum K, et al. A SARS-CoV-2 BioID-based virus-host membrane protein interactome and virus peptide compendium: new proteomics resources for COVID-19 research. bioRxiv. 2020:2020.08.28.269175. doi: 10.1101/2020.08.28.269175.
158. Guo K, Barrett BS, Morrison JH, Mickens KL, Vladar EK, Hasenkrug KJ, et al. Interferon resistance of emerging SARS-CoV-2 variants. Proc Natl Acad Sci U S A. 2022;119(32):e2203760119. Epub 20220722. doi: 10.1073/pnas.2203760119. PubMed PMID: 35867811; PubMed Central PMCID: PMCPMC9371743.
159. Shalamova L, Felgenhauer U, Wilhelm J, Schaubmar AR, Buttner K, Schoen A, et al. Omicron variant of SARS-CoV-2 exhibits an increased resilience to the antiviral type I interferon response. PNAS Nexus. 2022;1(2):pgac067. Epub 20220523. doi: 10.1093/pnasnexus/pgac067. PubMed PMID: 36713328; PubMed Central PMCID: PMCPMC9802332.
160. Shi G, Li T, Lai KK, Johnson RF, Yewdell JW, Compton AA. Omicron Spike confers enhanced infectivity and interferon resistance to SARS-CoV-2 in human nasal tissue. Nat Commun. 2024;15(1):889. Epub 20240130. doi: 10.1038/s41467-024-45075-8. PubMed PMID: 38291024; PubMed Central PMCID: PMCPMC10828397.
161. Doyle T, Moncorge O, Bonaventure B, Pollpeter D, Lussignol M, Tauziet M, et al. The interferon-inducible isoform of NCOA7 inhibits endosome-mediated viral entry. Nat Microbiol.

2018;3(12):1369-76. Epub 20181126. doi: 10.1038/s41564-018-0273-9. PubMed PMID: 30478388; PubMed Central PMCID: PMCPMC6329445.
162. Khan H, Winstone H, Jimenez-Guardeno JM, Graham C, Doores KJ, Goujon C, et al. TMPRSS2 promotes SARS-CoV-2 evasion from NCOA7-mediated restriction. PLoS Pathog. 2021;17(11):e1009820. Epub 20211122. doi: 10.1371/journal.ppat.1009820. PubMed PMID: 34807954; PubMed Central PMCID: PMCPMC8648102.
163. Willett BJ, Grove J, MacLean OA, Wilkie C, De Lorenzo G, Furnon W, et al. SARS-CoV-2 Omicron is an immune escape variant with an altered cell entry pathway. Nat Microbiol. 2022;7(8):1161-79. Epub 20220707. doi: 10.1038/s41564-022-01143-7. PubMed PMID: 35798890; PubMed Central PMCID: PMCPMC9352574.
164. Peacock TP, Brown JC, Zhou J, Thakur N, Sukhova K, Newman J, et al. The altered entry pathway and antigenic distance of the SARS-CoV-2 Omicron variant map to separate domains of spike protein. bioRxiv. 2022:2021.12.31.474653. doi: 10.1101/2021.12.31.474653.
165. Shuai H, Chan JF, Hu B, Chai Y, Yuen TT, Yin F, et al. Attenuated replication and pathogenicity of SARS-CoV-2 B.1.1.529 Omicron. Nature. 2022;603(7902):693-9. Epub 20220121. doi: 10.1038/s41586-022-04442-5. PubMed PMID: 35062016.
166. Hui KPY, Ho JCW, Cheung MC, Ng KC, Ching RHH, Lai KL, et al. SARS-CoV-2 Omicron variant replication in human bronchus and lung ex vivo. Nature. 2022;603(7902):715-20. Epub 20220201. doi: 10.1038/s41586-022-04479-6. PubMed PMID: 35104836.
167. Zhao H, Lu L, Peng Z, Chen LL, Meng X, Zhang C, et al. SARS-CoV-2 Omicron variant shows less efficient replication and fusion activity when compared with Delta variant in TMPRSS2-expressed cells. Emerg Microbes Infect. 2022;11(1):277-83. doi: 10.1080/22221751.2021.2023329. PubMed PMID: 34951565; PubMed Central PMCID: PMCPMC8774049.
168. Meng B, Abdullahi A, Ferreira I, Goonawardane N, Saito A, Kimura I, et al. Altered TMPRSS2 usage by SARS-CoV-2 Omicron impacts infectivity and fusogenicity. Nature. 2022;603(7902):706-14. Epub 20220201. doi: 10.1038/s41586-022-04474-x. PubMed PMID: 35104837; PubMed Central PMCID: PMCPMC8942856.
169. Fan Y, Li X, Zhang L, Wan S, Zhang L, Zhou F. SARS-CoV-2 Omicron variant: recent progress and future perspectives. Signal Transduct Target Ther. 2022;7(1):141. Epub 20220428. doi: 10.1038/s41392-022-00997-x. PubMed PMID: 35484110; PubMed Central PMCID: PMCPMC9047469.
170. Sette A, Crotty S. Adaptive immunity to SARS-CoV-2 and COVID-19. Cell. 2021;184(4):861-80. Epub 20210112. doi: 10.1016/j.cell.2021.01.007. PubMed PMID: 33497610; PubMed Central PMCID: PMCPMC7803150.
171. Mar KB, Van Dyke MC, Lopez AH, Eitson JL, Fan W, Hanners NW, et al. LY6E protects mice from pathogenic effects of murine coronavirus and SARS-CoV-2. bioRxiv. 2023. Epub 20230126. doi: 10.1101/2023.01.25.525551. PubMed PMID: 36747632; PubMed Central PMCID: PMCPMC9900800.
172. Consortium GT. The Genotype-Tissue Expression (GTEx) project. Nat Genet. 2013;45(6):580-5. doi: 10.1038/ng.2653. PubMed PMID: 23715323; PubMed Central PMCID: PMCPMC4010069.

2279 173. Blight KJ, McKeating JA, Rice CM. Highly permissive cell lines for subgenomic and genomic
2280 hepatitis C virus RNA replication. J Virol. 2002;76(24):13001-14. doi: 10.1128/jvi.76.24.13001-
2281 13014.2002. PubMed PMID: 12438626; PubMed Central PMCID: PMCPMC136668.
2282 174. Zhang L, Bukreyev A, Thompson CI, Watson B, Peeples ME, Collins PL, et al. Infection of
2283 ciliated cells by human parainfluenza virus type 3 in an in vitro model of human airway epithelium.
2284 J Virol. 2005;79(2):1113-24. doi: 10.1128/JVI.79.2.1113-1124.2005. PubMed PMID: 15613339;
2285 PubMed Central PMCID: PMCPMC538579.
2286 175. Hoffmann HH, Schneider WM, Rozen-Gagnon K, Miles LA, Schuster F, Razooky B, et al.
2287 TMEM41B Is a Pan-flavivirus Host Factor. Cell. 2021;184(1):133-48 e20. Epub 20201209. doi:
2288 10.1016/j.cell.2020.12.005. PubMed PMID: 33338421; PubMed Central PMCID:
2289 PMCPMC7954666.
2290 176. Benboudjema L, Mulvey M, Gao Y, Pimplikar SW, Mohr I. Association of the herpes simplex
2291 virus type 1 Us11 gene product with the cellular kinesin light-chain-related protein PAT1 results
2292 in the redistribution of both polypeptides. J Virol. 2003;77(17):9192-203. doi:
2293 10.1128/jvi.77.17.9192-9203.2003. PubMed PMID: 12915535; PubMed Central PMCID:
2294 PMCPMC187382.
2295 177. Lee D, Le Pen J, Yatim A, Dong B, Aquino Y, Ogishi M, et al. Inborn errors of OAS-RNase L
2296 in SARS-CoV-2-related multisystem inflammatory syndrome in children. Science.
2297 2023;379(6632):eabo3627. Epub 20230210. doi: 10.1126/science.abo3627. PubMed PMID:
2298 36538032.
2299 178. Mendoza EJ, Manguiat K, Wood H, Drebot M. Two Detailed Plaque Assay Protocols for the
2300 Quantification of Infectious SARS-CoV-2. Curr Protoc Microbiol. 2020;57(1):ecpmc105. doi:
2301 10.1002/cpmc.105. PubMed PMID: 32475066; PubMed Central PMCID: PMCPMC7300432.
2302 179. Polo JM, Davis NL, Rice CM, Huang HV, Johnston RE. Molecular analysis of Sindbis virus
2303 pathogenesis in neonatal mice by using virus recombinants constructed in vitro. J Virol.
2304 1988;62(6):2124-33. doi: 10.1128/JVI.62.6.2124-2133.1988. PubMed PMID: 2835514; PubMed
2305 Central PMCID: PMCPMC253309.
2306 180. Bick MJ, Carroll JW, Gao G, Goff SP, Rice CM, MacDonald MR. Expression of the zinc-finger
2307 antiviral protein inhibits alphavirus replication. J Virol. 2003;77(21):11555-62. doi:
2308 10.1128/jvi.77.21.11555-11562.2003. PubMed PMID: 14557641; PubMed Central PMCID:
2309 PMCPMC229374.
2310 181. Atasheva S, Kim DY, Akhrymuk M, Morgan DG, Frolova EI, Frolov I. Pseudoinfectious
2311 Venezuelan equine encephalitis virus: a new means of alphavirus attenuation. J Virol.
2312 2013;87(4):2023-35. Epub 20121205. doi: 10.1128/JVI.02881-12. PubMed PMID: 23221545;
2313 PubMed Central PMCID: PMCPMC3571482.
2314 182. Dalton KP, Rose JK. Vesicular stomatitis virus glycoprotein containing the entire green
2315 fluorescent protein on its cytoplasmic domain is incorporated efficiently into virus particles.
2316 Virology. 2001;279(2):414-21. doi: 10.1006/viro.2000.0736. PubMed PMID: 11162797.
2317 183. Dobin A, Davis CA, Schlesinger F, Drenkow J, Zaleski C, Jha S, et al. STAR: ultrafast universal
2318 RNA-seq aligner. Bioinformatics. 2013;29(1):15-21. Epub 20121025. doi:
2319 10.1093/bioinformatics/bts635. PubMed PMID: 23104886; PubMed Central PMCID:
2320 PMCPMC3530905.

184. Liao Y, Smyth GK, Shi W. The R package Rsubread is easier, faster, cheaper and better for alignment and quantification of RNA sequencing reads. Nucleic Acids Res. 2019;47(8):e47. doi: 10.1093/nar/gkz114. PubMed PMID: 30783653; PubMed Central PMCID: PMCPMC6486549.
185. Love MI, Huber W, Anders S. Moderated estimation of fold change and dispersion for RNA-seq data with DESeq2. Genome Biol. 2014;15(12):550. doi: 10.1186/s13059-014-0550-8. PubMed PMID: 25516281; PubMed Central PMCID: PMCPMC4302049.
186. Korotkevich G, Sukhov V, Budin N, Shpak B, Artyomov MN, Sergushichev A. Fast gene set enrichment analysis. bioRxiv. 2021:060012. doi: 10.1101/060012.
187. Liberzon A, Subramanian A, Pinchback R, Thorvaldsdottir H, Tamayo P, Mesirov JP. Molecular signatures database (MSigDB) 3.0. Bioinformatics. 2011;27(12):1739-40. Epub 20110505. doi: 10.1093/bioinformatics/btr260. PubMed PMID: 21546393; PubMed Central PMCID: PMCPMC3106198.
188. Fabregat A, Jupe S, Matthews L, Sidiropoulos K, Gillespie M, Garapati P, et al. The Reactome Pathway Knowledgebase. Nucleic Acids Res. 2018;46(D1):D649-D55. doi: 10.1093/nar/gkx1132. PubMed PMID: 29145629; PubMed Central PMCID: PMCPMC5753187.
189. Kanehisa M, Goto S. KEGG: kyoto encyclopedia of genes and genomes. Nucleic Acids Res. 2000;28(1):27-30. doi: 10.1093/nar/28.1.27. PubMed PMID: 10592173; PubMed Central PMCID: PMCPMC102409.
190. Agrawal A, Balci H, Hanspers K, Coort SL, Martens M, Slenter DN, et al. WikiPathways 2024: next generation pathway database. Nucleic Acids Res. 2024;52(D1):D679-D89. doi: 10.1093/nar/gkad960. PubMed PMID: 37941138; PubMed Central PMCID: PMCPMC10767877.
191. Schaefer CF, Anthony K, Krupa S, Buchoff J, Day M, Hannay T, et al. PID: the Pathway Interaction Database. Nucleic Acids Res. 2009;37(Database issue):D674-9. Epub 20081002. doi: 10.1093/nar/gkn653. PubMed PMID: 18832364; PubMed Central PMCID: PMCPMC2686461.
192. Nishimura D. BioCarta. Biotech Software & Internet Report: The Computer Software Journal for Scient. 2001;2(3):117-20.
193. Schmittgen TD, Livak KJ. Analyzing real-time PCR data by the comparative C(T) method. Nat Protoc. 2008;3(6):1101-8. doi: 10.1038/nprot.2008.73. PubMed PMID: 18546601.
194. Witte L, Baharani VA, Schmidt F, Wang Z, Cho A, Raspe R, et al. Epistasis lowers the genetic barrier to SARS-CoV-2 neutralizing antibody escape. Nat Commun. 2023;14(1):302. Epub 20230119. doi: 10.1038/s41467-023-35927-0. PubMed PMID: 36653360; PubMed Central PMCID: PMCPMC9849103.
195. Wang Z, Muecksch F, Raspe R, Johannsen F, Turroja M, Canis M, et al. Memory B cell development elicited by mRNA booster vaccinations in the elderly. J Exp Med. 2023;220(9). Epub 20230627. doi: 10.1084/jem.20230668. PubMed PMID: 37368240; PubMed Central PMCID: PMCPMC10300432.
196. Dittmann M, Hoffmann HH, Scull MA, Gilmore RH, Bell KL, Ciancanelli M, et al. A serpin shapes the extracellular environment to prevent influenza A virus maturation. Cell. 2015;160(4):631-43. doi: 10.1016/j.cell.2015.01.040. PubMed PMID: 25679759; PubMed Central PMCID: PMC4328142.
197. UniProt C. UniProt: the Universal Protein Knowledgebase in 2023. Nucleic Acids Res. 2023;51(D1):D523-D31. doi: 10.1093/nar/gkac1052. PubMed PMID: 36408920; PubMed Central PMCID: PMCPMC9825514.

198. Bruchez A, Sha K, Johnson J, Chen L, Stefani C, McConnell H, et al. MHC class II transactivator CIITA induces cell resistance to Ebola virus and SARS-like coronaviruses. Science. 2020;370(6513):241-7. Epub 20200827. doi: 10.1126/science.abb3753. PubMed PMID: 32855215; PubMed Central PMCID: PMCPMC7665841.
199. Lista MJ, Winstone H, Wilson HD, Dyer A, Pickering S, Galao RP, et al. The P681H Mutation in the Spike Glycoprotein of the Alpha Variant of SARS-CoV-2 Escapes IFITM Restriction and Is Necessary for Type I Interferon Resistance. J Virol. 2022;96(23):e0125022. Epub 20221109. doi: 10.1128/jvi.01250-22. PubMed PMID: 36350154; PubMed Central PMCID: PMCPMC9749455.
200. Shi G, Kenney AD, Kudryashova E, Zani A, Zhang L, Lai KK, et al. Opposing activities of IFITM proteins in SARS-CoV-2 infection. EMBO J. 2021;40(3):e106501. Epub 20201221. doi: 10.15252/embj.2020106501. PubMed PMID: 33270927; PubMed Central PMCID: PMCPMC7744865.
201. Prelli Bozzo C, Nchioua R, Volcic M, Koepke L, Kruger J, Schutz D, et al. IFITM proteins promote SARS-CoV-2 infection and are targets for virus inhibition in vitro. Nat Commun. 2021;12(1):4584. Epub 20210728. doi: 10.1038/s41467-021-24817-y. PubMed PMID: 34321474; PubMed Central PMCID: PMCPMC8319209.
202. Peacock TP, Goldhill DH, Zhou J, Baillon L, Frise R, Swann OC, et al. The furin cleavage site in the SARS-CoV-2 spike protein is required for transmission in ferrets. Nat Microbiol. 2021;6(7):899-909. Epub 20210427. doi: 10.1038/s41564-021-00908-w. PubMed PMID: 33907312.
203. Nchioua R, Schundner A, Kmiec D, Prelli Bozzo C, Zech F, Koepke L, et al. SARS-CoV-2 Variants of Concern Hijack IFITM2 for Efficient Replication in Human Lung Cells. J Virol. 2022;96(11):e0059422. Epub 20220511. doi: 10.1128/jvi.00594-22. PubMed PMID: 35543509; PubMed Central PMCID: PMCPMC9175628.
204. Xu F, Wang G, Zhao F, Huang Y, Fan Z, Mei S, et al. IFITM3 Inhibits SARS-CoV-2 Infection and Is Associated with COVID-19 Susceptibility. Viruses. 2022;14(11). Epub 20221118. doi: 10.3390/v14112553. PubMed PMID: 36423162; PubMed Central PMCID: PMCPMC9692367.
205. Shi G, Chiramel AI, Li T, Lai KK, Kenney AD, Zani A, et al. Rapalogs downmodulate intrinsic immunity and promote cell entry of SARS-CoV-2. J Clin Invest. 2022;132(24). Epub 20221215. doi: 10.1172/JCI160766. PubMed PMID: 36264642; PubMed Central PMCID: PMCPMC9753997.
206. Kenney AD, Zani A, Kawahara J, Eddy AC, Wang XL, Mahesh KC, et al. Interferon-induced transmembrane protein 3 (IFITM3) limits lethality of SARS-CoV-2 in mice. EMBO Rep. 2023;24(4):e56660. Epub 20230307. doi: 10.15252/embr.202256660. PubMed PMID: 36880581; PubMed Central PMCID: PMCPMC10074051.
207. Mathieson T, Franken H, Kosinski J, Kurzawa N, Zinn N, Sweetman G, et al. Systematic analysis of protein turnover in primary cells. Nat Commun. 2018;9(1):689. Epub 2018/02/17. doi: 10.1038/s41467-018-03106-1. PubMed PMID: 29449567; PubMed Central PMCID: PMCPMC5814408.
208. Szklarczyk D, Kirsch R, Koutrouli M, Nastou K, Mehryary F, Hachilif R, et al. The STRING database in 2023: protein-protein association networks and functional enrichment analyses for any sequenced genome of interest. Nucleic Acids Res. 2023;51(D1):D638-D46. doi: 10.1093/nar/gkac1000. PubMed PMID: 36370105; PubMed Central PMCID: PMCPMC9825434.

Figure 1

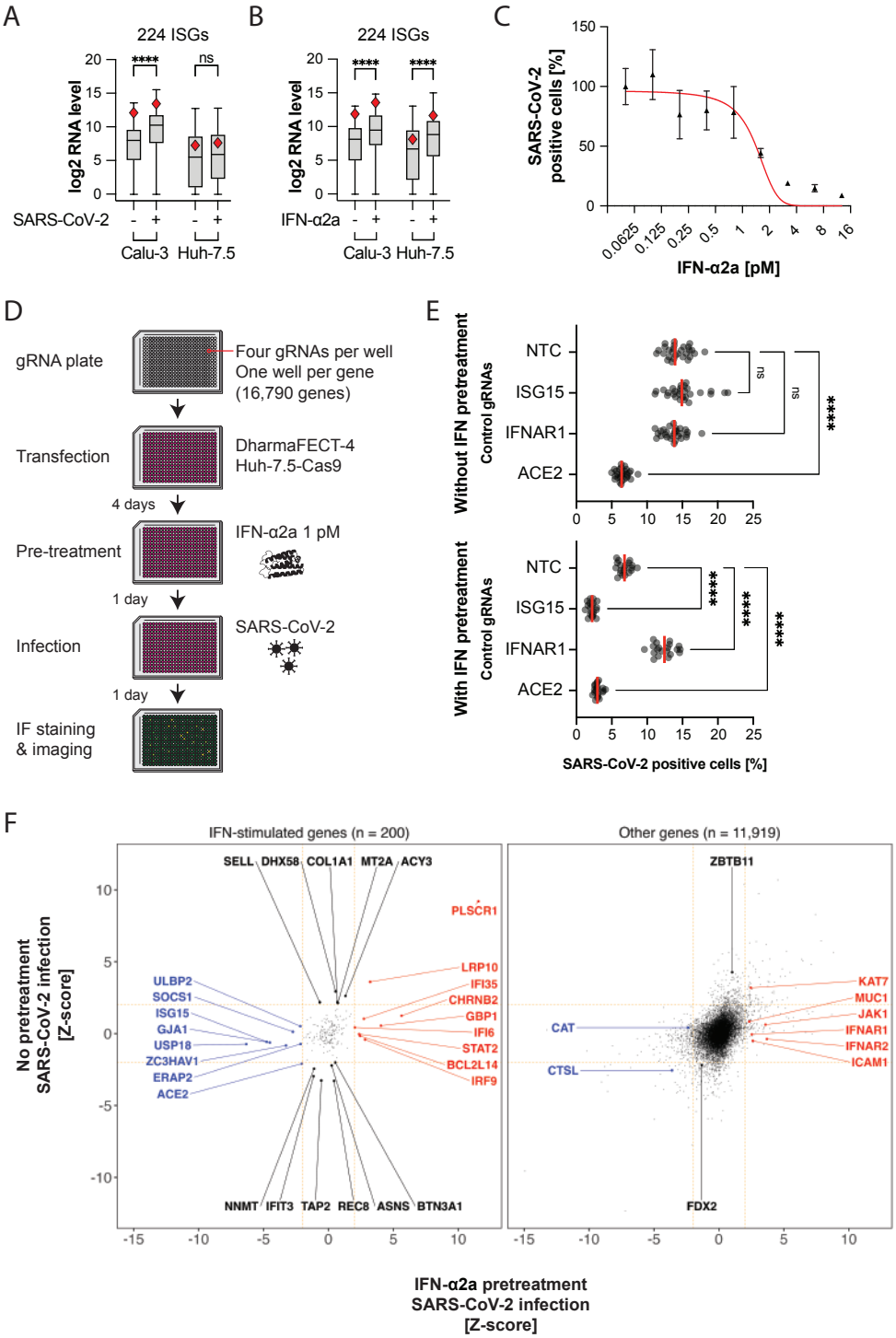
A
224 ISGs
log2 RNA level
****
ns
SARS-CoV-2
Calu-3
Huh-7.5
B
224 ISGs
log2 RNA level
****
****
IFN-α2a
Calu-3
Huh-7.5
C
SARS-CoV-2 positive cells [%]
IFN-α2a [pM]
D
gRNA plate
Four gRNAs per well
One well per gene
(16,790 genes)
Transfection
DharmaFECT-4
Huh-7.5-Cas9
4 days
Pre-treatment
IFN-α2a 1 pM
1 day
Infection
SARS-CoV-2
1 day
IF staining
& imaging
E
Without IFN pretreatment
Control gRNAs
NTC
ISG15
IFNAR1
ACE2
ns
ns
****
With IFN pretreatment
Control gRNAs
NTC
ISG15
IFNAR1
ACE2
****
****
****
SARS-CoV-2 positive cells [%]
F
IFN-stimulated genes (n = 200)
Other genes (n = 11,919)
No pretreatment
SARS-CoV-2 infection
[Z-score]
SELL
DHX58
COL1A1
MT2A
ACY3
PLSCR1
LRP10
IFI35
CHRNB2
GBP1
IFI6
STAT2
BCL2L14
IRF9
ULBP2
SOCS1
ISG15
GJA1
USP18
ZC3HAV1
ERAP2
ACE2
NNMT
IFIT3
TAP2
REC8
ASNS
BTN3A1
ZBTB11
KAT7
MUC1
JAK1
IFNAR1
IFNAR2
ICAM1
CAT
CTSL
FDX2
IFN-α2a pretreatment
SARS-CoV-2 infection
[Z-score]

Figure 2

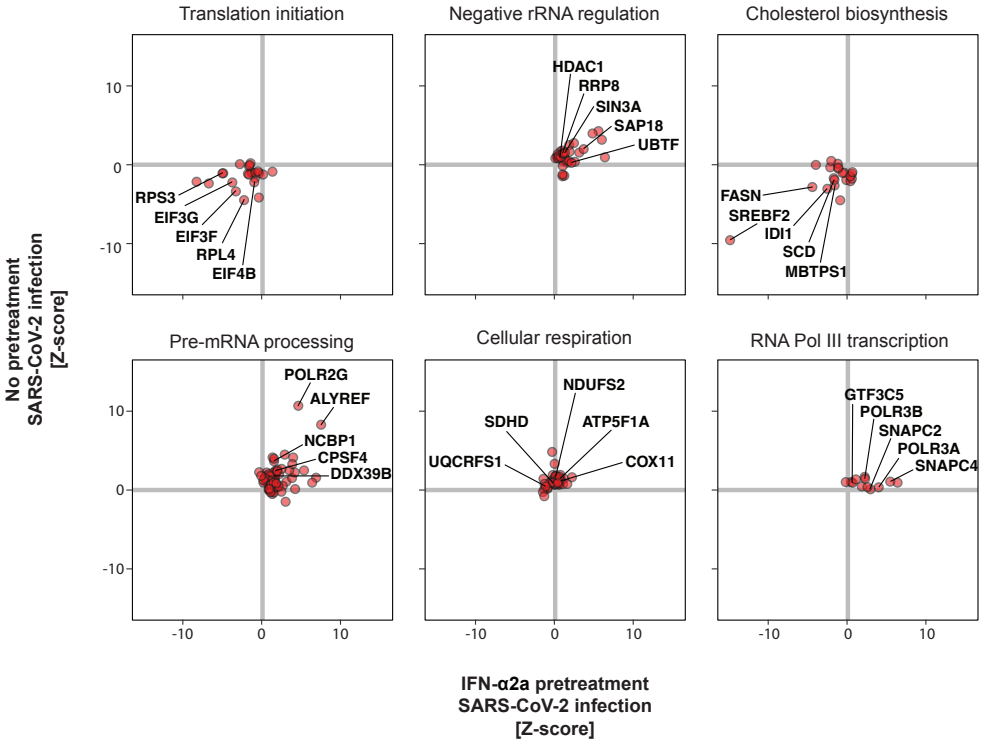
Translation initiation
Negative rRNA regulation
Cholesterol biosynthesis
Pre-mRNA processing
Cellular respiration
RNA Pol III transcription
RPS3
EIF3G
EIF3F
RPL4
EIF4B
HDAC1
RRP8
SIN3A
SAP18
UBTF
FASN
SREBF2
IDI1
SCD
MBTPS1
POLR2G
ALYREF
NCBP1
CPSF4
DDX39B
NDUFS2
SDHD
ATP5F1A
UQCRFS1
COX11
GTF3C5
POLR3B
SNAPC2
POLR3A
SNAPC4
10
0
-10
No pretreatment
SARS-CoV-2 infection
[Z-score]
IFN-α2a pretreatment
SARS-CoV-2 infection
[Z-score]

Figure 3

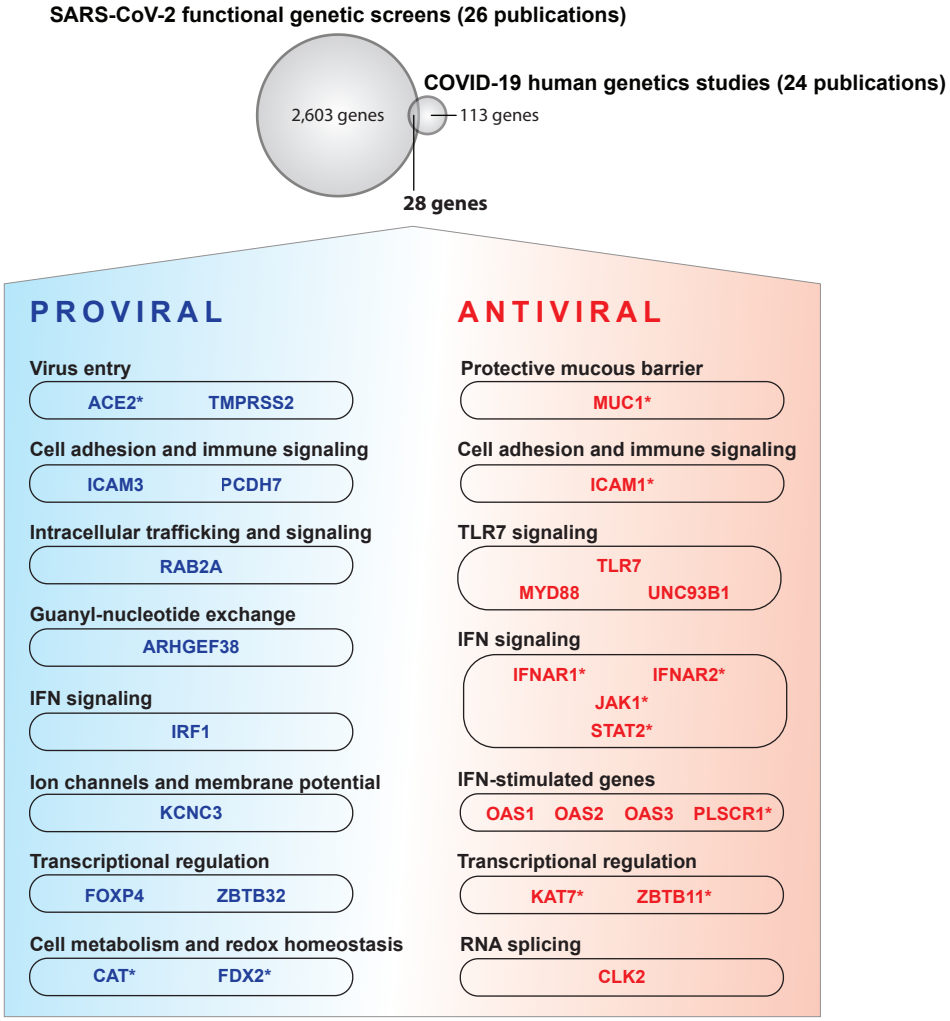

* Hit in arrayed CRISPR KO screen.

Figure 4

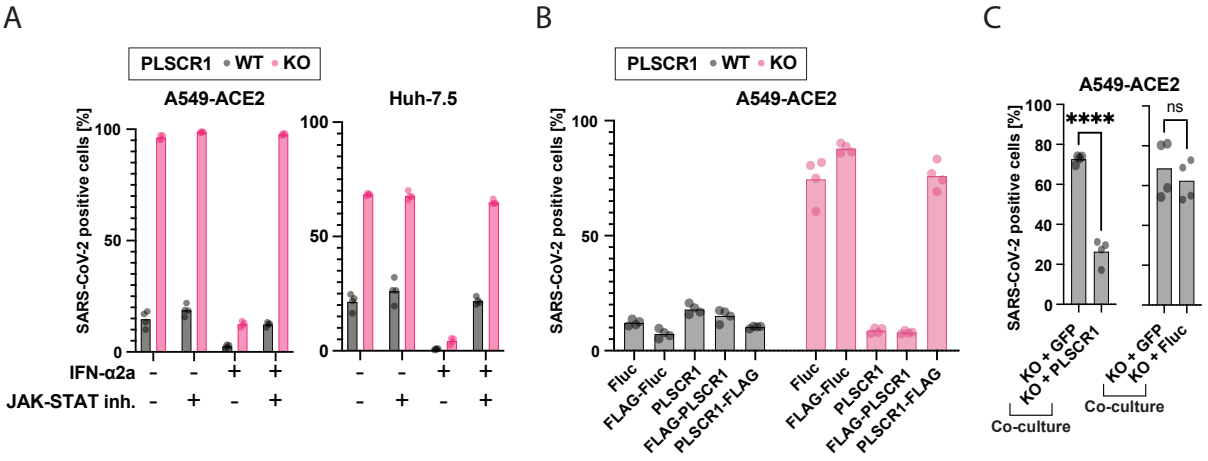
A
PLSCR1 WT KO
A549-ACE2
Huh-7.5
SARS-CoV-2 positive cells [%]
100
50
0
IFN-α2a - - + +
JAK-STAT inh. - + - +
B
PLSCR1 WT KO
A549-ACE2
Fluc
FLAG-Fluc
PLSCR1
FLAG-PLSCR1
PLSCR1-FLAG
C
A549-ACE2
****
ns
KO + GFP
KO + PLSCR1
KO + Fluc
Co-culture

Figure 5

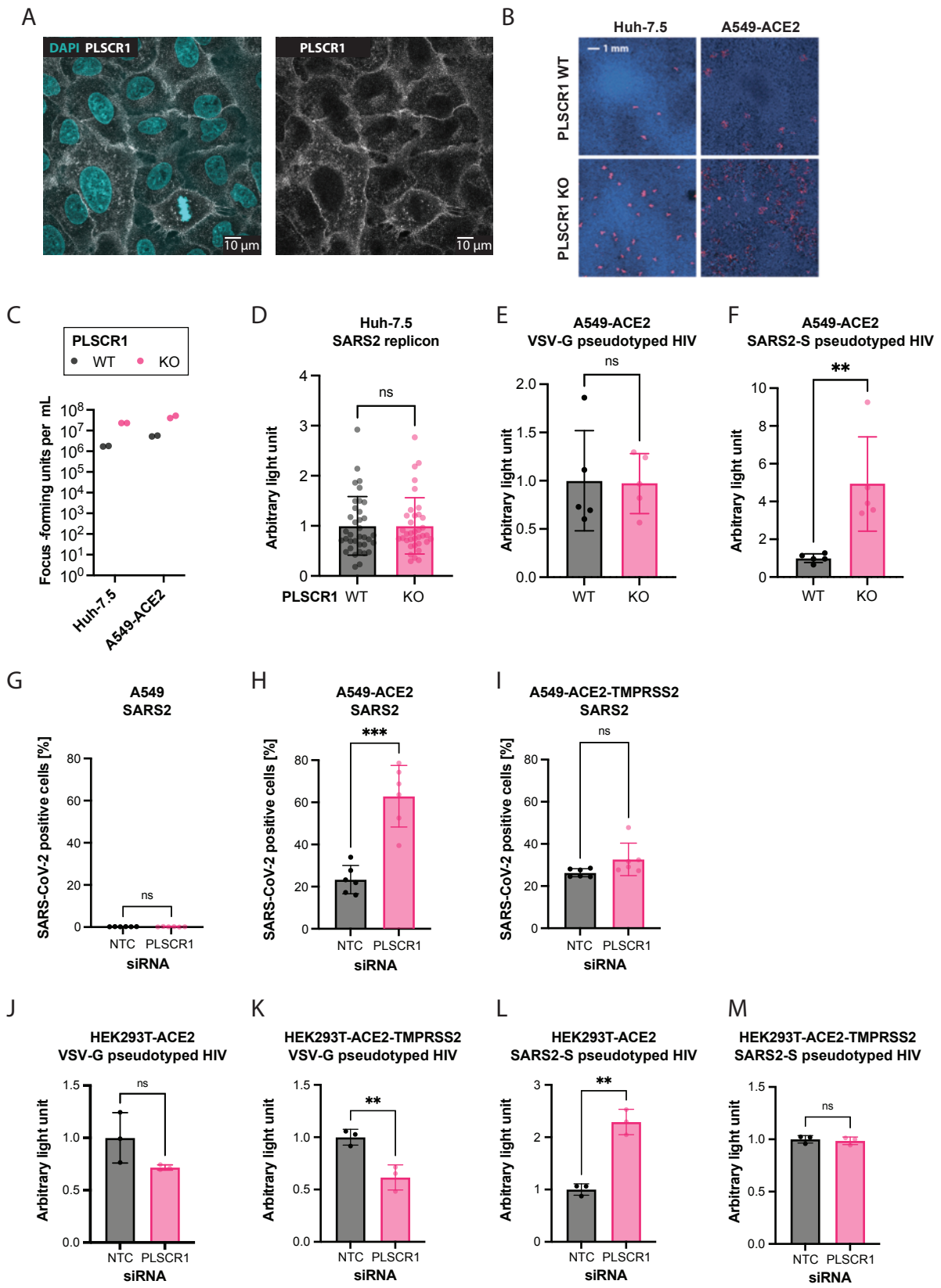
A
DAPI PLSCR1
10 µm
PLSCR1
10 µm
B
Huh-7.5
A549-ACE2
1 mm
PLSCR1 WT
PLSCR1 KO
C
PLSCR1
WT
KO
Focus -forming units per mL
Huh-7.5
A549-ACE2
D
Huh-7.5
SARS2 replicon
ns
Arbitrary light unit
PLSCR1 WT KO
E
A549-ACE2
VSV-G pseudotyped HIV
ns
Arbitrary light unit
WT KO
F
A549-ACE2
SARS2-S pseudotyped HIV
**
Arbitrary light unit
WT KO
G
A549
SARS2
ns
SARS-CoV-2 positive cells [%]
NTC PLSCR1
siRNA
H
A549-ACE2
SARS2
***
SARS-CoV-2 positive cells [%]
NTC PLSCR1
siRNA
I
A549-ACE2-TMPRSS2
SARS2
ns
SARS-CoV-2 positive cells [%]
NTC PLSCR1
siRNA
J
HEK293T-ACE2
VSV-G pseudotyped HIV
ns
Arbitrary light unit
NTC PLSCR1
siRNA
K
HEK293T-ACE2-TMPRSS2
VSV-G pseudotyped HIV
**
Arbitrary light unit
NTC PLSCR1
siRNA
L
HEK293T-ACE2
SARS2-S pseudotyped HIV
**
Arbitrary light unit
NTC PLSCR1
siRNA
M
HEK293T-ACE2-TMPRSS2
SARS2-S pseudotyped HIV
ns
Arbitrary light unit
NTC PLSCR1
siRNA

Figure 6

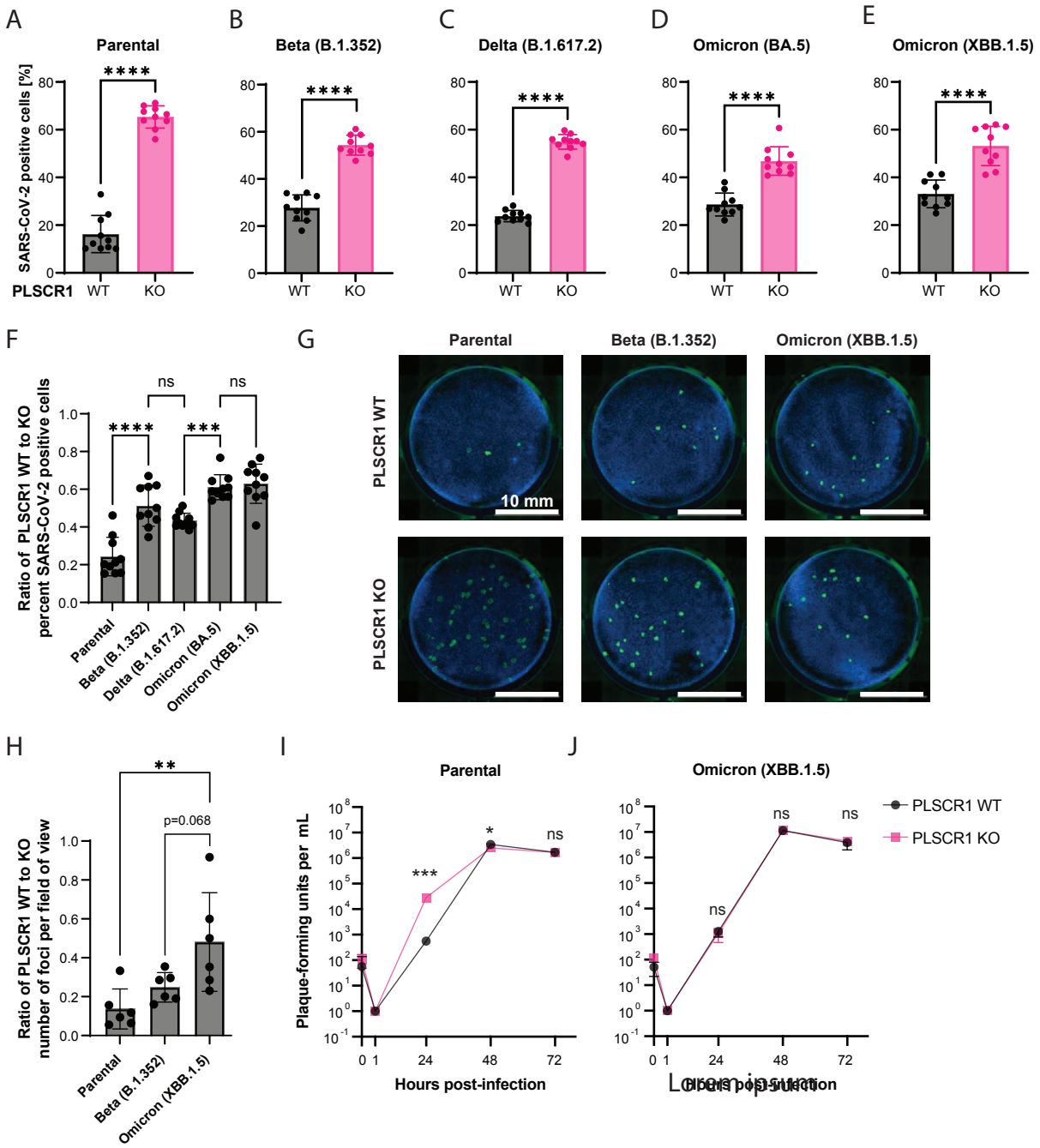
A
Parental
B
Beta (B.1.352)
C
Delta (B.1.617.2)
D
Omicron (BA.5)
E
Omicron (XBB.1.5)
SARS-CoV-2 positive cells [%]
****
PLSCR1
WT
KO
F
Ratio of PLSCR1 WT to KO percent SARS-CoV-2 positive cells
ns
***
Parental
Beta (B.1.352)
Delta (B.1.617.2)
Omicron (BA.5)
Omicron (XBB.1.5)
G
PLSCR1 WT
PLSCR1 KO
10 mm
H
Ratio of PLSCR1 WT to KO number of foci per field of view
**
p=0.068
I
Plaque-forming units per mL
Hours post-infection
J
PLSCR1 WT
PLSCR1 KO

Figure 7

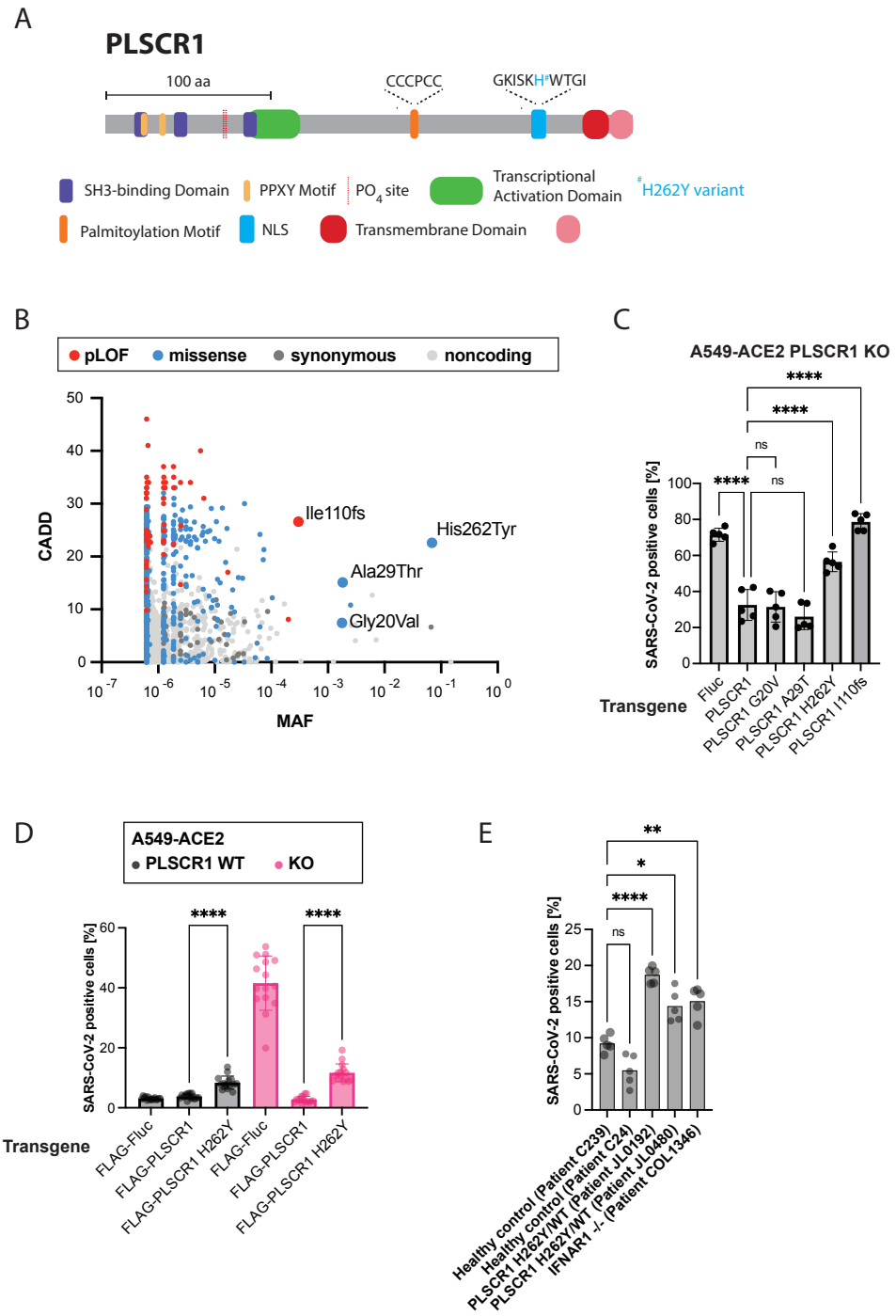
A
PLSCR1
100 aa
CCCPCC
GKISKH#WTGI
SH3-binding Domain
PPXY Motif
PO4 site
Transcriptional Activation Domain
#H262Y variant
Palmitoylation Motif
NLS
Transmembrane Domain
B
pLOF
missense
synonymous
noncoding
CADD
MAF
Ile110fs
His262Tyr
Ala29Thr
Gly20Val
C
A549-ACE2 PLSCR1 KO
SARS-CoV-2 positive cells [%]
Transgene
Fluc
PLSCR1
PLSCR1 G20V
PLSCR1 A29T
PLSCR1 H262Y
PLSCR1 I110fs
D
A549-ACE2
PLSCR1 WT
KO
SARS-CoV-2 positive cells [%]
Transgene
FLAG-Fluc
FLAG-PLSCR1
FLAG-PLSCR1 H262Y
E
SARS-CoV-2 positive cells [%]
Healthy control (Patient C239)
Healthy control (Patient C24)
PLSCR1 H262Y/WT (Patient JL0192)
PLSCR1 H262Y/WT (Patient JL0480)
IFNAR1 -/- (Patient COL1346)

Supplementary figure 1

A

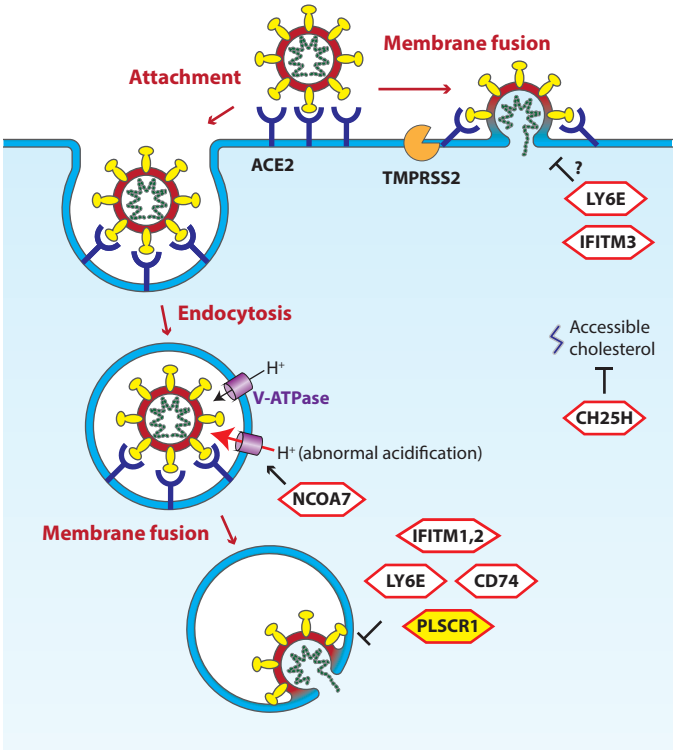

B

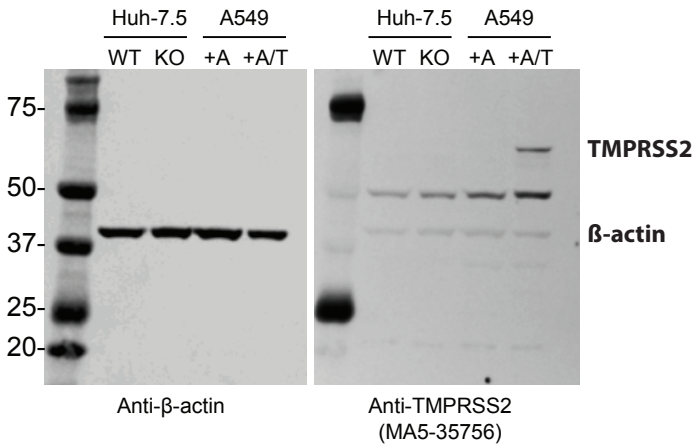

Supplementary figure 2

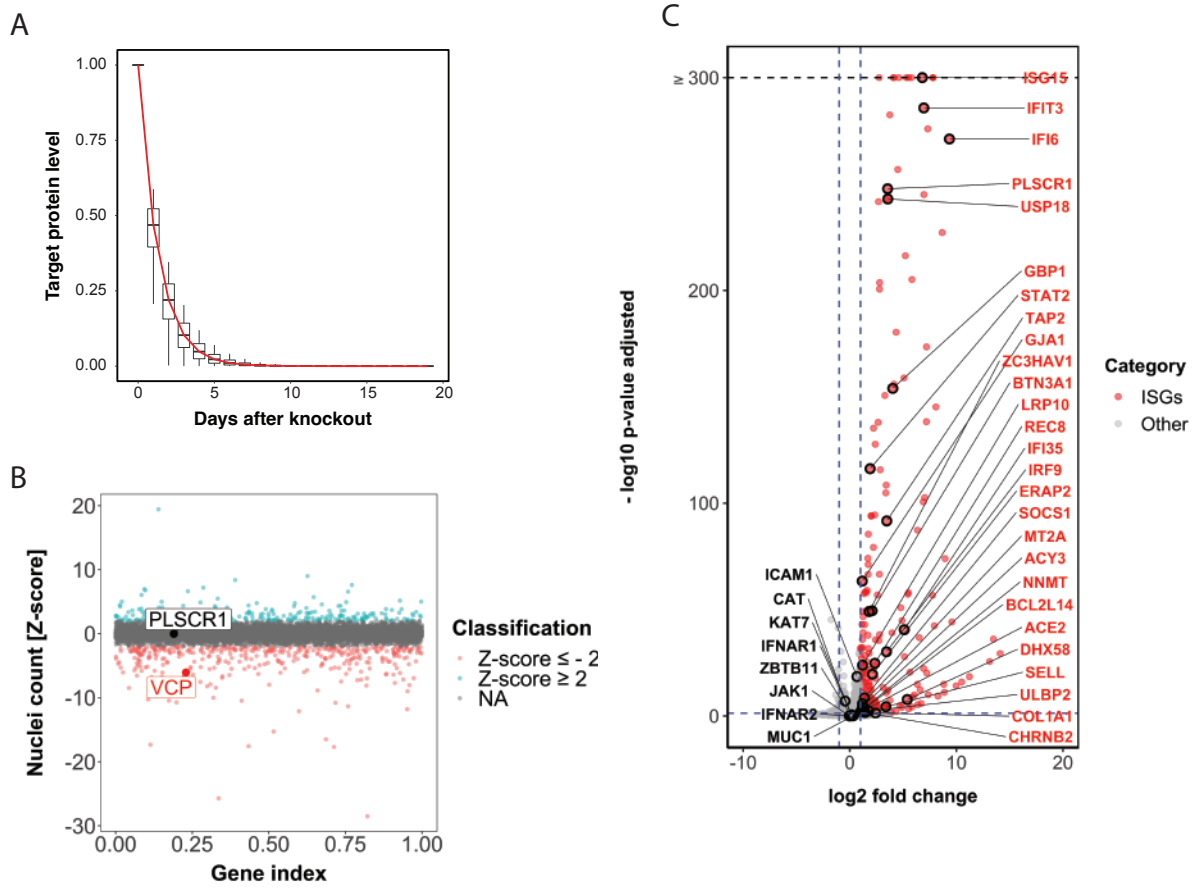

D

	ANTIVIRAL WITHOUT IFN • Respiratory electron transport[1] • Oxidative phosphorylation[4] • The citric acid cycle[1] • Aurora B pathway[3] • Sumoylation of DNA replication proteins[1] • Budding and maturation of HIV virion[1]	**ANTIVIRAL WITH OR WITHOUT IFN** • Processing of pre-mRNA[1] • mRNA splicing[1] • Transcriptional regulation by small RNAs[1] • RNA Pol II transcribes snRNAs[1] • HATs acetylate histones[1] • Inhibition of DNA recombination at telomere[1]
PROVIRAL WITH IFN • Attachment and entry[1] • Sumoylation of immune response proteins[1] • Eukaryotic translation[1] • Signaling by Robo receptors[1] • SREBF in cholesterol and lipid homeostasis[2] • SREBP signaling[2]		**ANTIVIRAL WITH IFN** • IFN-α pathway[5] • RNA Pol III transcription initiation[1] • RNA Pol III chain elongation[1] • Transcription-coupled nucleotide excision repair[1] • RHO BTB GTPase cycle[1]
PROVIRAL WITH OR WITHOUT IFN • rRNA processing[1] • Cotranslational protein targeting to membrane[1] • Regulation of lipid metabolism by PPARalpha[1] • Cholesterol biosynthesis by SREBP SREBF[1] • Metabolism of steroids[1] • S1P pathway[5]	**PROVIRAL WITHOUT IFN** • Receptor-mediated mitophagy[1] • SARS-CoV-2 modulates autophagy[1] • Vesicle mediated transport[1] • Assembly of LPL and LIPC lipase complexes[1] • ARAP pathway[5] • Keap1-NFE2L2 pathway[1] • Signal transduction by L1 cell adhesion molecules[1]	

No pretreatment SARS-CoV-2 infection [Pathways]

IFN-α2a pretreatment SARS-CoV-2 infection [Pathways]

Supplementary figure 3

A

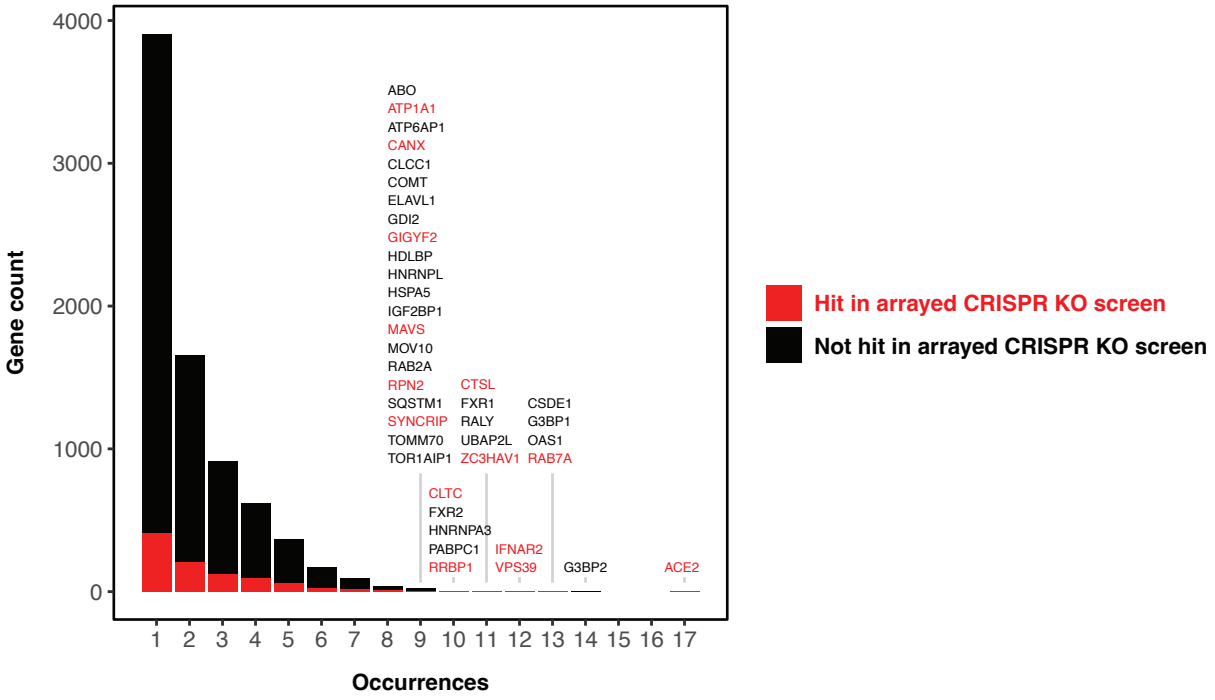

B

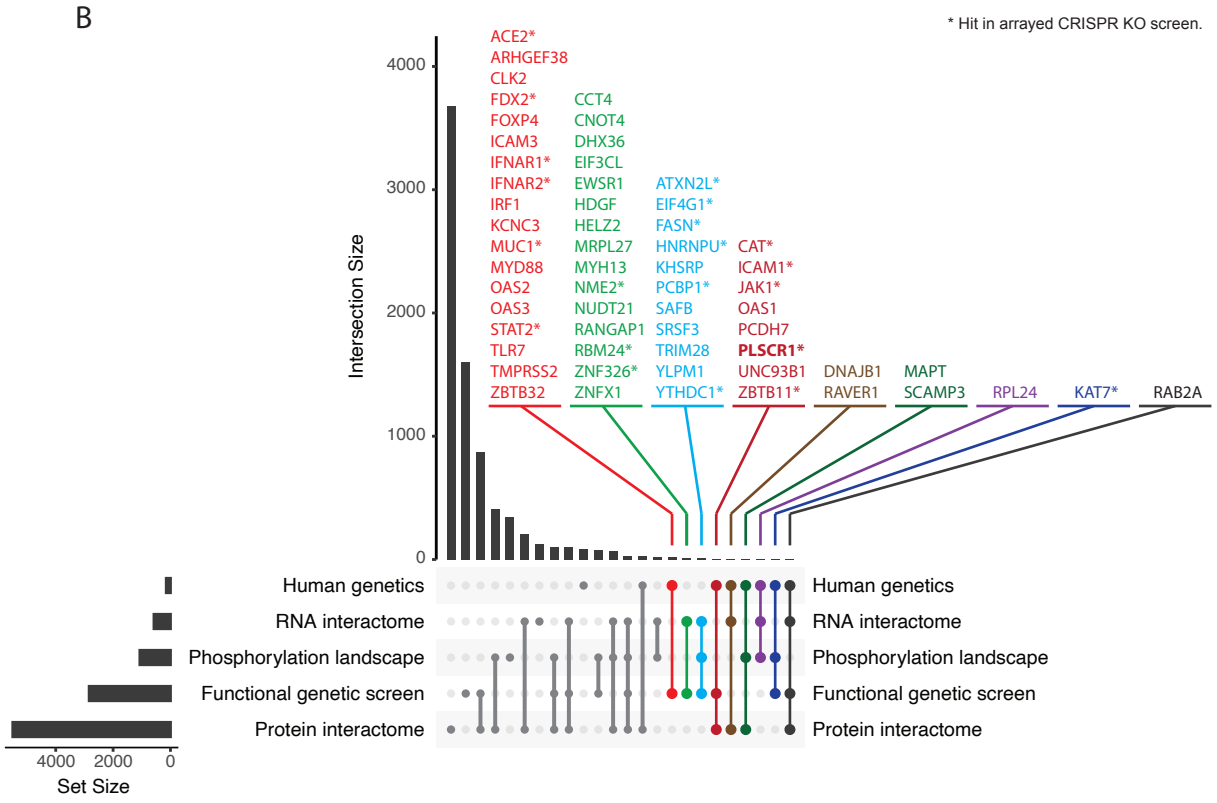

Supplementary figure 4

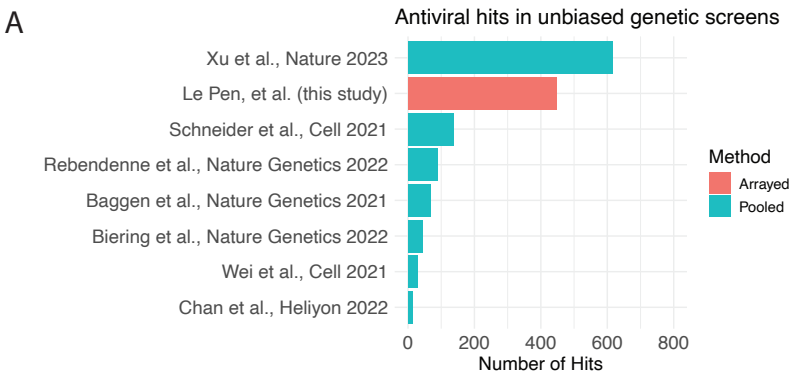

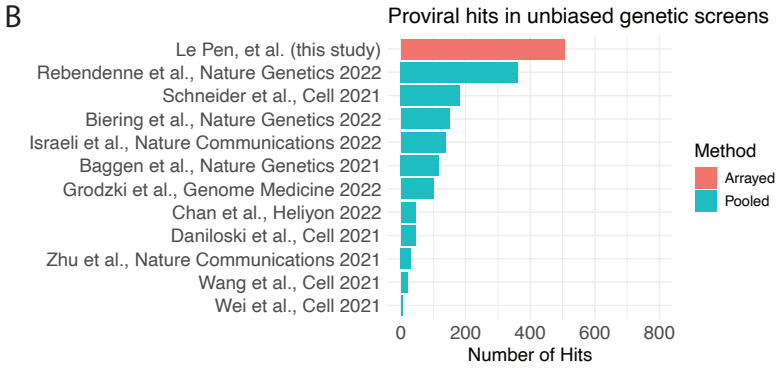

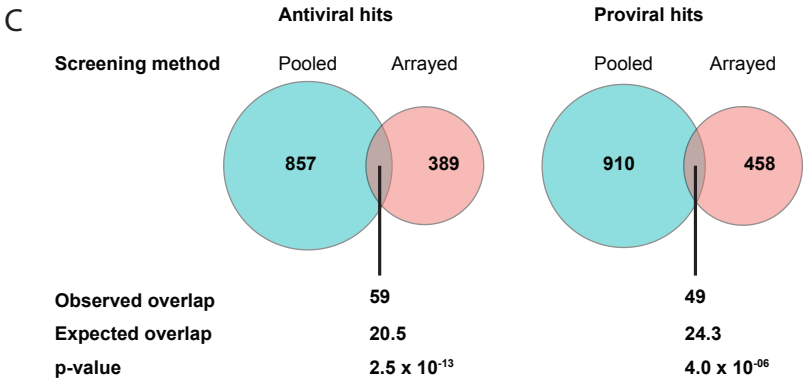

Supplementary figure 5

A

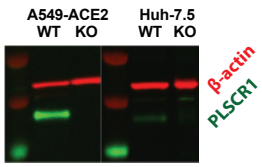

B

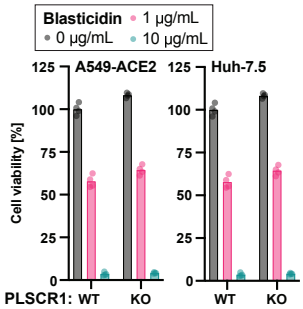

C

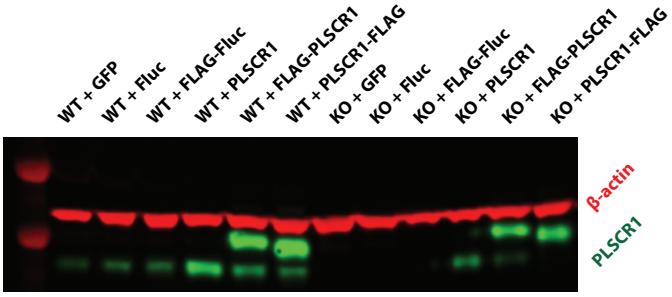

D

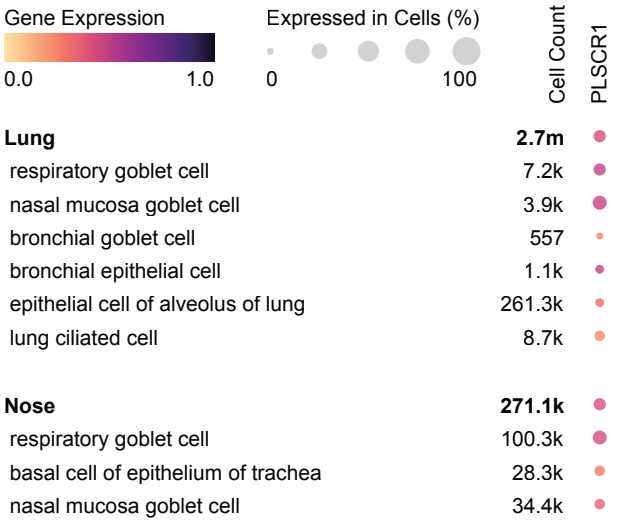

Supplementary figure 6

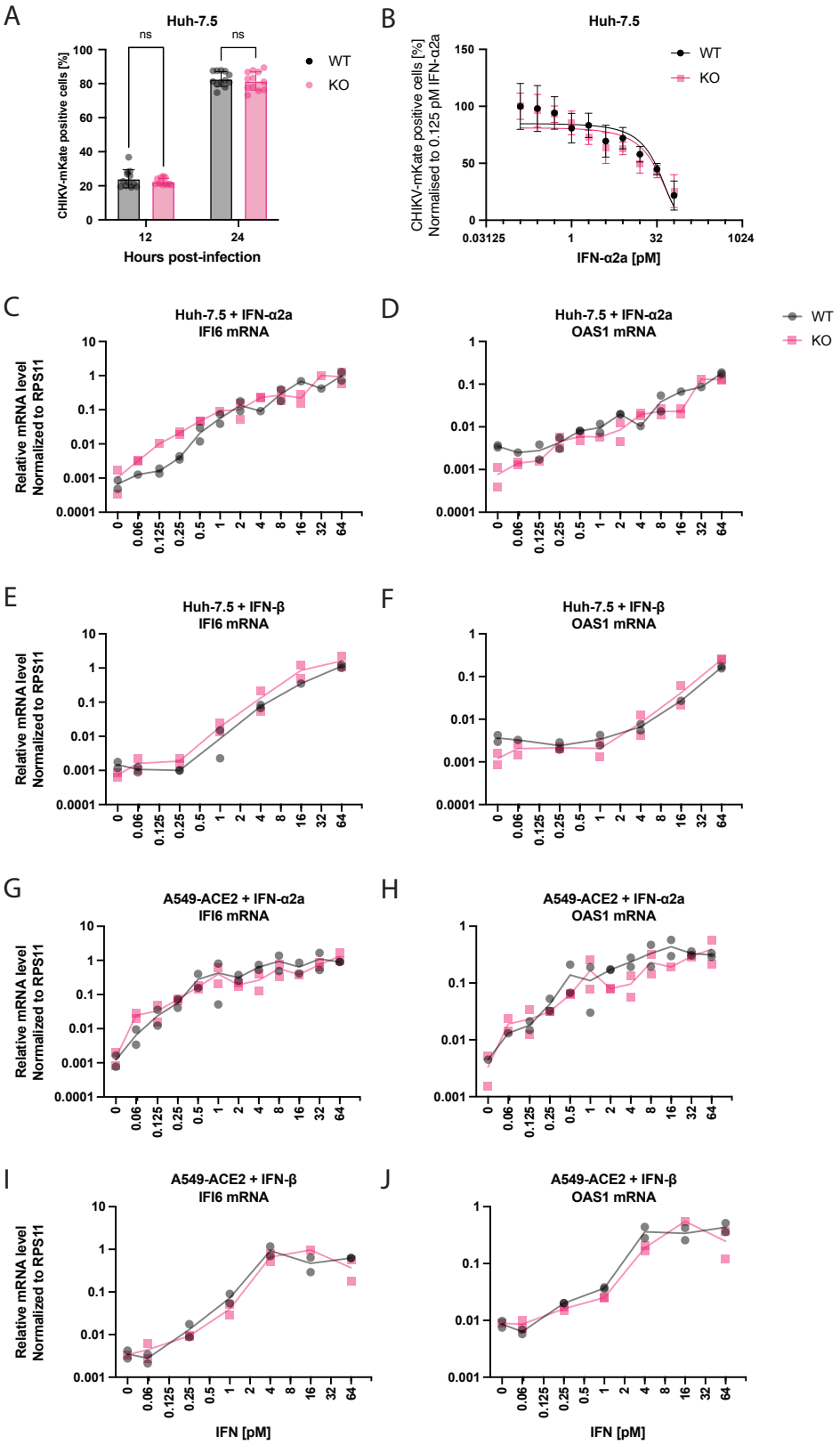

Supplementary figure 7

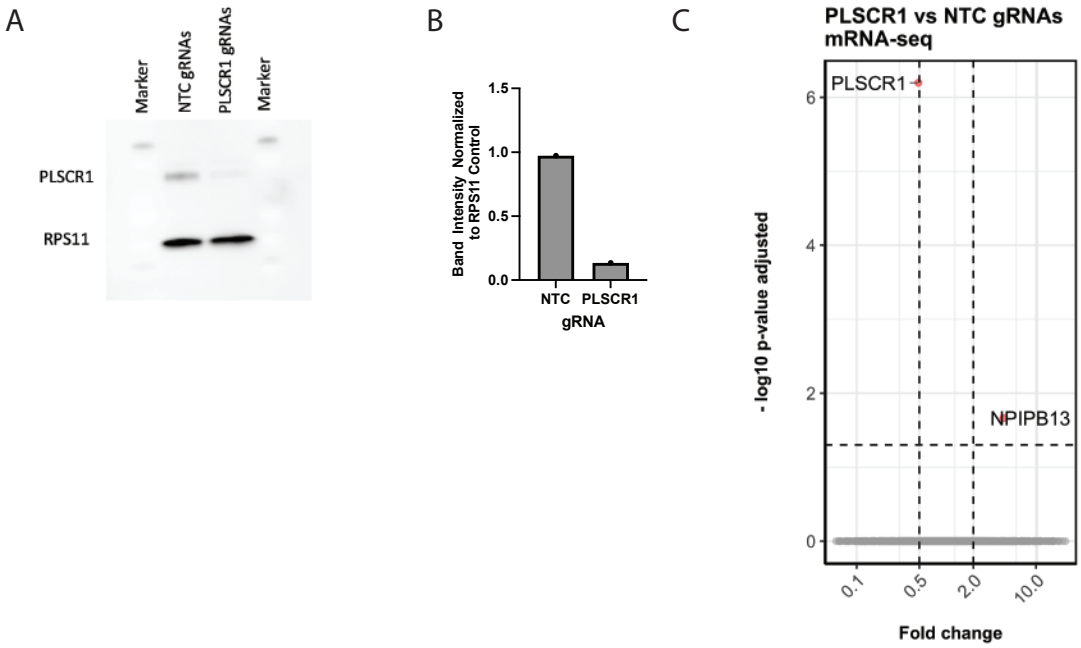

Supplementary figure 8

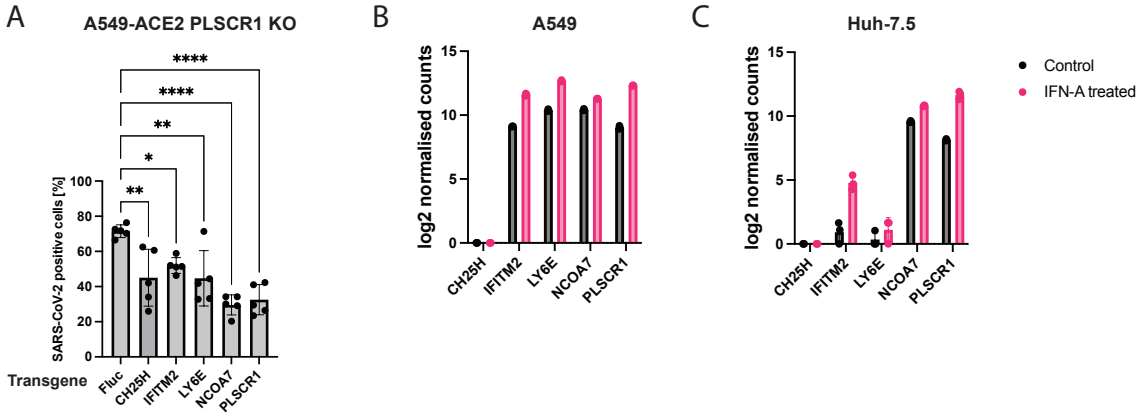

Supplementary figure 9

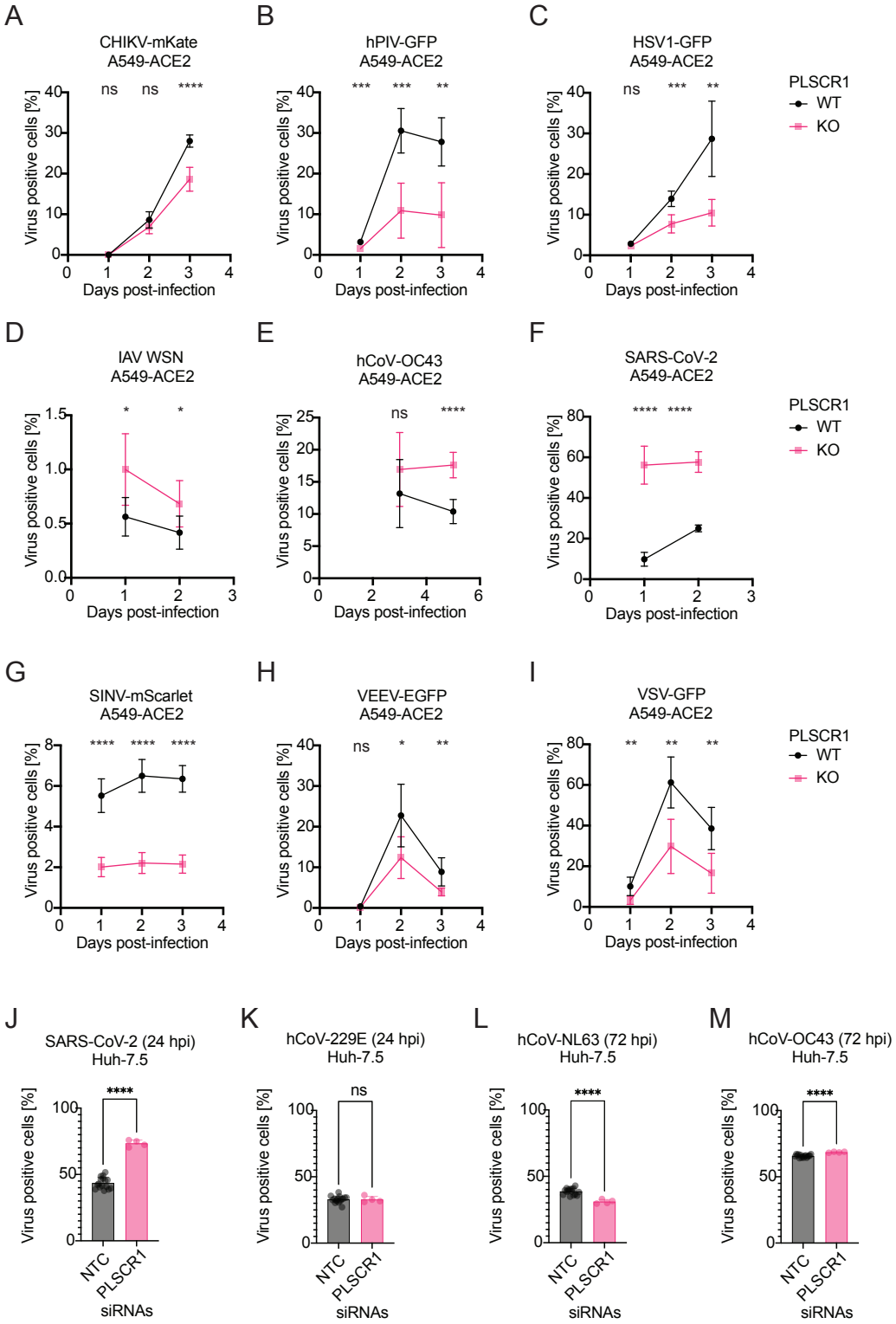

Supplementary figure 10

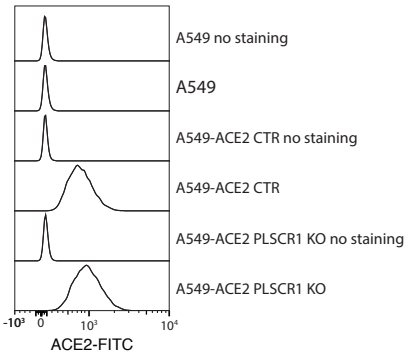

Supplementary figure 11

A

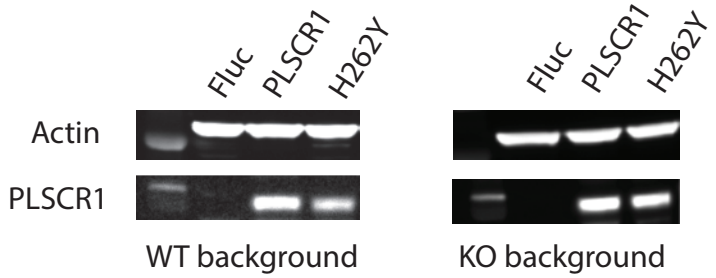

B

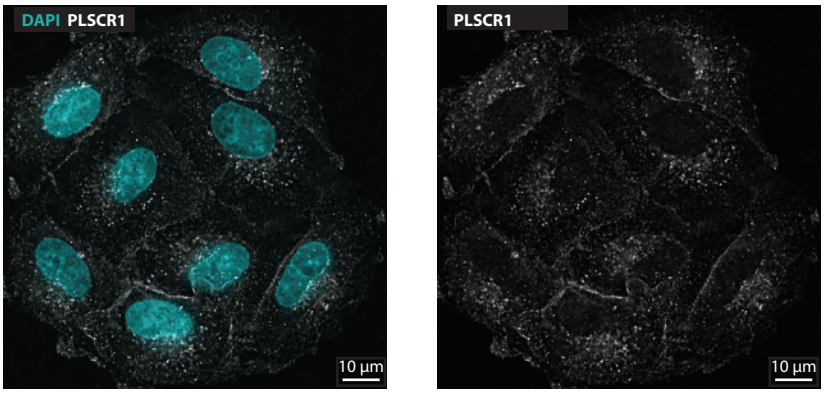

C

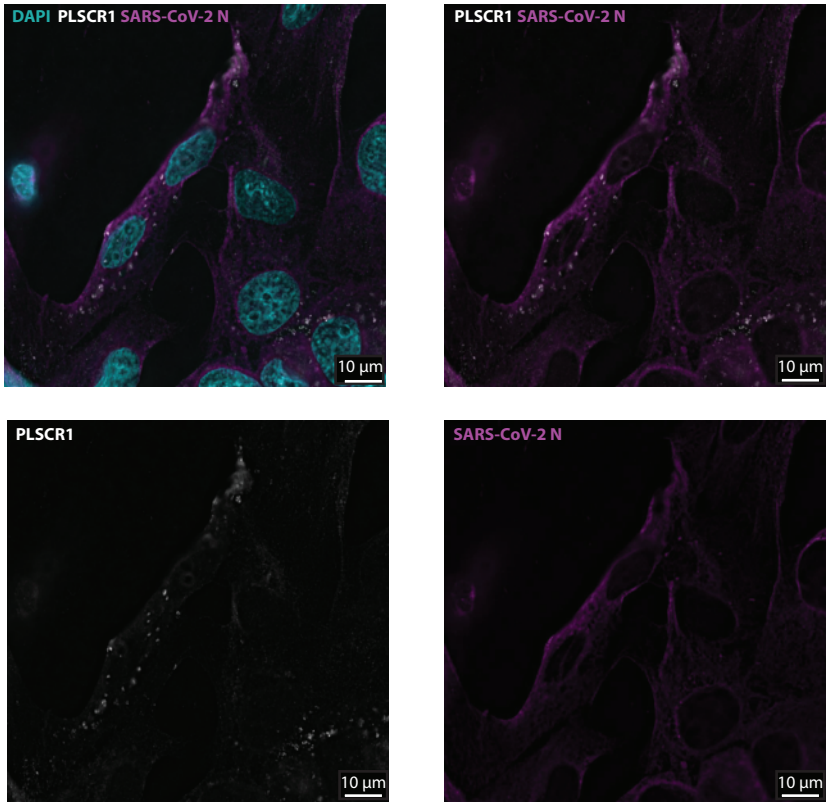

Supplementary figure 12

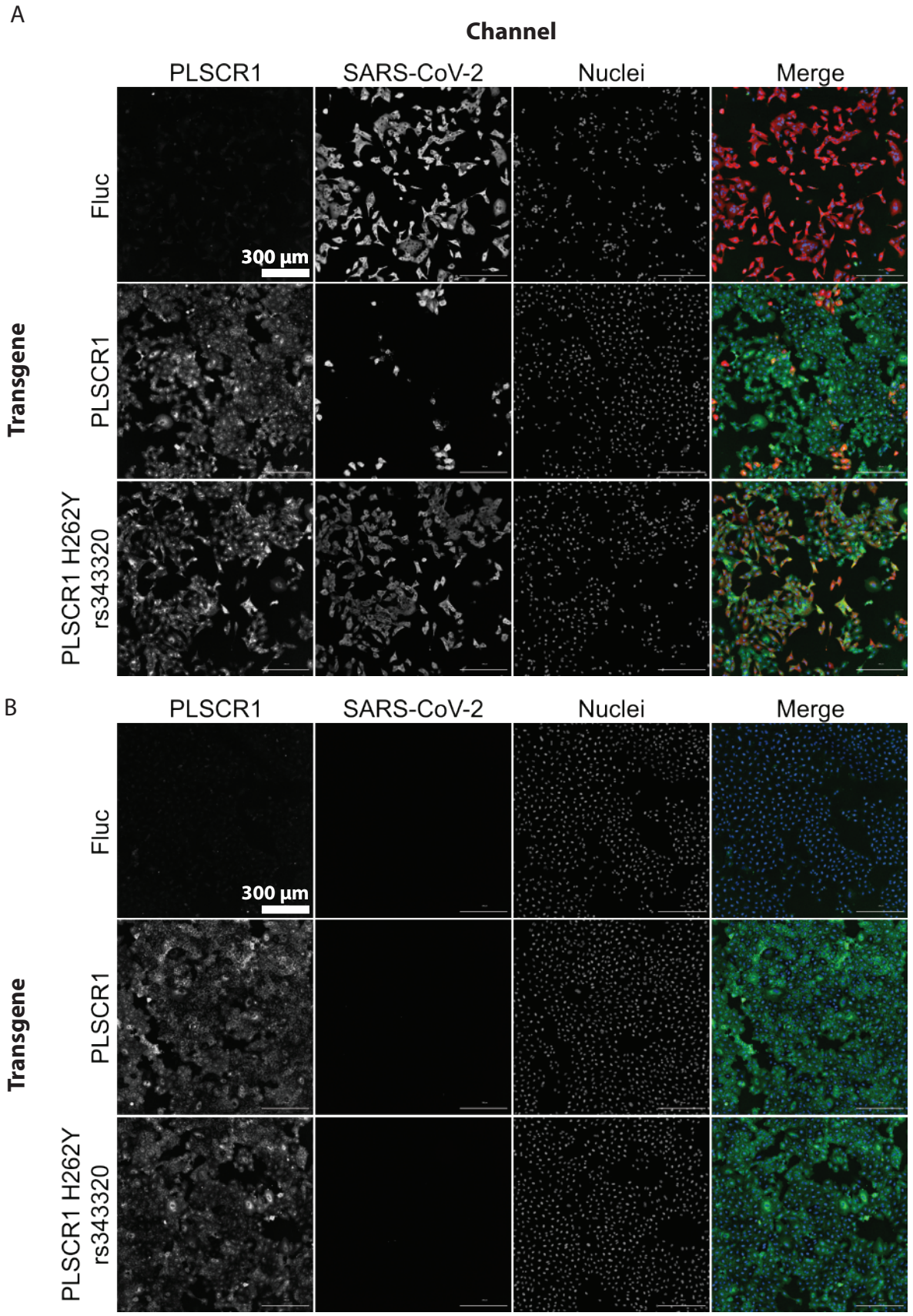

Supplementary figure 13

A

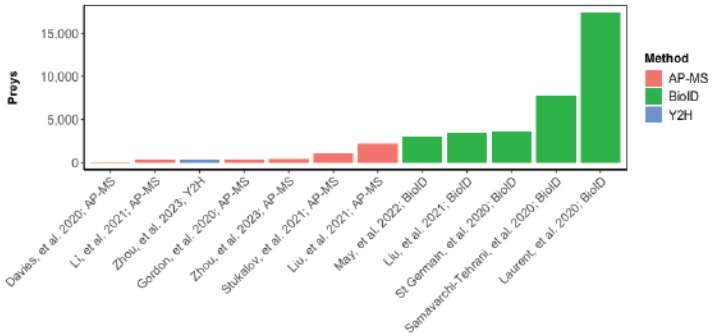

B

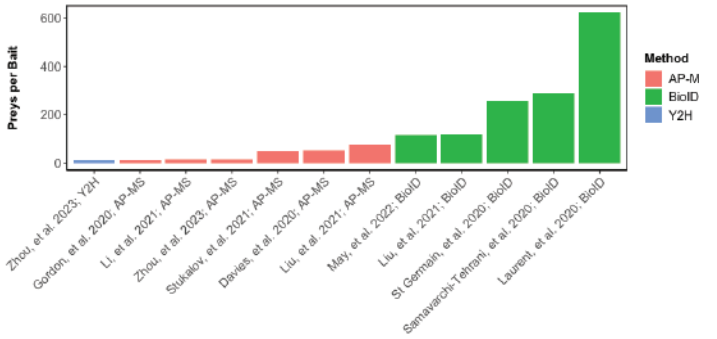
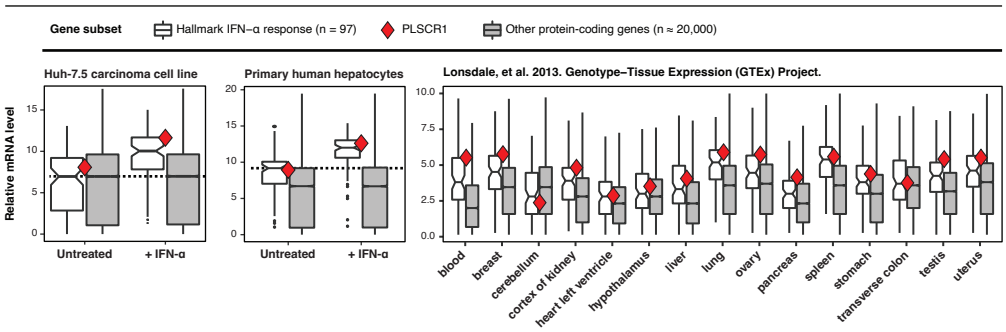
Supplementary figure 14